The Pennsylvania State University
The Graduate School

STRUCTURING AN INTEGRATIVE APPROACH FOR FIELD DEVELOPMENT PLANNING USING ARTIFICIAL INTELLIGENCE AND ITS APPLICATION TO TOMBUA LANDANA ASSET IN ANGOLA

A Dissertation in
Energy and Mineral Engineering
by
Sarath Pavan Ketineni

Submitted in Partial Fulfillment
of the Requirements
for the Degree of

Doctor of Philosophy

December 2015

The dissertation of Sarath Pavan Ketineni was reviewed and approved* by the following:

Turgay Ertekin
Head, John and Willie Leone Family Department of Energy and Mineral Engineering
Professor of Petroleum and Natural Gas Engineering
George E. Trimble Chair in Earth and Mineral Sciences
Chair of Committee
Dissertation Advisor

John Yilin Wang
Associate Professor of Petroleum and Natural Gas Engineering
Director of 3S Laboratory

Eugene Morgan
Assistant Professor of Petroleum and Natural Gas Engineering

Sridhar Anandakrishnan
Professor of Geosciences

Luis F. Ayala H.
Professor of Petroleum and Natural Gas Engineering
Associate Department Head for Graduate Education

*Signatures are on file in the Graduate School.

Abstract

Field development studies are at the forefront of common engineering practices in petroleum industry to maximize the returns on a given asset. In early stages of reservoir depletion, it is often a challenging task to accurately determine reservoir properties that are representative of the actual field. Reservoir modeling is the traditional way that engineers performed to develop field development and depletion plans. Due to different scales of data obtained from various sources like seismic data, well logs, cores, and production data, there is a lot of uncertainty in solving the inverse problem of estimating formation rock and fluid properties from the field data. Increase in complexity of formations and scarcity of reservoir data have made reservoir characterization a challenging task. Soft computing techniques have gained popularity in petroleum industry to identify complex patterns that exist between various reservoir data collected from multiple sources and be able to successfully characterize a reservoir.

In this work, a work-flow is developed for devising a comprehensive reservoir characterization tool based on artificial neural network. A case study of Chevron's Tombua Landana Asset is used in demonstrating the tenets of the work-flow.

The reservoir under consideration is highly heterogeneous in terms of property distribution and is believed to be highly channelized. The ANN based tool will assist in identifying sweet spots by predicting optimal well location/path/completion parameters and production schedule.

The multilayer feed forward back propagation based neural network tool developed is able to capture the correlations that exist amongst seismic data, well logs, completion data, and production data. Well logs are correlated using surface seismic attributes and geometric location of wells with an average testing error of less than 15%. The range of testing errors is in between 1-30%. The tool enables the user to predict the entire well log suite for even a horizontal well of user defined configuration through a graphic user interface. Having correlated seismic data with well logs, synthetic well logs are generated for the entire area of seismic coverage. To predict production data, along with seismic data and well logs, schedule of production and interference factors are incorporated as functional links. Upon analyzing the relevancies of input data, functional links based on geographic location and injection wells are included to make the prediction more reliable and robust. Production performance networks comprising cumulative oil, gas and water production performance prediction modules are developed to forecast performance of wells at undrilled locations. Oil networks indicated an average error of 21% in blind testing cases. Highly variable gas production could also be correlated with the seismic data and well log data within 32% error. Water production networks indicated a high error of 46% on blind testing cases. Oil, gas and water production forecast maps are generated using production performance networks. Maps generated indicate flow paths that exist in the field.

Monte Carlo simulations are performed to predict P10/P50/P90 OOIP maps. The developed model enables reservoir engineers to construct well paths based on synthetic log cubes generated in conjunction with Monte Carlo OOIP estimates. Genetic algorithms can be used to optimize selection of new well locations and well paths enabling production from sweet spots. Further analysis using NPV (net present value) calculations is integrated with production predictions to identify the potential producer locations and well paths.

Table of Contents

List of Figures

List of Tables

List of Symbols

Roman

a : Tortuosity factor or Lithology dependent constant in Archie's equation

A : Area (acres)

B_o : Formation volume factor of oil phase (RB/STB)

B_g : Formation volume factor of gas phase (RB/SCF)

B_w : Formation volume factor of water phase (RB/STB)

F : Formation factor ranges from 0 to 1, ratio of resistivities

h : Thickness of reservoir (ft)

m : Cementation factor in Archie's equation

NPV : Net present value in dollars,$

OOIP : Original oil in place (STB)

OGIP : Original gas in place (SCF)

OWIP : Original water in place (STB)

p : Pressure (psi)

$P10$: 10% Probability of finding a certain value

$P50$: 50% Probability of finding a certain value

$P90$: 90% Probability of finding a certain value

q_g : Gas flow rate ($MSCF/day$)

q_o : Oil flow rate (STB/day)

q_w : Water flow rate (STB/day)

q_{cum} : Cumulative flow rate (STB/day)

S_o : Oil saturation

S_g : Gas saturation

S_w : Water saturation

R_t : Fluid saturated rock resistivity

R_o : Water filled rock resistivity

R_w : Brine resistivity

t : Time (day)

Greek

ϕ : Porosity

ρ_b : bulk density (gm/cm^3)

ρ_f : Fluid density (gm/cm^3)

ρ_{ma} : Matrix density (gm/cm^3)

Subscripts

i : Initial conditions

o : Oil phase

w : Water phase

g : Gas phase

Acknowledgments

I would like to sincerely thank Dr. Turgay Ertekin for his invaluable guidance and immense patience throughout my time here as his student. I have been extremely lucky to have a supervisor who cared so much about my work as well as personal life, and who responded to my questions and queries so promptly. Energy and Mineral Engineering department at Penn State has provided with me all the resources and avenues for me to perform up to my abilities and strengths. I would like to extend my gratitude towards all the professors and staff, specially Jaime Harter who work tirelessly to keep the department vibrant and welcoming. Thanks to Chevron Corporation for providing the data for this research.

I thank Dr. Sridhar Anandakrishnan, Dr. Luis Ayala. Dr. John Yilin Wang and Dr. Eugene Morgan for serving on my committee and helping me navigate through obstacles and guide me in right direction to research. Their valuable suggestions have made a significant difference.

Dr. Elizabeth Hajek and Dr. Rudy Slingerland have been been of great help in navigating obstacles through research and I owe them for letting me use sedimentary lab for working on my research.

I owe my loving thanks to my father Rama Rao, mother Prameela, brother Subramanyam, sister Vidyavathi for their unconditional love and support. They

have been my pillars of support. Special thanks to friends, Phani, Siddhart, Soumyadeep, Taha, Vaibhav, Rajesh, Yogesh, Amir, Aditya, Ravi, Kelvin, Kristen, Doug for their help when most needed.

Chapter 1

Introduction

With the ever increasing demand for oil and gas in modern day, it has become necessary for engineers to develop economic ways of evaluating and producing from an asset. A detailed reservoir model is necessary to maximize the value of a hydrocarbon asset. Field development strategies, infill well drilling, forecasting reservoir performance are made based on reservoir characterization studies.

Traditional ways of reservoir modeling include building static models through extensive petrophysical analyses combined with dynamic history matching via reservoir simulation to establish the reserves in place and propose field development strategies. These methods are time and labor intensive, and several approximations are made throughout this process when data is limited, and sparse in nature. The challenge in modern day reservoirs is no longer to predict the presence of hydrocarbons, but to quantify the uncertainty of reservoir predictions and minimize risk associated with that (Wong et al., 2002).

Reservoir characterization increases in complexity as the reservoir becomes increasingly heterogeneous. Core data measured at a wellbore will no more act as a representative sample, hence would require a statistically large number of samples to encompass the entire reservoir. In the recent times, seismic data

is proven to be useful in estimating the interwell geologic information, thereby aid in understanding heterogeneous reservoirs better. Rock physics discipline deals with finding correlations that exist between seismic data and reservoir rock and fluid properties. But, it is important to effectively reconcile and precisely integrate various sources and scales of data obtained from 3D seismic, well logs, core and production information. The challenge in the conventional models is to preserve the reservoir complexity while shortening their runtime. Most often reservoir parameters are adjusted by trial and error to obtain a history matched model. Conventional methods of characterizing these reservoirs are not effective, therefore, alternative methods should be explored to find a probable solution that can efficiently understand the complexities of the reservoirs.

Soft computing techniques have tolerance for imprecision and uncertainty, and are efficient, low cost, and robust (Nikravesh and Aminzadeh, 2001). Identifying non-linear patterns in reservoir studies can significantly help in assisting reservoir characterization. In recent times, artificial neural networks are being increasingly used in science, finance and engineering for their aforementioned capabilities.

Therefore, this research focuses on building an artificial intelligence based tool to characterize a heterogeneous reservoir by integrating geological, geophysical and dynamic production data. The proposed methodology can be applied to a wide variety of reservoirs to evaluate the production potential and suggest an optimal field development strategy. Inter assisting expert systems based on artificial neural network technology are developed that establish the complex relationship between seismic data, well log data and production data. The dissertation is divided into different chapters to describe development of the integrated artificial intelligence based tool.

- Chapter 2 outlines the literature reviewed and presents information pertinent to the latest research in the field of reservoir characterization.
- Chapter 3 provides a general description of problem statement and objectives
- Chapter 4 discusses the methodology developed in this study. Inter assisting expert systems comprising of synthetic well log networks and production performance networks are presented.
- Chapter 5 presents a case study on which the current methodology has been tested. The case study presented is Chevron's Tombua Landana asset from Block 14 Angola offshore.
- Chapter 6 showcases the results and discussion of expert systems developed in this study. Blind testing results are used to illustrate the robustness and accuracy of the developed model.
- Chapter 7 summarizes the work, and major conclusions of this study along with recommendations for future research.

Chapter 2

Literature Review

2.1 Reservoir characterization

The process of quantitative assignment of reservoir properties such as porosity, permeability, and fluid contacts, etc. is known as reservoir characterization (Mohaghegh et al., 1996). Field scale characterization of reservoirs is crucial in providing the link between exploration/discovery process and the development/reservoir management process. Geologic concepts developed during the exploration stage are continuously tested and modified as appropriate during reservoir development and production. Uncertainties associated with the inverse problem of estimating reservoir properties through observed data need to be thoroughly understood for efficient reservoir management. Properties such as porosity, permeability, lithology, fluid type, etc. can be obtained using seismic reservoir characterization methods.

Areal extent of the reservoir is usually obtained from seismic exploration analysis. Reservoir thickness, porosity, and water saturation are derived from petrophysical well log analysis combined with core data analysis. Core data provide high resolution information surrounding the well bore however they suffer from sampling bias. The

obtained core data could be a small isolated section and may not be able to capture the macroscopic features of the reservoir. Well logs provide medium resolution information in the vicinity of wellbore. Seismic data and well log data are explained further in the following sections.

2.1.1 Seismic exploration

There are several exploration methods such as seismic, gravity, magnetic, etc. used in measuring physical properties of the subsurface in order to understand the petroleum reservoirs. Seismic data acquisition is the most commonly used method in obtaining a comprehensive image of the reservoir (Artun et al., 2005). In this method, energy source located either on the surface of the earth or submerged in water (for offshore applications) generates low frequency sound waves. These sound waves are reflected off earth's surface that comprise of information relating to geologic interfaces and amplitudes at two way travel times (TWTT) are recorded via series of geophones. Depending on the location of energy sources and geophones, seismic profiles can be recorded in 2-D or 3-D. The latest technology is to shoot a seismic survey with time and is referred to as 4-D seismic survey or 3-D time lapse seismic survey. These 4-D seismic surveys can be used to track the saturation changes over time for secondary recovery applications (Yilmaz, 2001). The data gathered across these geophones over a horizontal distance can be compiled to create a cross section of the earth (Berger and Anderson, 1981). In a 3-D seismic survey, data recorded from numerous closely spaced seismic lines called inlines and crosslines, provide a high spatially sampled measure of subsurface reflectivity. A visual description of the two different types of common seismic surveys is provided in Figure 2.1

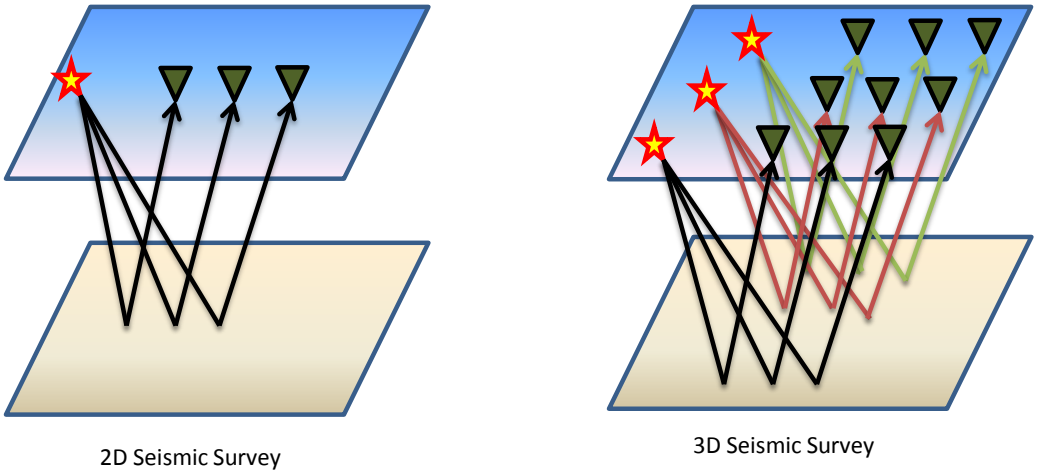

Figure 2.1. Visual description of 2D and 3D seismic survey

Though seismic data is measured at a lower vertical resolution compared to a well log, the areal coverage is extensive and spans over the entire filed. Seismic data are primarily utilized by geophysicists to recreate the subsurface structure and identify potential oil and gas producing regions.

Seismic attributes: Seismic attributes are information derived from the seismic data either by direct measurement or by processing important seismic characteristics such as time, amplitude, frequency and attenuation. Seismic attributes could be either horizon based or sample based. The process of adding seismic traces to improve the signal to noise ratio is called staking. Seismic attributes computed post stacking tends to loose offset and azimuth information, but they are preferred due to the reduced amount of data. In practice, most interpreters use instantaneous amplitude or some variation of amplitude attribute as the primary diagnostic tool. Amplitude is related to reflectivity providing information on subsurface impedance contrasts. Instantaneous phase and frequency attributes are used in tracking

reflection continuity, bed thickness and bed spacing respectively. In the current work, amplitude based attributes are extensively used.

Any computation on the seismic trace can be categorized as a seismic attribute. Attributes could be 3-D, 2-D and even a scalar value for the entire zone/region/surface. Figure 2.2 outlines all the possible attributes that could be computed from seismic data. These attributes contain several parameters that represent reservoir characteristics and fluid properties.

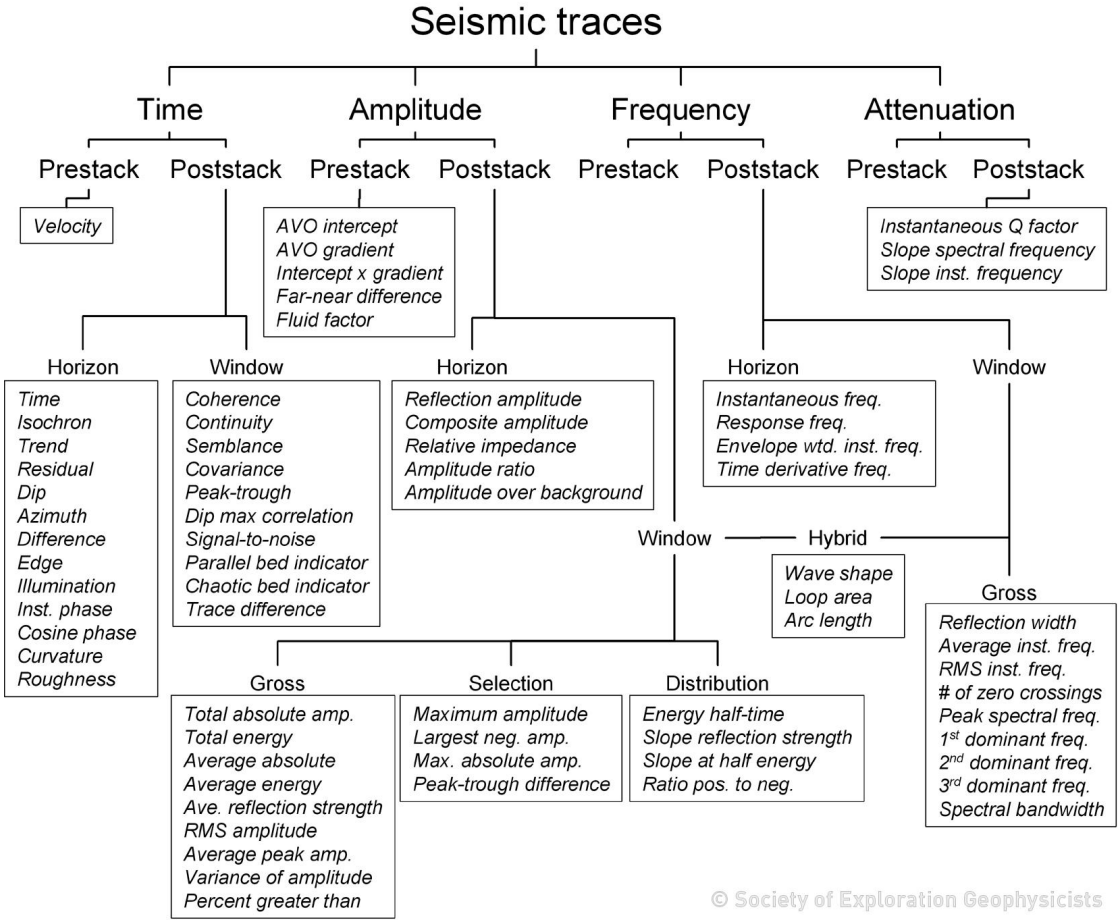

Figure 2.2. Classification of seismic attributes (Brown, 2001)

A velocity model is used as a bridge between time and depth domains. Seismic surveys are recorded in time domain, where amplitudes are plotted against two

way travel times. Geophysicists develop a velocity model taking into account the stratigraphic variations based on lithology. This velocity model is used to commute between time and depth domain. Check shot surveys are used for quality control to tie well log with the seismic trace information.

Seismic data can also be utilized to obtain a spatial distribution of reservoir properties via principal component analysis (PCA) techniques. PCA is a long established technique to analyze multivariate seismic attribute data sets to make predictions of rock properties and help refine definition of reservoir geometry and quality (Higgs et al., 2005).

2.1.2 Well logs

Well logs provide continuous measurements of physical parameters in the nearby wellbore region. Usually most wells (conventional logs such as spontaneous potential, gamma ray, density, resistivity, and induction) are logged upon drilling and completion. The primary objectives of wireline logging are to identify the reservoir, estimate hydrocarbon in place and estimate recoverable hydrocarbon through estimation of petrophysical parameters like porosity, permeability, hydrocarbon saturation and lithology of the zones. Hydrocarbons and reservoir rocks are insulators, whereas connate water and brine are saline and good conductors. The basic relationship between electrical resistivity and formation properties was first developed by Archie,1942 (Archie et al., 1942).

He observed that rock resistivity is directly proportional to the resistivity of brine, R_w and formation factor F. Formation factor is determined by the porosity and pore structure factors like cementation factor m and lithology dependent constant a as indicated in Equation 2.1.

$$
\begin{aligned}
R_o &= F * R_w \\
F &= \frac{a}{\phi^m} = \frac{R_o}{R_w} \\
S_w^n &= \frac{R_o}{R_w}
\end{aligned}
\tag{2.1}
$$

The porosity of a zone can be estimated from a single porosity log or a combination of porosity logs, in order to correct for the variable lithology effects in complex reservoirs. When using a single density porosity log, the true porosity is derived from interpolation of values between values from matrix mineral and the pore fluid as indicated in Equation 2.2

$$\rho_b = \phi * \rho_f + (1 - \phi)\rho_{ma} \tag{2.2}$$

where, ρ_b is the bulk density, ϕ is porosity, ρ_{ma} is the matrix density and ρ_f is the fluid density.

The most common way of determining net pay is to select intervals based on log derived cutoffs. The petrophysical cutoffs are determined based on the observed field data. Gamma ray log provided information on extent of sand/shale present in the formation. Resistivity logs help in distinguishing hydrocarbon rich zones from water saturated zones.

2.1.3 Monte Carlo simulations

Monte Carlo(MC) simulations are a broad class of computational algorithms that rely on repeated sampling to obtain numerical results with probabilistic estimates. This method was first invented and published by Metropolis and

Stanislaw(1949) (Metropolis and Ulam, 1949) while working at Los Alamos National Laboratory.From then on, it has been used in engineering, physical sciences, computational biology, computer graphics, applied statistics, finance and other fields.

Monte Carlo simulations are highly useful in risk assessment while estimating the volumetric reserves of hydrocarbon reservoirs (Murtha et al., 1994). This method is also popularly used to predict lithology, stratigraphic sequence from seismic data. Statistical distributions of porosity, thickness, area, water saturation, recovery factor, and oil formation factor affect the simulated original oil in place. These simulations can help in establishing probabilities of expected parametric values. Much of risk analysis techniques estimate a parameter within a range of values rather than a single value. Original oil in place is one of the most important parameters while evaluating a reservoir for its potential.

The oil in place is calculated through the Equation 2.3 :

$$OOIP(bbls) = 7758 \times A(acres) \times netpay(ft) \times \phi \times \frac{1 - S_{wi}}{B_{oi}(RB/STB)} \tag{2.3}$$

Think of the parameters A, $netpay$, ϕ, S_{wi}, and B_{oi} as input parameters and $OOIP$ as the output. Once all the parameters are specified, $OOIP$ can be calculated as a point value. But if the parameters are considered random variables with corresponding probability distribution functions describing them, a trial consists of randomly selecting one value for each of the input parameter and calculating an output. A simulation is a succession of thousands of repeated trials; the outputs are recorded and plotted on a histogram or cumulative distribution function. $P10$ is described as 10% probability of finding that particular output value, $P50$ is 50% probability and $P90$ is 90% probability that the output is going

to assume a certain value. These three parameters can be used to perform risk analysis by incorporation of NPV to the associated outcomes.

Monte Carlo simulations involve sampling based on probabilities to approximate the solution of a mathematical or physical problem in a statistical way. Pseudo wells were created by deGroot(1996) (De Groot and Bril, 1996)using this method. He demonstrated how these results can be driven to produce only plausible cases by having geologic constraints that enforce bounds on parametric values and steer the simulation to honor realistic scenarios. In this dissertation, MC simulations are used to establish OOIP values generated from synthetic logs. Further explanation is provided in Section 6.2. There are several reservoir characterization studies that had used seismic data, well log data through soft computing techniques and had proven to be robust in finding quick alternate solutions. Relevant case studies are presented in Section 2.1.4.

2.1.4 Case studies

Geostatistics is known to map spatial variations in estimating reservoir properties, but these models often suffer when the information available does not encompass a representative section of the reservoir. Reservoir characterization is often a challenging task during early stages of reservoir depletion owing to uncertainty associated with extrapolating the limited filed data to the entire field. One of the reasons large percentage of oil left in ground is due to macroscopic heterogeneities in the oil reservoirs. Oil wells tap into only a small fraction of reservoirs due to impermeable layers, which effectively act as a series of disconnected oil traps. Having closely spaced infill wells is not an economic decision due to the high cost associated

with drilling wells today. This calls for improved reservoir characterization techniques that can provide better reservoir definitions.

Hard computing protocols like reservoir simulation, geophysical modeling, and facies modeling are labor and time intensive. Several methods have been proposed in literature that includes stochastic methods, deterministic methods, and soft computing methods. Out of which soft-computing methods have tolerance for imprecision, uncertainty and are low cost, robust and efficient. Soft computing techniques are further explained in Section 2.2.

Bravo et al.(2014) (Bravo et al., 2014) presented a summary of the applications of artificial intelligence in exploration and production. Through their survey, it is evident that artificial neural network technology is gaining popularity in solving problems with data mining, pattern recognition, proxy models, and automated workflows.

Based on various case studies examined, it is known that simplified reservoir models built merely from production data, well interference and well log correlations may not capture the inherent heterogeneity and complex reservoir rock and fluid properties in an accurate way.

Field development studies conducted by Thararoop et al.(2008) (Thararoop et al., 2008) showed that production data, completion information, interference effects, and reservoir characteristics from seismic data can be mapped using artificial neural network. Spatial maps of gas production have revealed new sweet spots which otherwise could not be identified based on production data alone. The work however did not incorporate the information of well logs and had considered seismic data only at the completed zones. This study assumes that all the productive zones have been perforated which could not be completely accurate.

Rolon et al.(2009) (Rolon et al., 2009) used ANNs to generate synthetic well logs. They used a combination of wireline logs to predict the missing log using ANN and found it superior compared to multiple-regression. However their results did not include any information from seismic data. The regression values found were consistently under 0.9. This methodology involves obtaining few wireline logs prior to establishing the correlation to find the other missing logs. There was no way presented to predict the well logs at undrilled locations. Utilizing seismic data, if a correlation was built to estimate synthetic logs, it could potentially define the heterogeneities across the entire field.

Bansal et al.(2013) (Bansal et al., 2013) demonstrated a workflow employing artificial neural network for analyzing a tight gas reservoir in West Texas. Production surfaces were created based on an inter-assisting artificial expert system that comprised of a synthetic well log generation and production performance networks. They successfully mapped the complex relationships between seismic data, well log data, completion parameters, and production information for the case study considered. In this work, seismic attributes are considered based on horizons which included geologist's bias into interpretation of pay zones. To date, none of the earlier studies were able to correlate seismic data with horizontal well logs. Typically synthetic well logs are derived based on seismic inversion methods from P-wave or S-wave transformations, but no attempt to use the entire range of seismic attributes available to characterize the well log has been made so far. In this dissertation, a novel methodology capturing the attributes that correlate to directional well logs is created.

Several works in the past utilized neural networks to predict lithology, permeability, and fluid saturation from well logs and seismic data, as well as generation of synthetic well logs ((Hart et al., 2002), (Nikravesh and Aminzadeh, 2001), (Mohaghegh

et al., 2000)) or pseudo-wells (De Groot and Bril, 1996). A combination of seismic attributes is used to derive the reservoir properties using neural networks, by Aminzadeh et al.(2000) (Aminzadeh et al., 2000), and Taner(2001) (Taner et al., 2001). In the proposed methodology of this dissertation, a novel technique of utilizing seismic data is presented that has not been used before. Computation of seismic attributes between horizons tends to carry an interpretation bias from the geologists and geophysicists involved. Not enough work has been done in correlating seismic data either with directional well logs or production associated with them. Till date none of the studies have incorporated the schedule of production while correlating seismic data to production rates. In this dissertation, time dependence and interwell interference from nearby producers and injectors is accounted for. This work attempts to bridge the gaps found in correlating horizontal wells with seismic data. Further explanation is provided in Section 6.3

2.2 Soft computing techniques

Soft computing is the collection of techniques that are based on human cognitive processes. These methods are known for their ability to handle uncertainty and imprecision. The objective of the soft computing methods is to produce low cost, analytic and complete solutions for complex systems where traditional computational methods have not yielded satisfactory results. Soft computing techniques are comprised of fuzzy logic, neuro-computing, genetic algorithms, and probabilistic computing. Artificial neural networks are one of the main branches of soft computing that has been extensively used in numerous applications in signal processing, image processing, pattern recognition, etc.

2.2.1 Artificial neural networks

Artificial neural networks (ANN) were first introduced in late 1940's by McColloch and Pitts(1943) (McCulloch and Pitts, 1943) and later gained significance with invention of perceptrons by Rosenblatt(1958) (Rosenblatt, 1958). With the advances in computing power, Hopfield(1982) (Hopfield, 1982), Kohonen(1982) (Kohonen, 1982), and Hecht-Nielsen(1987) (Hecht-Nielsen, 1987) have reinvigorated the use of artificial neural networks.

ANN mimics the components of biological nervous system with an axon, soma and dendrite (Yegnanarayana, 2009). Each input is represented by a neuron, and then information is passed on through a series of transfer functions to the output neuron. There are hidden layers in between inputs and outputs and have a transfer function associated with them. Typical structure of an artificial neural network is indicated in the Figure 2.3

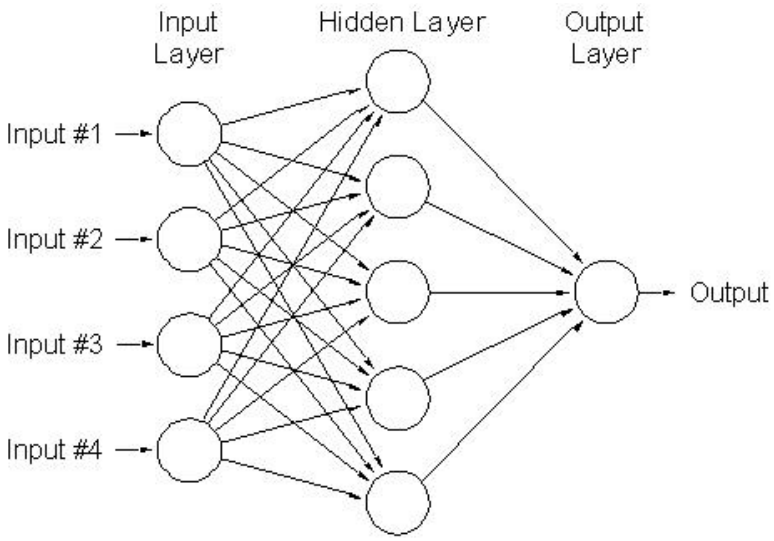

Figure 2.3. Sample artificial neural network

There is a library of transfer functions from where a user can pick based on the problem being studied. *Tansig* and *logsig* functions are widely used in generating synthetic well logs (Gharehlo, 2012).

Tansig function: This function is also known as bipolar sigmoid. In the function the net input is converted between -1 and 1 by the Equation 2.4,

$$f(x) = \frac{2}{1 - e^{-2x}} - 1 = \frac{e^{x} - e^{-x}}{e^{x} + e^{-x}} \tag{2.4}$$

Logsig function: This function is also known as bipolar sigmoid. In this function the net input is converted between 0 and 1 by the Equation 2.5

$$f(x) = \frac{1}{1 + e^{-x}} \tag{2.5}$$

Once input and a corresponding output are specified for a neural network, an error surface is composed based on the difference between the desired system response and real system output. This error information is propagated back to the system to make necessary adjustments to weights during the learning stage in a systematic fashion according to the learning algorithm specified. The process is repeated until the errors get reduced to a preset tolerance level. User needs to select the number of hidden layers and number of neurons in each layer along with the transfer functions associated with each layer.

Learning the complicated patterns and ability to successfully map the input data to output data highly depends on the type of learning algorithms employed. From literature, it is observed that error back propagation learning algorithm seems to suit best for the reservoir characterization problems (Bansal et al., 2013).

Feed-Forward back propagation network as indicated in Figure 2.4 takes the input in forward direction. As the computed error through network is propagated backward, weights and biases are adjusted. These kinds of networks are used to solve static problems; whereas cascade feed forward back propagation is used in time dependent problems. In predicting the flow rate or cumulative flow rates from wells, cascade feed forward back propagation networks serve as a better choice.

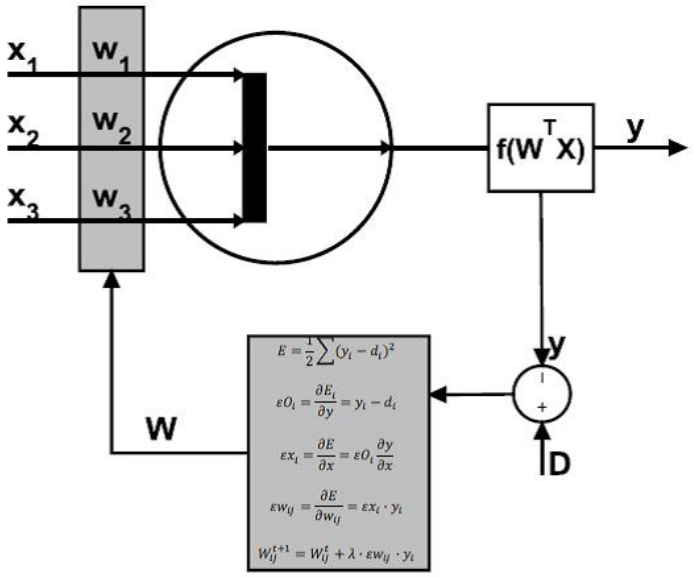

Figure 2.4. Artificial neural network training using backpropogation algorithm (Gharehlo, 2012)

A brief list of ANN applications in petroleum industry is listed in Table 2.1 (Shahkarami et al., 2014)

2.2.2 Fuzzy logic

Zadeh(1965) (Zadeh, 1965) first introduced fuzzy logic almost 50 years ago. Unlike Boolean logic, fuzzy logic allows the object to belong both true and false with different degrees of membership from zero to one. It has been designed to handle

Table 2.1. A brief list of applications of ANN in petroleum industry

Well Log interpretation	(Baldwin et al., 1989) (Lim et al., 2004) (Nikravesh et al., 1998a)
Well test data analysis	(Al-Kaabl et al., 1990) (Ershaghi et al., 1993) (Athichanagorn et al., 1995) (Sultan et al., 2002)
Reservoir characterization	(Mohaghegh et al., 1995) (Ouenes et al., 1997) (Singh et al., 2008) (Bansal et al., 2013) (Thararoop et al., 2008)
Seismic attributes calibration, Seismic pattern recognition , Inversion of seismic waveforms	(McCormack et al., 1993) (Yang et al., 1991) (Roth and Tarantoia, 1992)
Prediction of PVT data	(Gharbi et al., 1997) (Osman et al., 2001) (Oloso et al., 2009)
Identifying fractures and faults	(Sadiq et al., 2000) (Aminzadeh et al., 2005)
Detecting hydrocarbons and forecast formation damage	(Zhou et al., 1994) (Aminzadeh et al., 2005) (Nikravesh et al., 1998b) (Kalam et al., 1996)

concept of partial truth. This logic mimics the human mind to effectively employ the modes of reasoning that is approximate rather than exact. The imprecise nature of geophysical and geological information makes fuzzy set theory an appropriate tool to utilize in reservoir characterization studies. Given the set of input-output patterns, many fuzzy rules can be developed to cover the entire functional space. The major applications of fuzzy logic include seismic interpretation, stratigraphic modeling and well logging (Bois,1984 (Bois, 1984); Nordlund,1996 (Nordlund, 1996);Cuddy,2000 (Cuddy et al., 2000)). In this current work, fuzzy logic is used to determine the lithology based on well logs and also used to identify the net pay zones.

Chapter 3

Statement of the Problem and Objectives

The increasing costs of drilling exploratory wells, and obtaining field-wide data in offshore fields have prompted reservoir engineers to look for more robust ways to estimate properties at unexplored locations. As a reservoir engineer, one needs to find ways to gain insight into issues of uncertainty in reservoir simulations, and try to eliminate them based on models from available information. So to characterize heterogeneous formations, a system needs to be developed to provide a comprehensive reservoir analysis tool that could analyze Chevron's Tombua Landana asset. The challenge lies in integrating different sources and scales of data to help build a model with accurate predictive capability in identifying reservoir properties. The first aspect is to predict reservoir properties away from wellbores and identify net pay along with uncertainty bounds. The second aspect of characterization is to be able to predict the production performance of a chosen location that in turn could be used to propose the infill wells.

The envisioned artificial intelligence tools will operate on the basis of learning obtained from the training data sets (seismic data, well logs, production data, and completion data).Therefore, the objectives of the current study can be summarized as:

- To develop synthetic well log generation network that captures the relation between seismic data and log values,
- To develop a production performance network that captures the relation between production data, seismic data and well logs,
- Perform Monte Carlo simulation to capture uncertainties in prediction of porosity, net pay and other relevant parameters using P10/P50/P90 forecasts,
- Generation of net pay surfaces, gas/oil/water in place maps, ultimate recovery estimations and infill drilling opportunities,
- Optimal drainage pattern for field development to maximize the production from infill drilling.

Chapter 4

Proposed Methodology

As described earlier, this research aims to structure an integrative approach to characterize a reservoir using the available data and predict reservoir properties away from wellbores, and also identify production potential which together aid in field development planning. This process entails three steps namely data preparation, neural network training and prediction.

In data preparation, anomalies are identified and a consistent data set is assembled that forms a part of the input. This involves screening of well logs for consistency, availability, and quality. Seismic data and velocity model are checked with respect to seismic well ties available through checkshot data. Seismic attributes computed, are plotted to identify anomalous trends. These attribute trends are investigated to check if they add any additional information. In this process, seismic attributes providing null values are discarded. A detailed procedure of calculating seismic attributes and the resolutions is further explained in Chapter 5. Well logs provide information at a high resolution of 0.5 ft, they need to be converted to a resolution comparable to seismic data while correlating them.

Neural network training is performed using MATLAB[1] by generating several architectures, and establishing an optimum architecture that performs well consistently across a variety of data sets. Mean square error performance is used as a criterion to stop the training process. Several training algorithms are tested for optimal performance.

Synthetic well logs are created at all the locations where seismic data is available using the synthetic well log network. Oil, water and gas production performance networks enable the generation of production surface maps and help in forecasting production in future. Monte Carlo simulations coupled with production performance networks will help in identifying the infill well locations.

4.1 Well logs

Well logs are detailed petrophysical observations around well bore that inform reservoir engineers of the subsurface properties. To integrate the well log data into the static model or full field reservoir model, there are several ways. The challenge however lies in prediction of properties at interwell locations, where often interpolation is used to estimate the properties. The following are the types of well logs studied in this work:

- *GR (Gamma ray)*: measures the naturally occurring gamma radiation that helps in characterizing the rock type in the borehole. It is not a function of grain size or carbonate content, only the proportion of radioactive elements, which may be related to the proportion of shale content. It is used to interpret the depositional environment.

[1]MATLAB (matrix laboratory) is a multi-paradigm numerical computing environment and fourth-generation programming language developed by Mathworks.

- *NPHI (Neutron Porosity)*: measure the hydrogen content in a formation. Provides us with useful information on fluid filled porosity values. In shale-free, water-bearing formations, the hydrogen concentration reflects the porosity and lithology.

- *PHIT (Total Porosity)*: measures the porosity of clean sand

- *RHOB (Bulk Density)* : measures bulk density, which can estimate the porosity of the formation through the wellbore. These logs along with sonic logs are used in calculating impedance that is used in seismic well tie process. This can help identify evaporite minerals, detect gas-bearing zones and determine hydrocarbon density.

- *RESD (Deep Resistivity)*: measures the electrical resistivity of the formation. High resistivity indicates presence of hydrocarbon bearing formation. It is also useful in picking tops and bottoms of formations and correlating between wells.

4.2 Seismic data

Seismic attributes are computed at the chosen stratal slices as described in section 5.2.1. All the available attributes from Petrel[2] are considered in this study to maximize the available seismic information. The chosen amplitude based attributes describe heterogeneity, stratigraphic sequence, map direct hydrocarbon indicators, isolated geologic features, formation thickness, and porosity/fluid changes. All the available attributes are extracted through the surface attribute model and then

[2]Petrel is a Schlumberger owned Windows PC software application intended to aggregate oil reservoir data from multiple sources

analyzed individually to identify the uniqueness of attribute computations at the well locations. Attributes that resulted in zero values at all the well locations are identified as redundant and hence removed from the input data. Appendix A provides the list of seismic surface attributes used in this study. The descriptions of the seismic attributes used in the study is provided in Section 5.2.1.

Amplitudes from seismic traces are directly correlated to acoustic impedance, which in turn used bulk density log values. Hence it is expected to have a direct correlation with bulk density log. In selecting the methodology to map the reservoir, it is critical that the chosen input parameters will effectively represent the important variables that capture the heterogeneity of the system under consideration. It is known that production rate at a well location is related to a combination of well logs and seismic attributes from literature. In this work, an attempt will be made to recognize the pattern that exists between seismic data and well logs via synthetic well log generation networks. Once synthetic well logs are populated over the entire seismic coverage, logs in conjunction with seismic data will then be mapped to production data using a production performance network. The production network is expected to capture the interference effects of nearby producers and injectors in oil, gas and water predictions. Using Monte-Carlo simulations, P10/P50/P90 surfaces of reservoir properties will be generated from the synthetic well logs. This comprehensive reservoir tool will then enable generation of log surfaces; net pay maps indicating sweet spots, spatial oil, gas, water maps, and assists in optimizing the field development plan.

An inter-assisting group of artificial neural networks as indicated in Figures 4.1 and 4.2 will be developed consisting of the following networks

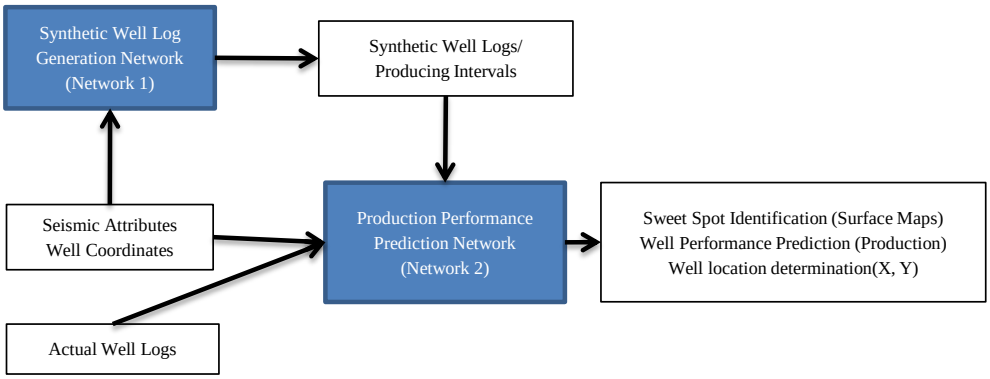

Figure 4.1. Proposed methodology overview

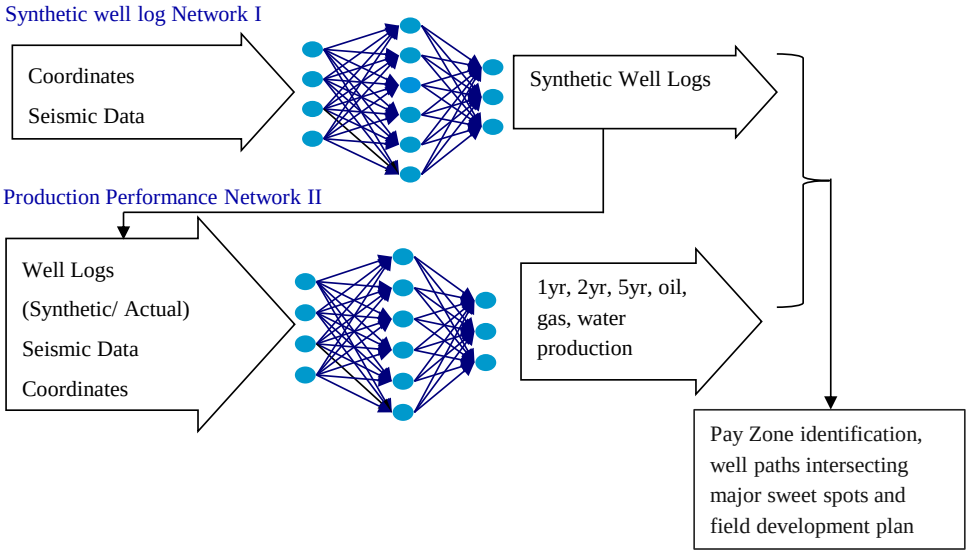

Figure 4.2. Proposed methodology detailed - module wise

In addition to the input and output parameters indicated in the proposed methodology, functional links based on the physical relationships that exist between input and output parameters will be employed wherever necessary.

Chapter 5

Case Study - Tombua Landana Asset

5.1 Location

In 2015, Angola's oil production has surged owing to a variety of wide-ranging, high potential plays (Koning, 2014). Production of 2.0 million bopd has been achieved starting from 750,000 bopd a decade ago. Even though first drilling for oil happened in 1915, it's not until 1956 the Benfica oil field, near Luanda marked the significant oil production in Angola. Since 1996, several deep water to ultra-deep-water blocks have been identified and put to production.As indicated in Figure 5.1, deep water assets have been contributing to more than 80% of the oil production in Angola in the recent past.

Tombua Landana is located in Block 14 approximately 100 km offshore from Cabinda in Angola with a water depth ranging from 200m to 1500m. Chevron is the majority stakeholder (31%) along with Agip Angola (20%), Sonangol (20%), Total Angola (20%), and Petrogal (9%). The area of the current study is 56km×55km. The block lies in the lower Congo basin and produces medium light crude oil. The first exploration well was drilled in 1999 and is currently undergoing

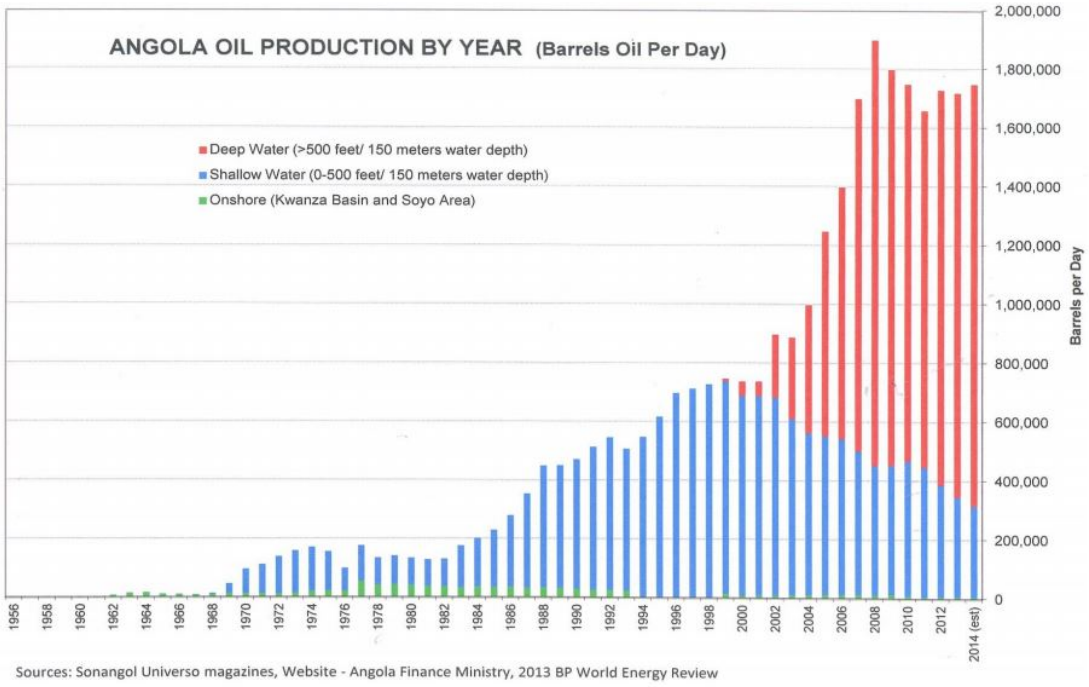

Figure 5.1. Angola's oil production 1956-2014(Koning, 2014)

secondary recovery through water injection. Additional production and injection well opportunities are pursued to improve the recovery factor. This asset is believed to have 350 million barrels of oil in place and 60 million barrels has been produced out of 20 wells as of October 2012.

5.1.1 Geologic setting of Angola

High quality turbidite sands deposited in a middle bathyal slope valley/incised canyon environment make up the reservoirs(Higgs et al., 2005). Reservoir sands are believed to form vertically stacked and nested channel complexes that both erode and aggrade preexisting sediments . The turbidite complexes are known to be 500-2,000m wide, 10-60m thick, composed on intercutting sand-rich turbidite channels, shale-rich mudflows, debris flows and slumps.

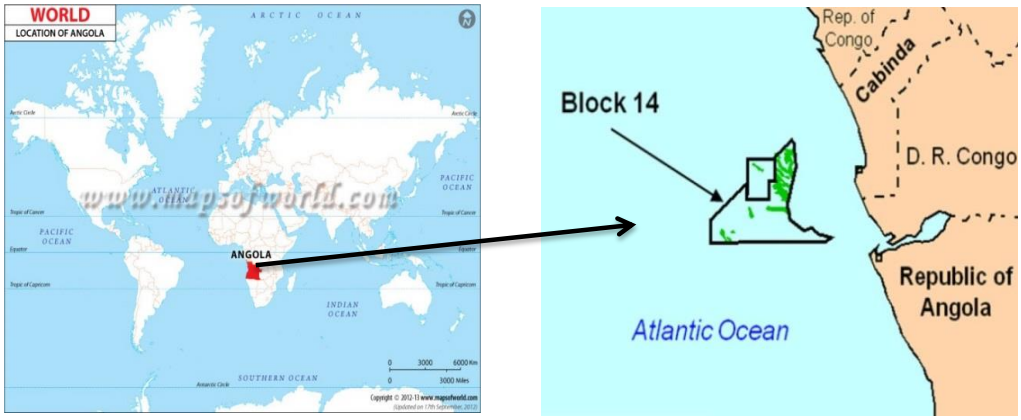

Figure 5.2. Location of Block 14 Angola offshore(Mapsofworld, 2014)

Traps comprise of channels draped over four-way structural highs or in normal fault trap geometries and are likely controlled by Aptian salt movement and subsequent late stage extensional faulting (Figure 5.3).

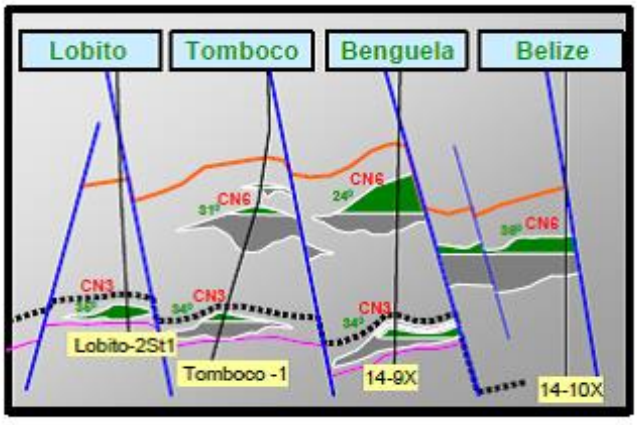

Figure 5.3. Schematic cross section through BBLT discovery wells showing stacked channel traps which are influenced by later extensional faulting (Higgs et al., 2005)

Combination of Labe and Lower Malembo serve as source rocks with the onset of peak oil generation at 13 Ma and 5 Ma. Migration pathways into the Miocene channels are provided by deep penetration normal faults. Typically, all Miocene

sands in trap position have encountered hydrocarbons of various quality and quantity (Higgs et al., 2005).

5.2 Data availability/Inputs

All the available data is summarized in Figure 5.4. Seismic data is the geophysical information that yields seismic attributes at each of the inline and crossline locations. Directional surveys in combination with check shot data is used to verify the time slice intersections of wells and their corresponding depths. Production rates are used in building the production performance networks. Perforation information is used as a functional link to inputs. Results are discussed in Chapter 6.

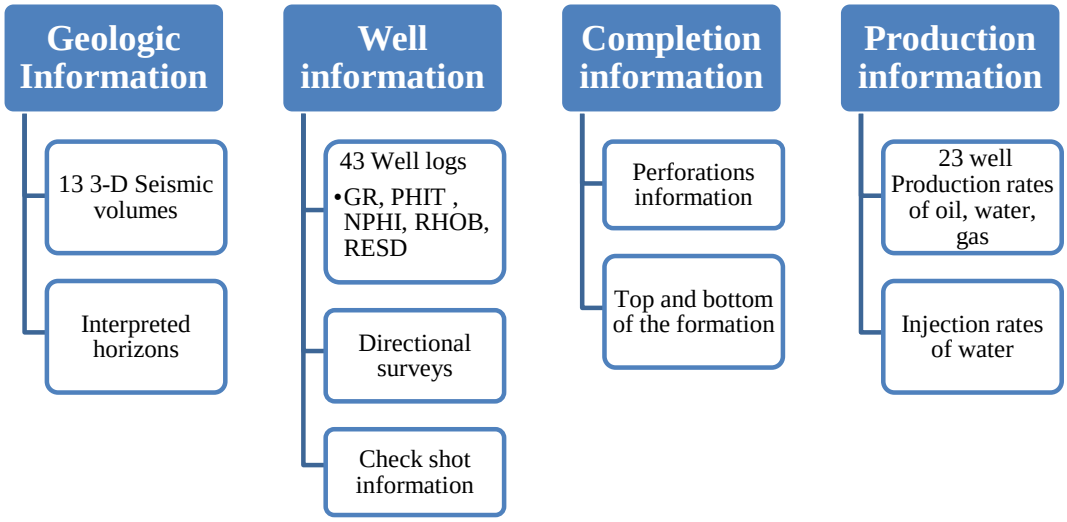

Figure 5.4. Available data from Tombua Landana

5.2.1 Seismic data input

Seismic data in the form of attributes at a given X, Y location (corresponding to a well point) is computed by inverse square interpolation method from four nearest

neighboring seismic data points as indicated in Figure 5.5. Hence, the training data input is a matrix with 42 surface attribute values as rows at each X, Y, with 38 columns corresponding to the well locations for a given surface. 39 attribute values are calculated from seismic data and X, Y, Z coordinates constitute the remaining three attributes.

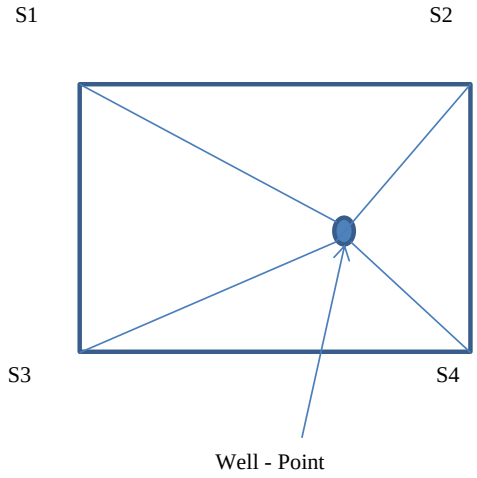

Figure 5.5. Inverse square interpolation

The following is a description of the available surface attributes in Petrel[2]. The Table 5.1 outlines the list of the seismic attributes used in this study.

Arc length: Arc length measures reflection heterogeneity, and can be used to quantify lateral changes in reflection patterns. It is calculated using the following formula:

$$Arc\ Length = \frac{\sum_{j=1}^{n-1} \sqrt{amp(j) - amp(j+1)^2 + Z^2}}{(n-i) \times sample - rate} \tag{5.1}$$

where, Z is in milliseconds in time domain, or in feet or meters in depth domain. Arc length is a stratigraphic sequence indicator.

Average duration of negative loops: Gives the average duration of all negative loops in a given interval. It is undefined if there is no loop (a loop requires two

Table 5.1. Surface attributes considered in this study

S.no	Attribute Name	S.no	Attribute Name
1	Arc Length	21	Threshold >0
2	Average Energy	22	Time at Max Amplitude
3	Average Magnitude	23	Time at Min Amplitude
4	Average Peak	24	Average duration of negative loops
5	Average Trough	25	Average duration of positive loops
6	Interval Average-Arithmetic	26	Average loop duration
7	Maximum Amplitude	27	Average negative amplitude
8	Maximum Magnitude	28	Average negative trough value
9	Mean Amplitude	29	Average peak value between zero crossings
10	Median	30	Average positive amplitude
11	Minimum Amplitude	31	Average positive peak value
12	Most of	32	Average trough value between zero crossings
13	Number of negative crossings	33	Half energy
14	Number of positive crossings	34	Maximum loop duration
15	Number of Zero crossings	35	Minimum loop duration
16	RMS Amplitude	36	Positive to negative ratio
17	Standard deviation of amplitude	37	Standard deviation of loop duration
18	Sum of Amplitudes	38	Sum of negative amplitudes
19	Sum of Magnitudes	39	Sum of positive amplitudes
20	Extract value		

zero crossings)

$$D_{an} = \frac{\sum_{i=I,k} di}{K} \tag{5.2}$$

where, di represents loops with negative amplitude and K is the number of negative loops.

Average duration of positive loops: Gives the average duration of positive loops in a given interval. It is undefined if there is no loop with two zero crossings

with positive amplitudes.

$$D_{ap} = \frac{\sum_{i=I,k} di}{K} \tag{5.3}$$

where, di represents loops with negative amplitude and K is the number of positive loops.

Average energy:This is the squared RMS amplitude. This attribute is a measure of reflectivity within a time or depth window and can be used to map direct hydrocarbon indicators in a zone. Average energy is computed using the following formula:

$$Average\ Energy = \frac{\sum_{i}^{n} amp^2}{k} \tag{5.4}$$

where, k is the number of live samples.

Average loop duration: Average loop duration is defined as the average duration of all loops. It is undefined if there is no loop (requires two zero crossings). Its reciprocal (e.g. $500/D_{av}$ if the sample rate is 4 ms), gives an approximate average frequency of the seismic data within the extraction window.

$$D_{av} = \frac{\sum_{i=l,m} di}{m} \tag{5.5}$$

where, di represents loops with positive and negative amplitude and m is the number of loops.

Average magnitude: This operation measures the reflectivity within a time or depth window, but is less sensitive to large numbers than RMS amplitude. Average magnitude is computed using the following formula:

$$M_{avg} = \frac{\sum_{i=i}^{n} |amp|}{k} \tag{5.6}$$

where, k is the number of live samples. This attribute can be used as a hydrocarbon indicator as well as isolated geologic features which express themselves as anomalous amplitudes relative to background values.

Average negative amplitude: Gives the average of all negative amplitudes values within the analysis window. The amplitude range to be included in the calculation can be controlled with the parameter selector. The data range to be included can be within the defined interval or outside the defined interval. By default, all data values will be used.

Average negative trough value: Measures the negative reflectivity within a time or depth window. Only trough values which are negative are included in the average. This allows discrimination of local minima in the positive lobes of the seismic waveform.

Average peak value: This is the average of all peak values in a window. These peak values can be local maximums, in which case negative peaks are also averaged in. This attribute can be a measure of the positive reflectivity within a time/depth window. Large or small values can be used as a direct hydrocarbon indicator.

Average peak value between zero crossings: This operation is similar to the average peak value, but instead of taking all peak values, only the largest peak between each pair of zero crossings is taken.The output can provide a better measure of reflectivity when tracking a single event.

Average positive amplitude: Gives the average of all positive amplitudes values within the analysis window. The amplitude range to be included in the calculation can be controlled with the parameter selector. The data range to be included can be within the defined interval or outside the defined interval. By default, all data values will be used.

Average positive peak value: This operation is similar to average peak value,

but instead of taking all peak values, only the peaks in the positive lobe of the seismic waveform are taken.

Average trough value: This operation measures the average of negative reflectivity within a time or depth window. Its uses are similar to those of average peak value.

Average trough value between zero crossings: This operation is similar to average peak value, but instead of taking all peak values, only the largest negative peak between each pair of zero crossings is taken. This attribute can give a better measure of reflectivity when tracking a single event.

Extract value: Extract value is the utility to extract the input seismic value relative to a single horizon or an existing interpretation. This utility allows one to produce surface attribute maps from seismic volumes created as volume attributes with methods not available directly as surface attributes or from volumes created with seismic calculator options.

Interval average: Calculates the average over an interval based on one of the following methods; arithmetic, harmonic, geometric, RMS, summation, minimum, maximum, most of or median. Provides one with the same interval averaging options that were available in pre-Petrel 2007.1

Maximum amplitude: Measures reflectivity within a time or depth window. Returns the maximum positive number in the defined window. It is used to detect positive direct hydrocarbon indicators such as bright spots.

Maximum loop duration: Defined as the maximum duration (longest half-cycle) of all loops, both positive and negative in the extraction window. It is undefined if there is no loop (requires two zero crossings).

$$D_{mx} = max_{i=l,k}(d_i) \tag{5.7}$$

Maximum magnitude: Measures reflectivity within a time or depth window. Returns the maximum positive number in the defined window. It is used to detect positive direct hydrocarbon indicators such as bright spots.

Mean amplitude: This is the arithmetic mean of the amplitude and is a measure of trace bias. If the seismic trace has general bias, perhaps from the data processing, this can be removed from the seismic volume using the graphic equalizer attribute and removing the zero hertz component. Mean amplitude is computed using the following formula:

$$Amp_{mean} = \frac{(\sum_i^n amp)}{k} \tag{5.8}$$

where, k is the number of live samples. Positive or negative bias may indicate the presence of bright spots.

Median: The median of the analysis window can be found by arranging all the values from lowest to highest value and picking the middle one (i.e. 50% of the values in the window are below the median value). The median is less sensitive to extreme values (outliers) than the computation of the mean.

Minimum amplitude: This operation measures the reflectivity within a time or depth window. This is the maximum negative number in the defined window. It is used to detect negative direct hydrocarbon indicators such as bright spots.

Minimum loop duration: It is defined as the minimum duration (shortest half-cycle) of all loops, both positive and negative in the extraction window. It is undefined if there is no loop (requires two zero crossings).

$$D_{mn} = max_{i=l,k}(d_i) \tag{5.9}$$

Most of: The most of attribute captures the most commonly occurring data value within the analysis window. A histogram is computed from the input window and the value from the bin with the highest count is output for each trace location.

Number of negative zero crossings: This operation results in a value representing a counter for the number of zero crossings encountered within the analysis window that match the criteria of the sample values going from negative values to positive. Changes in the number of zero crossings can be related to the complexity of the stratigraphy. A high number of zero crossings generally indicates a greater degree of vertical lithologic complexity.

Number of positive zero crossings: This operation results in a value representing a counter for the number of zero crossings encountered within the analysis window that match the criteria of the sample values going from positive values to negative. Changes in the number of zero crossings can be related to the complexity of the stratigraphy. A high number of zero crossings generally indicates a greater degree of vertical lithologic complexity.

Number of zero crossings: This operation results in a value representing a counter for the number of zero crossings encountered within the analysis window that match the criteria of the sample values going both from positive values to negative ranges and from negative to positive ranges. See also number of negative zero crossings.

Positive to negative ratio: Ratio of positive to negative is the number of positive values in an interval, divided by the number of negative values in the interval. If there are no negative values found in the interval to be used as a divisor, the application returns a value of zero. This operation can be used to look for lateral changes in thickness and also lithology, such as a pinchout or a sand that is thickening within a shale sequence.

RMS Amplitude: RMS amplitude is the square root of the sum of the squared amplitudes, divided by the number of live samples as shown in the following formula:

$$RMS_{amp} = \sqrt{\frac{(\sum_i^n amp^2)}{k}} \tag{5.10}$$

where, k is the number of live samples. RMS amplitude can map directly to hydrocarbon indications in the data and other geologic features which are isolated from background features by amplitude response.

Standard deviation of amplitude: Standard deviation of amplitude measures the variability of the seismic amplitude values within the extraction window. It is undefined if n is less than 2.

$$D_s = \left\{ \frac{\sum_{i=l,n} (d_i - D_{av})^2}{(n-1)} \right\}^{0.5} \tag{5.11}$$

where, D_{av} is the average duration and n is the number of loops.

Sum of amplitudes: This is arithmetic mean of the amplitude, multiplied by number of samples in the window. This operation provides a measure of brightness multiplied by the formation thickness (time or depth) and may be regarded as a measure of brightness volume. The sum of amplitudes over the given window is calculated as follows:

$$Amp_{sum} = \sum_i^n amp \tag{5.12}$$

A large value may indicate a high net sand ratio

Sum of magnitudes: This operation measures the reflectivity within a time or depth window, but multiplied by the number of samples in the window. The operation can be used in a similar way to sum of amplitudes but is independent of amplitude sign. The sum of magnitudes over a given window is calculated as

follows:

$$M_{sum} = \sum_{i}^{n} |amp| \tag{5.13}$$

Sum of negative amplitudes: This is the arithmetic mean of the negative amplitudes, multiplied by the number of samples in the window. This operation provides a measure of brightness multiplied by the formation thickness (time or depth) and can be regarded as a measure of brightness volume. A large value may indicate a high net sand ratio.

Sum of positive amplitudes: This is the arithmetic mean of the positive amplitudes, multiplied by the number of samples in the window. This operation provides a measure of brightness multiplied by the formation thickness (time or depth) and may be regarded as a measure of brightness volume. A large value may indicate a high net sand ratio.

Threshold value: The threshold value attribute computes the percentage of samples that satisfy the threshold value parameter. The threshold value is controlled by the data range selected with the value parameter. One can select the threshold as greater than, less than, or equal to the defined data range value. Amplitudes in the seismic data can be analyzed using the user-defined threshold values that may infer porosity or fluid changes, when amplitude driven.

Time at maximum amplitude: This operation results in a z-value (time or depth) as the output attribute, where the z-value corresponds to the vertical position of the maximum amplitude within the analysis window.

Time at minimum amplitude: This operation results in a z-value (time or depth) as the output attribute, where the z-value corresponds to the vertical position of the minimum amplitude within the analysis window.

In the surface attribute extraction workflow, stratal slice of constant two-way travel time (TWTT) are used to compute the seismic attributes. Unlike earlier studies (Bansal et al., 2013) and (Thararoop et al., 2008), the current work does not consider any mapped horizons to prevent interpretation bias. Further explanation on extraction of seismic attributes in provided in Section 5.3. Impedance contrast attributes are computed, but did not help in improving the correlations with well log data. Hence, attributes based on amplitude alone are used in this study.

5.2.2 Well log data input

The well logs are relatively high resolution data compared to the seismic data. Well logs in LAS files along with their directional surveys are provided by Chevron Corporation. The entire length of the well log is divided into three zones for improved characterization. The resolutions used in this study have been obtained after several iterations of data extraction and correlation processes as outlined in Section 6.1. The synthetic log network is developed to predict 150 average well log values in a given zone. Zone-1, top surface corresponds to TWTT=1800ms and bottom surface corresponds to TWTT=2200ms. Zone-2 extends from 2200 ms to 2600 ms and Zone-3 from 2600 ms to 3000 ms. Figure 5.6 displays a sample interval averaged gamma ray log for Zone-1. These values are computed along the trajectory of the well bore following equally spaced points in measured depth (For e.g. Zone-1: Top surface corresponds to TWTT=1800ms and bottom surface corresponds to TWTT=2200ms). Data preparation detailing zonal information is outlined in section 5.3.

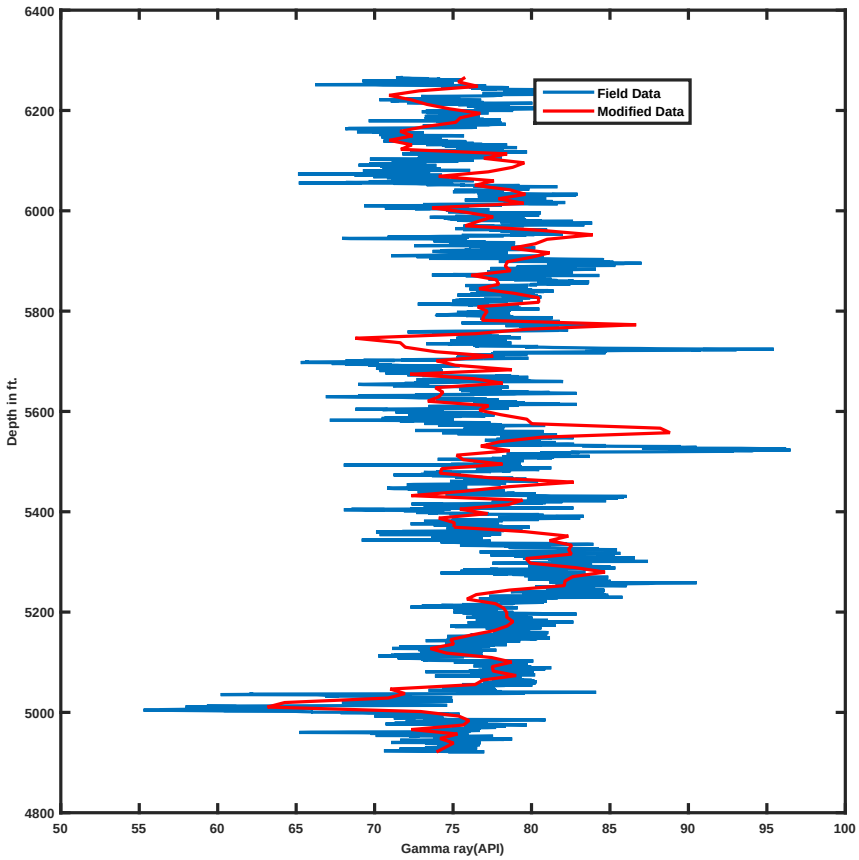

Figure 5.6. Comparison of field observed data with modified data

To maintain the consistency of the data for training purposes, 38 out of 43 wells are used to train the ANN model for GR prediction of zones one, two and three. The target data set is 150 $\times$ 38 (150 $-$ rows correspond to the number of interval averaged gamma ray values, and 38 columns correspond to the number of wells used for developing the model). Figure 5.6 indicates the actual gamma ray and interval averaged value of the gamma ray vs. depth

The top and bottom corresponding to a time surface are calculated through interpolating checkshot data. If the depth of the well is found shallower than the given the time surface, bottom depth is set at the bottom of the wellbore. Various

resolutions of the well logs are tested and it was found that dividing the well log into 150 values between each zone resulted in highest correlation coefficients.

High resolution well logs are developed in this module. 150 log values in each seismic zone (400 ms) for the wells (two expert systems to predict five types of well logs)

- GR/NPHI/PHIT Network (three networks one for each zone)
- RESD/RHOB Network (three networks one for each zone)

Gamma ray, neutron porosity log, total porosity log with first network and deep resistivity and bulk density, with second network each predicting 150 interval averaged log values at equally spaced values of measured depth in a zone/well.

5.2.3 Production data

Cumulative oil, water and gas produced based on the observed data is represented in the following surface maps. As of September 2012, 58 MMSTB of oil has been produced from this field. The field was put on to production in 2006 and continues to produce with ongoing water injection that supports the reservoir pressure. Figure 5.7 indicates the surface map of the cumulative oil produced from TOMBUA LANDANA field. Yellow color indicates high values of cumulative oil close to 11 MMSTB. The northern region has one of the most prolific wells in the field.

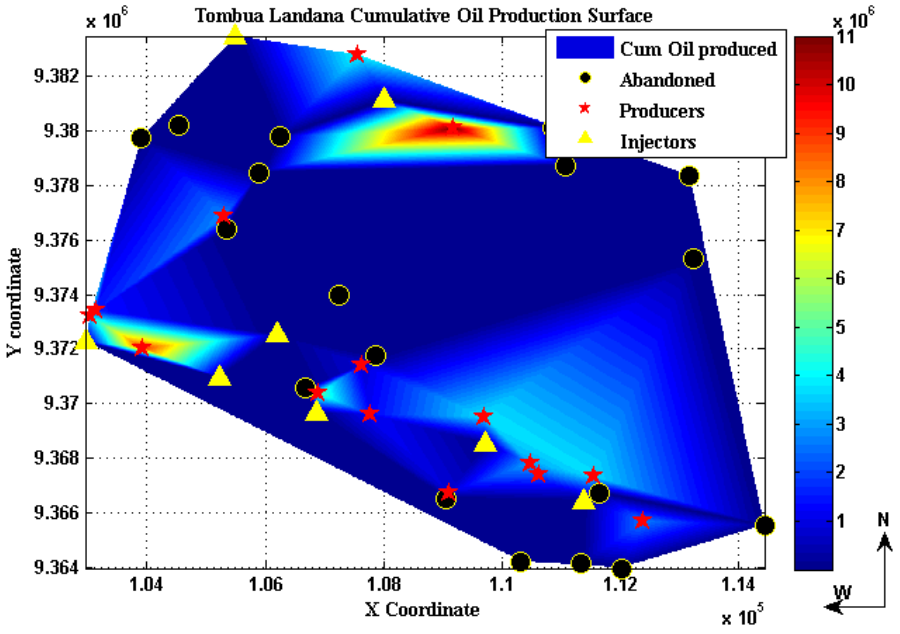

Figure 5.7. Cumulative oil production in STB observed until September 2012

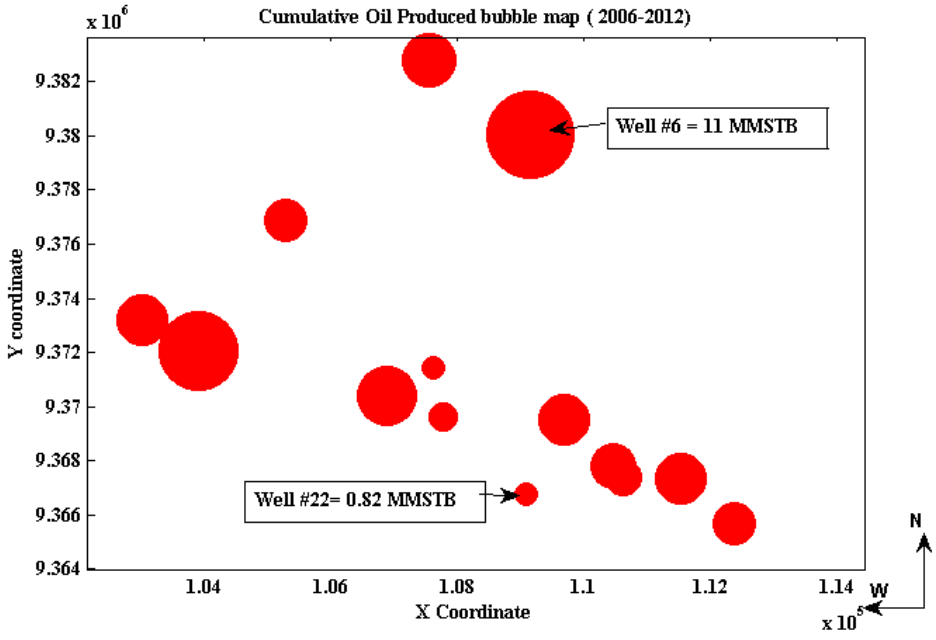

Figure 5.8. Cumulative oil production bubble map observed until September 2012

The earliest well, Well #6 in the Landana region (Northern region) as shown in Figure 5.8 has produced 11 million barrels until September 2012, and is still on production. Well #22 is the well with least cumulative oil produced of 0.82 million barrels and is located on the southern fringe of the considered area.

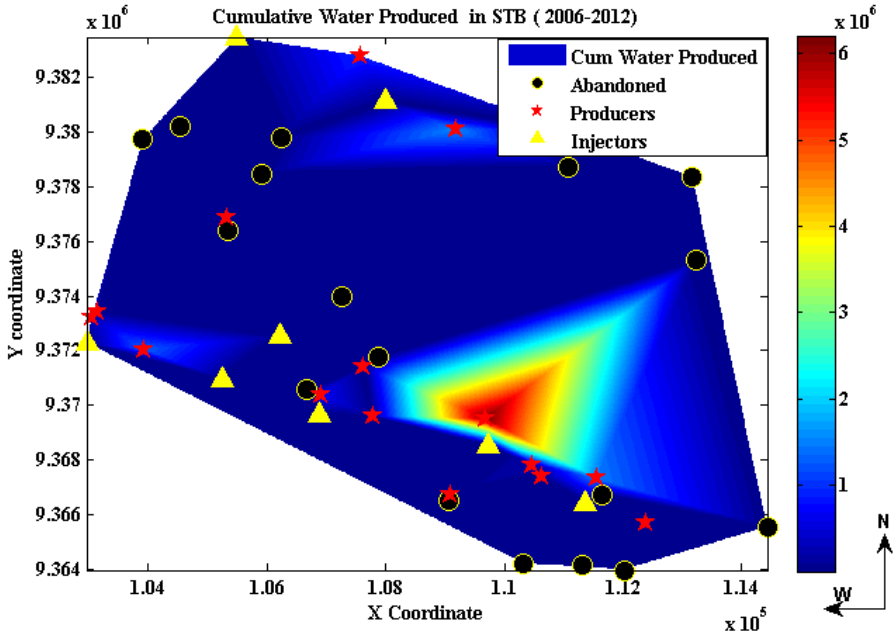

Figure 5.9. Cumulative water production in STB observed until September 2012

The bright red spot in Figure 5.9 indicates the well with highest water production. There are two injectors operating nearby, which could have been probable cause for the high water production observed at this location. Figure 5.10 showcases the cumulative gas produced from until September 2012.

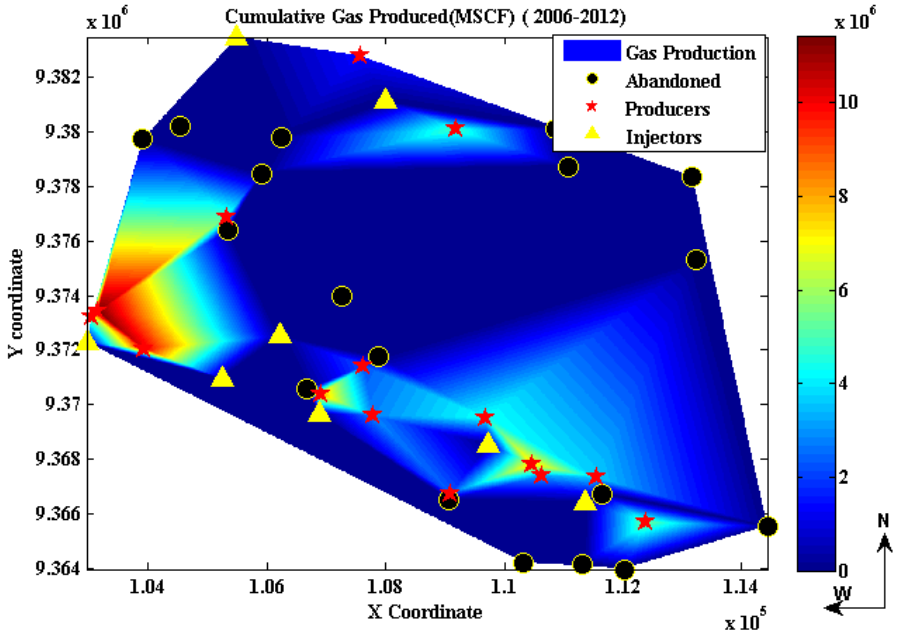

Figure 5.10. Cumulative gas production in MSCF observed until September 2012

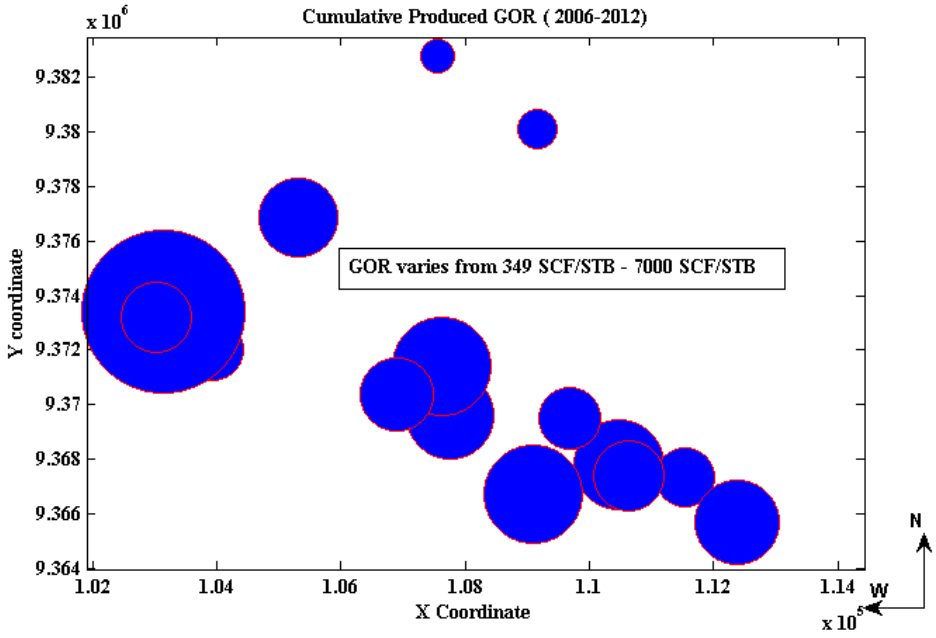

Figure 5.11. Cumulative produced GOR (SCF/STB) bubble map

Gas oil ratio (GOR) variation is highlighted in Figure 5.11. Gas oil ratios vary widely in this region ranging from 350 *SCF/STB* to 7000 *SCF/STB*. Based on the well operating conditions and the bottomhole pressure, gas oil ratio fluctuates throughout the life of the well. Ideally, if the reservoir is being produced above bubble point pressure, GOR remains constant. In this case, the pressure is sometimes lower than the bubble point pressure and ongoing injection does seem to have an effect on the producing GOR. Figure 5.11 shows that the western region of the reservoir under consideration generally has higher GOR values. Highest GOR value is from a well that has less than 1 year of production history. Average GOR value observed in this region is 2000 *SCF/STB*.

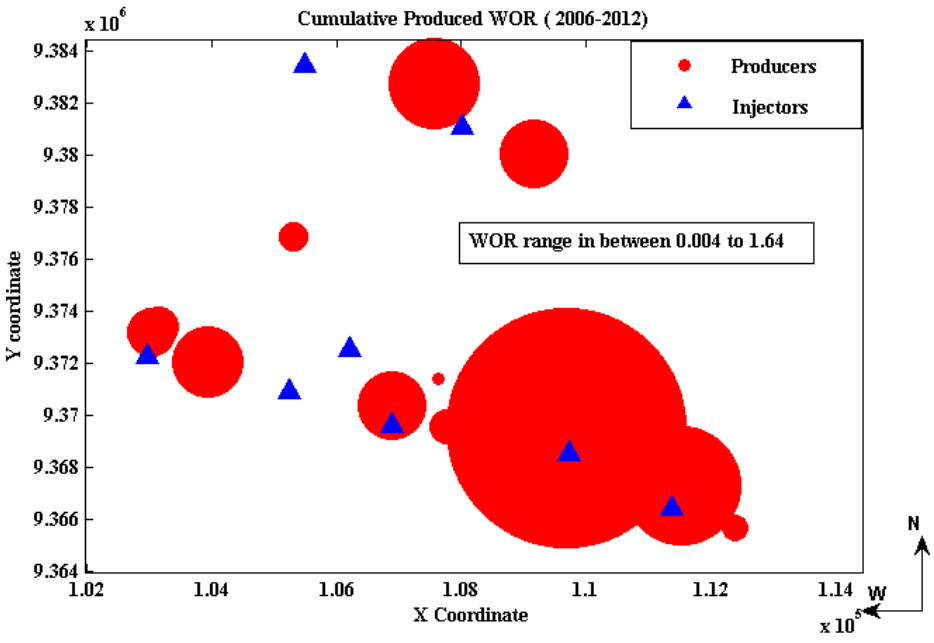

Figure 5.12. Cumulative produced WOR bubble map

Water oil ratio (WOR) is defined as number of barrels of water produced for every barrel of oil produced. This ratio qualitatively indicates the water cut evolution (see Figure 5.12) that is evident in the field. It is interesting to note

that wells in the southern part of the reservoir tend to produce more water than northern parts. The injector wells do influence the water cut observed in the nearby producers. In the current work, the influence of the injectors on the producing WOR is captured in water production network.

The histogram of all the production wells with their production times is presented in Figure 5.13. Wells with less than one year history are not used in the current study. Some of the wells encountered very low amounts of oil, so they were either recompleted to a different zone or production rates declined quickly reaching abandonment conditions. One of the production wells with less than two years history is converted to an injection well.

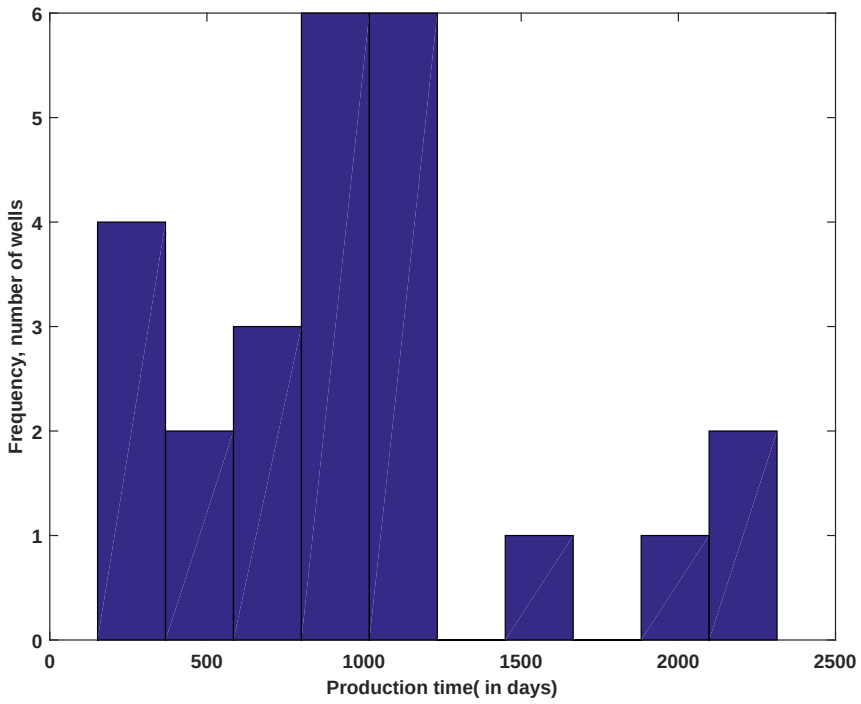

Figure 5.13. Histogram of wells with their production times

5.3 Data Preparation

In order to capture the information obtained through 3-D seismic surveys, a 'surface attribute' based approach is used to extract seismic data at the top of the chosen surfaces. For converting the seismic volumes from SGY files to multihorizon surface attributes, a project is created in Petrel.

To exclude geophysical interpretation bias, the seismic information is considered in its raw format without the horizons provided in the data. In the current work, the full angle stack file is cropped in between two way travel times 1800-3000ms. The chosen seismic volume has over nine million traces with spacing of 12.5 meters between each of the inlines/crosslines representing an area of $56km \times 55km$ of Block 14, Angola. Computational efficiency has driven creation of low resolution surfaces. Time slices/surfaces are created at every 40 ms starting from 1800ms to 3000ms by skipping 5 inlines and 5 crosslines. The resulting surfaces have a resolution of 75 meters (resolution reduced from 3007×3351 to 750×835 as indicated in Figure 5.14). Surface attributes at top of each of these time surfaces are extracted and converted to interpretation as illustrated in Figure 5.15. Appendix A lists the surface attributes currently considered as the seismic input data set.

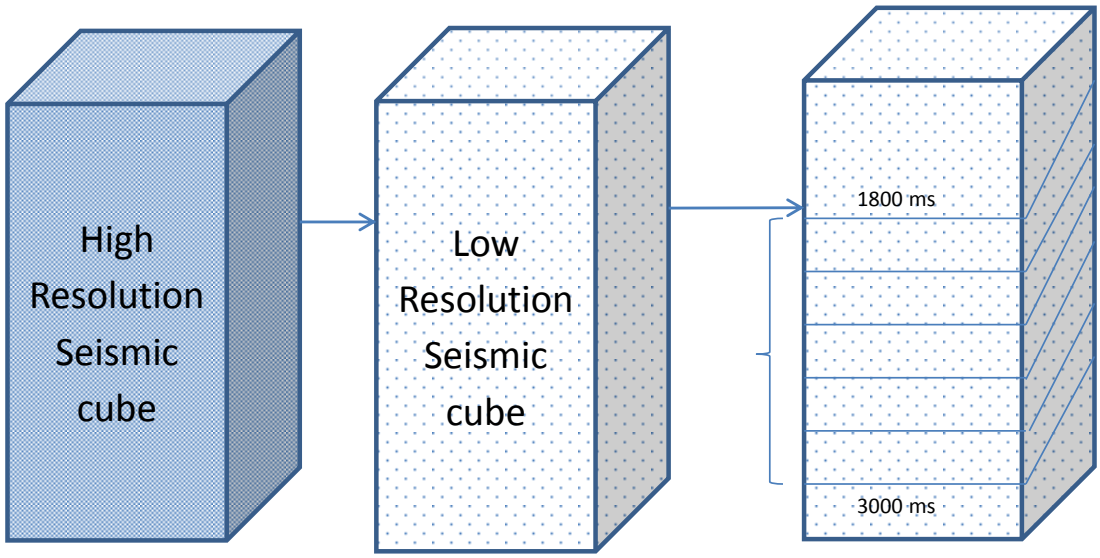

Figure 5.14. Seismic data preparation - time based stratal slices considered

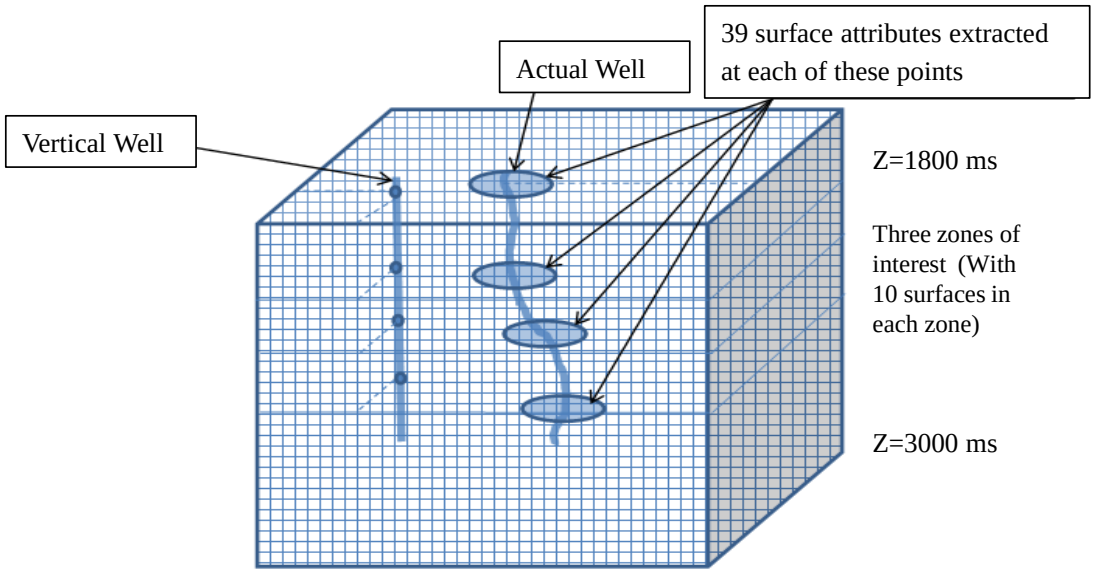

Figure 5.15. Seismic surface attributes considered

Seismic attributes that required a loop to be completed for computations could not computed at certain locations resulting in null values. A boundary is created

around the seismic data set and attribute values within the boundary are computed using convergent interpolation technique available in Petrel. See Figures 5.16 and 5.17.

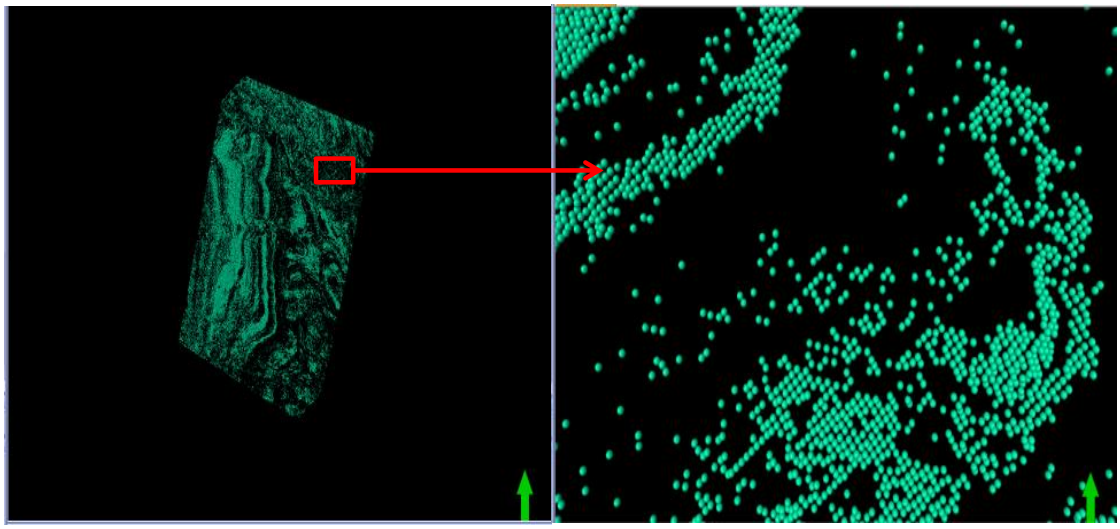

Figure 5.16. Visual representation of missing data in the initial surface attribute computation module

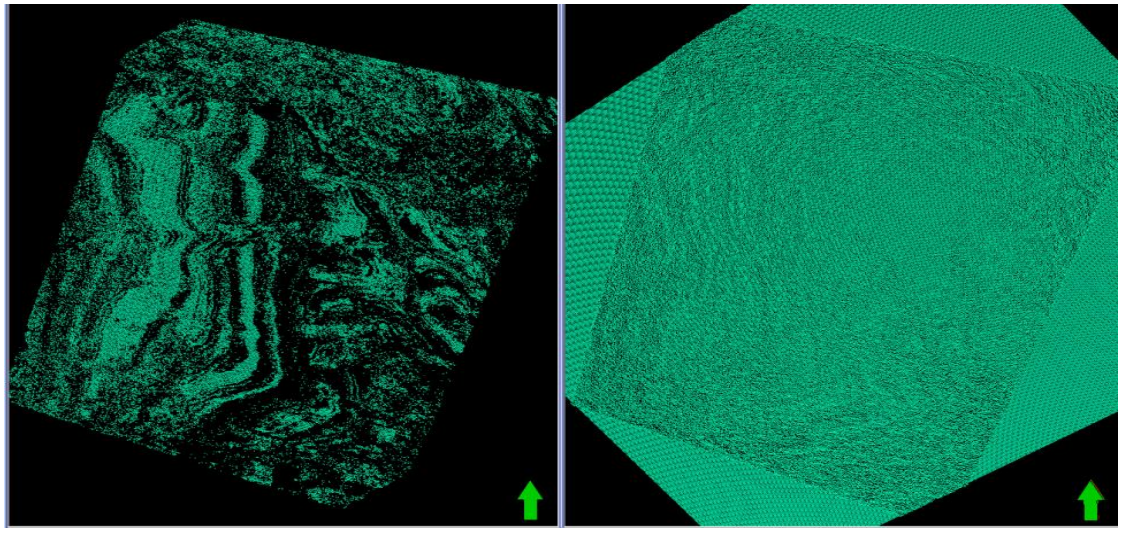

Figure 5.17. Comparison between the densities of the 60k points (Low Res) vs. 157k points (Full Res)

Obtained seismic attribute data set comprises of 157,348 × 42 matrixes at each of the 30 surfaces. (157,348 rows correspond to the total number of locations at which surface attributes are computed, 42 columns indicate 39 attributes followed by X coordinate and Y coordinate and Z coordinate). Zone-1 is defined as 1800-2200ms and Zone-2 as 2200-2600 ms and Zone-3 as 2600-3000 ms. The division of these zones at the current resolution is a result of the improved correlation coefficients observed in the synthetic well log networks.

Four sample surface attributes arc length, peak value, minimum loop duration, and number of zero crossings computed at 2800 ms are shown in the Figure 5.18.

Production data is processed to obtain the curve fit parameters that result in cumulative flow rate being described with three parameters a, b, c using the following power law formula. Figure 5.19 represents the cumulative flow rate data of Well #5 along the assumed curve fit parameters.

$$q_{cum}(STB) = at^b + c \tag{5.14}$$

Various curve fitting models are considered as indicated in Table 5.2 with their corresponding average regression values. These values correspond to cumulative oil production profiles.

Table 5.2. Curve fitting models considered for cumulative oil production

Type of Model	Curve fit equation	R^2	Adjusted R^2
Model 1 (Exponential)	$q_{cum}=ae^{bt}$	0.898	0.897
Model 2 (Polynomial)	$q_{cum}=at^2+bt+c$	0.996	0.996
Model 3 (Power)	$q_{cum}=at^b+c$	0.994	0.994

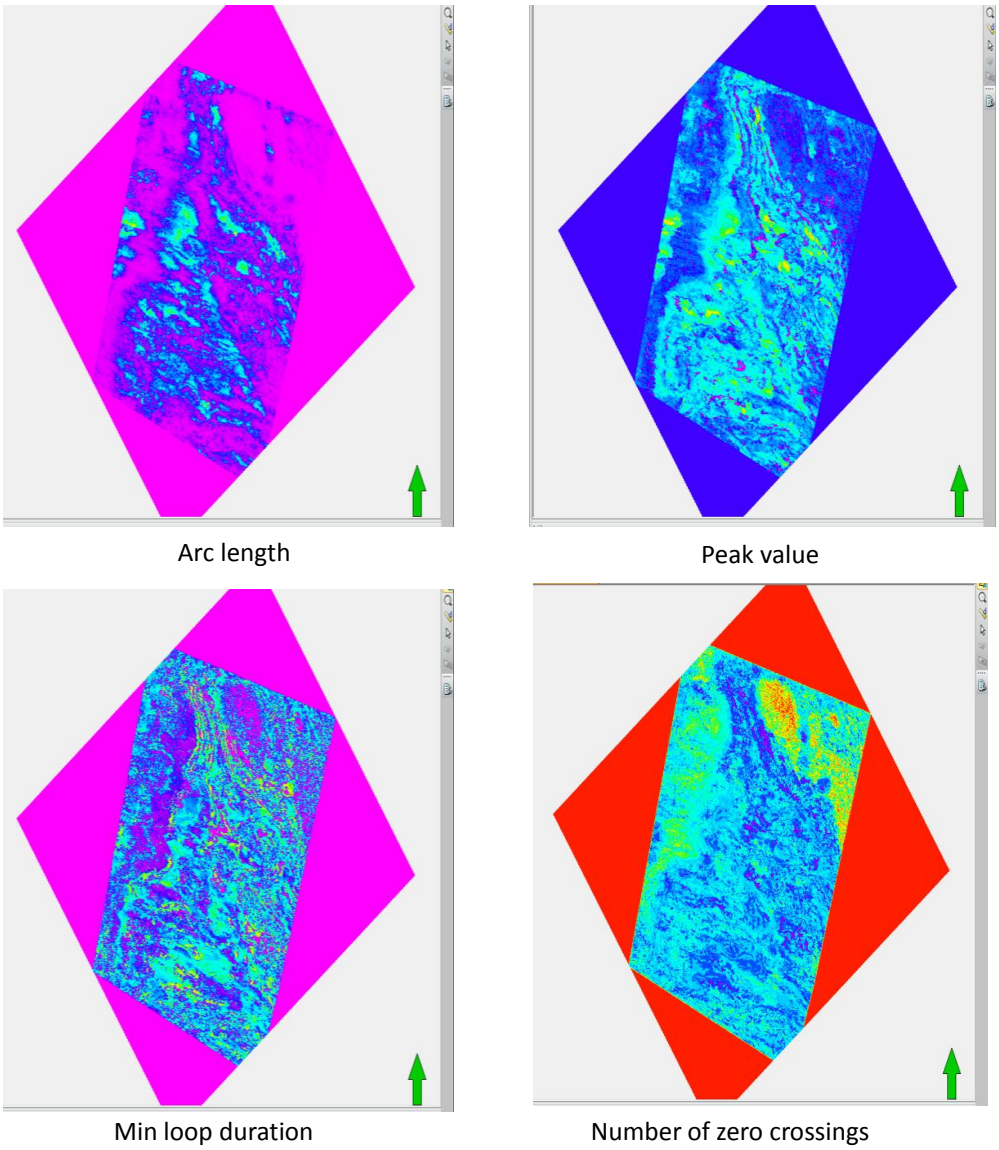

Figure 5.18. Sample surface attributes computed at 2800 ms surface

From Table 5.3, it is evident that Model 2 and Model 3 are able to characterize the cumulative flow rate profiles with high regression coefficients. However, in finding an optimum architecture, it was found that curve fit parameters a, b, c based on Model 3 are predicted with higher correlation coefficients and lower blind

test errors consistently. Following Model 3, the ranges of parameters observed for each of the oil, gas and water networks are listed in the tables below:

Table 5.3. Curve fit parameters for cumulative oil production

Parameter	Min	Max	Average
a	1.33e+03	1.05e+05	2.79e+04
b	0.4401	1.0526	0.7539
c	-7.43e+05	1.26e+05	-1.55e+05

Table 5.4. Curve fit parameters for cumulative gas production

Parameter	Min	Max	Average
a	3.28e+03	2.38e+05	6.12e+04
b	0.5079	1.0983	0.7313
c	-1.36e+06	2.23e+05	-3.68e+05

Table 5.5. Curve fit parameters for cumulative water production

Parameter	Min	Max	Average
a	6.09e-13	2.29e+05	2.58e+04
b	0.0067	6.1043	1.5301
c	-2.55e+05	1.49e+04	-4.06e+04

The parameters predicted for cumulative water production profiles have a wide range of the parameters a, b, c observed. These extreme variations in the curve fit parameters make the model predictions difficult to converge. Hence alternate ways of correlating water production profiles are explored (Details are illustrated in Section 6.3.3).

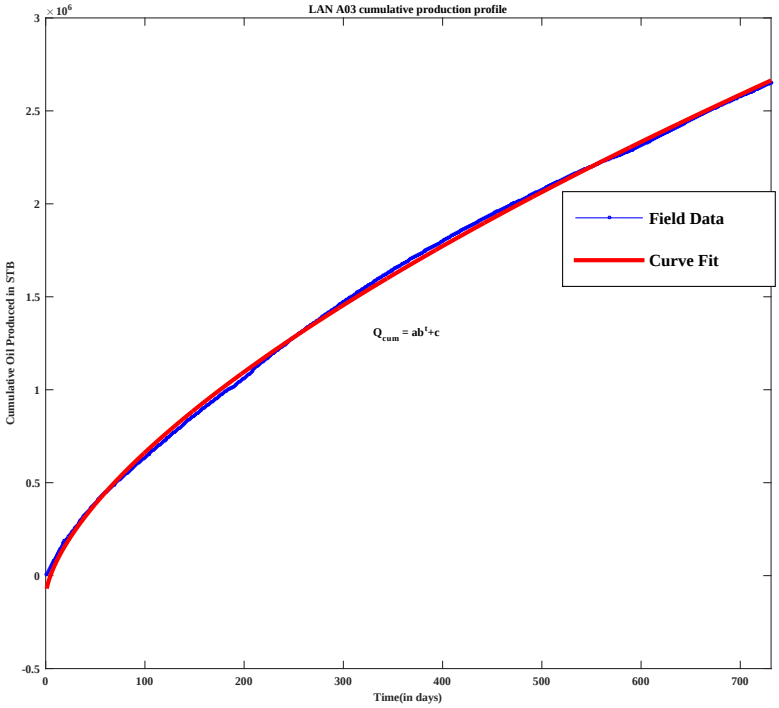

Figure 5.19. Cumulative production profile of well #5 indicating goodness of curve fit

5.4 ANN architectures and performance criterion

Obtaining an optimal architecture is of prime importance in bridging the uncertainty in predictions. In the current work, a new methodology has been developed that employs the parallel processing capabilities of MATLAB with the help of a script that enables efficient search for optimal network architecture.

Mean square error regression is used as a criterion while training the networks. Various training algorithms are tested during this stage to accelerate the convergence. Scaled conjugate gradient method of training has proved to be the most successful training method compared to other available methods. This network training function updates weight and bias values according to the scaled conjugate gradient

method. Levenberg-Marquardt and BFDS Quasi-Newton and Conjugate gradient with Powell/Beale restarts are amongst the other training algorithms tested. Gradient descent with momentum weight and bias learning function was implemented as a learning algorithm. Number of epochs was limited at 10,000 to avoid overfitting the data. The goal for training was set at 10^{-4}. In all the numerical experiments conducted, 80% (30 wells) data is used for training, 10% (4 wells) data is used for validation and 10%(4 wells) data is used for testing purposes in case of synthetic log networks. In some synthetic log networks the sample data set is limited to 34 wells to ensure consistency and availability of all the logs in the suite. For production performance networks, 14 wells consistently had data that could be used. So 80%(12 wells) data is used for training, 10%(one well) for validation, and 10%(one well) for testing. Mean average testing error for a given synthetic log network is computed according to Equation 5.15:

$$e = 100 * \sum_{i=1}^{n_{test}} \sum_{j=1}^{Length} \frac{(Predictedvalue_{i,j} - Targetvalue_{i,j})}{Targetvalue_{i,j}} \frac{1}{(n_{test})(Length)} \quad (5.15)$$

Where, $n_{test} = 3$ or 4 , Depending on the number of testing cases available for each of the networks

Length=150 log values for all the networks.

Even for the production performance networks, similar criterion is used in generating the optimal architectures. In evaluating the error, month by month production is computed and error is composed based on average monthly percentage error in cumulative flow rates.

5.4.1 Parallel computation algorithm

In the current work 100,000 artificial neural network architectures are tested and data sets are shuffled 6 times for each of the architectures . The speed of convergence depends of various factors namely error tolerance, learning algorithm used, number of cores in the computer, processor speed and data set itself. In this work it typically took from 8hrs-24 hrs for the program to return the optimal architecture for each of the synthetic well log architectures. The inputs for these architectures like range of number of neurons, transfer functions, minimum and maximum number of layers, learning algorithms, error performance criterion are manually adjusted based on the performance. The workflow illustrated in Figure 5.20 enables implementation of parallel computational ability in MATLAB helping user to save time in generating multiple scenarios and evaluating them.

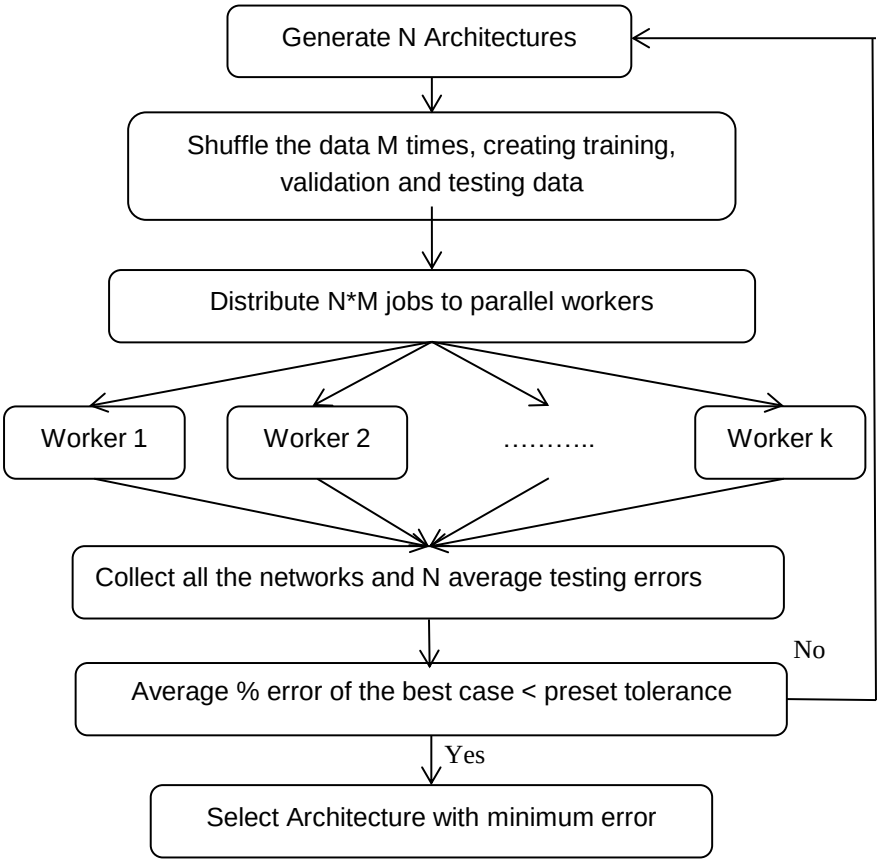

Figure 5.20. Parallel computation algorithm

Chapter 6

Results and Discussions

6.1 Synthetic well log networks

Synthetic well log networks correlate seismic attributes to well logs and help in generating synthetic well logs across the entire area of the reservoir. Initially the well logs are trained individually with the seismic attribute data and later it has been observed that combining the well logs and using them together as target has improved the correlations. In the past works, a variety of wireline logs have been individually predicted with limited to moderate success. In this work, an attempt is made to test the hypothesis that well log signatures are codependent. During trials with individual well log pattern identification networks, blind test errors of greater than 15% were observed for GR log. Several numerical experiments concluded that neutron porosity log (NPHI), gamma ray log (GR) and total porosity log (PHIT) together yield better correlations and reduced error in the blind tests. Bulk density log (RHOB) and deep resistivity logs (RESD) together did perform better than individual networks. Therefore six network architectures are established, two network architectures for each of the three zones.

The resolution of the well log parameters was critical to obtaining meaningful correlations. Predicting the well logs at 0.5 ft resolution resulted in extreme variations that often resulted in noisy data. On moving to coarser resolutions, there is a risk of losing detailed information provided by the log signature. At the same time, the lowest possible vertical resolution that could be obtained from a seismic trace data in the current field considered is 4ms. Hence resolutions of well logs, and seismic data were altered intelligently to improve the correlations. This process has resulted in the final resolutions used in generating synthetic well log networks.

Using the parallel processing algorithm outlined in Figure 5.20, about 100,000 architectures are tested to arrive at optimal architecture. It has been observed that *tansig* and *logsig* transfer functions performed better than the rest of the available transfer functions. The maximum and minimum was set at 300 and 100 neurons for the hidden layers. The optimal architecture obtained for Zone-1 NPHI GR PHIT network has three hidden layers with *logsig*, *tansig*, *logsig* and 368, 398, and 99 neurons. *Purelin* is used for the output later. To improve the prediction, mean log values are added as an output functional links for all the synthetic log networks. The optimal network architecure is shown in Figure 6.1.

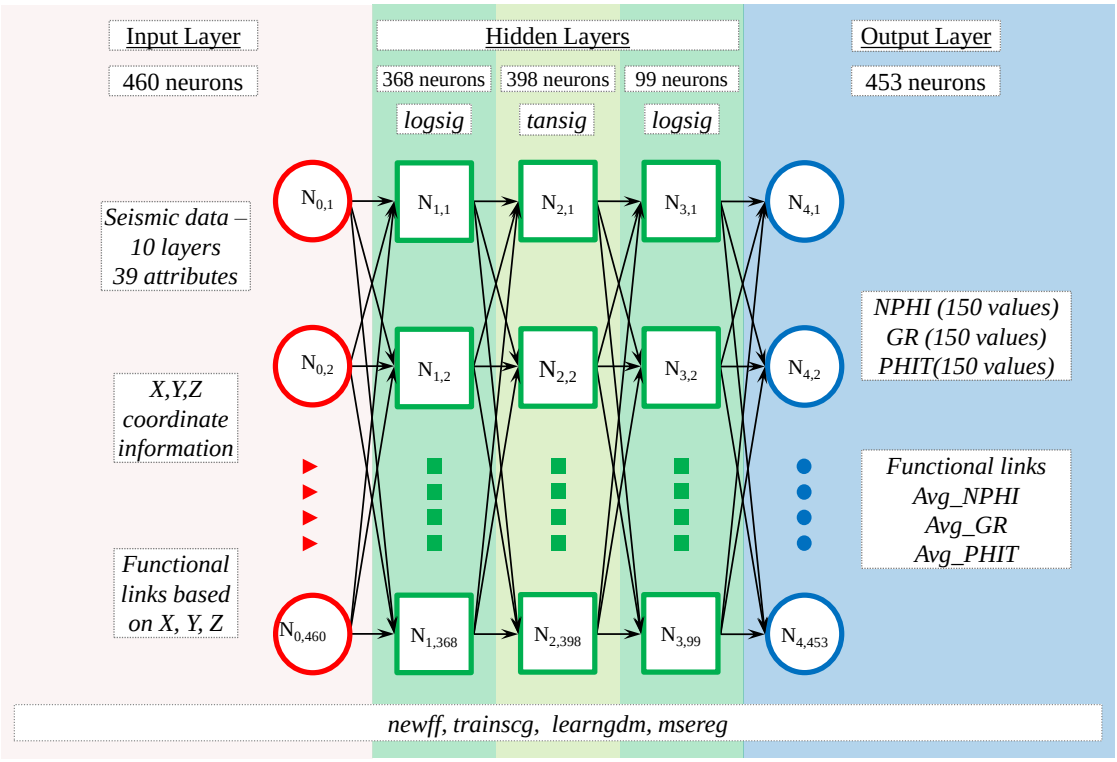

Figure 6.1. Zone one - three log architecture

Zone one blind testing results for three log architecture

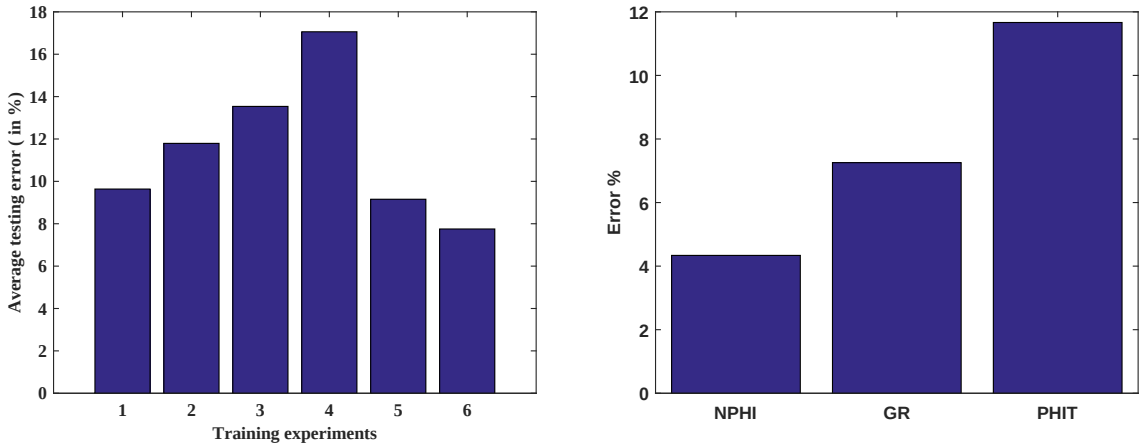

(a) Blind testing errors observed during numerical experiments

(b) For three different logs, Errors observed in blind testing

Figure 6.2. Blind testing errors observed

Figure 6.2 showcases the errors encountered while generating the optimal architecture. The figure on the left displays the blind testing average error results observed with the optimal architecture on six numerical trials. In each of the numerical trials , data sets are randomly shuffled to obtain a different training, testing and validation data. The figure on the right shows the blind testing error observed in prediction of individual logs.

Figure 6.3 shows the relevancy of the input attributes in predicting the suite of NPHI, GR and PHIT logs for Zone-1. All the seismic attributes more or less had similar contributions around 3%. Sum of negative amplitudes and average peak value between zero crossings have turned out to be slightly significant on comparison with other seismic attributes. Sum of negative amplitudes provides a measure of brightness multiplied by the formation thickness and may be regarded as a measure of brightness volume. This explains the reason GR log is found to be highly correlated with seismic data in Zone-1 as a result the observed blind testing error is less than 10%

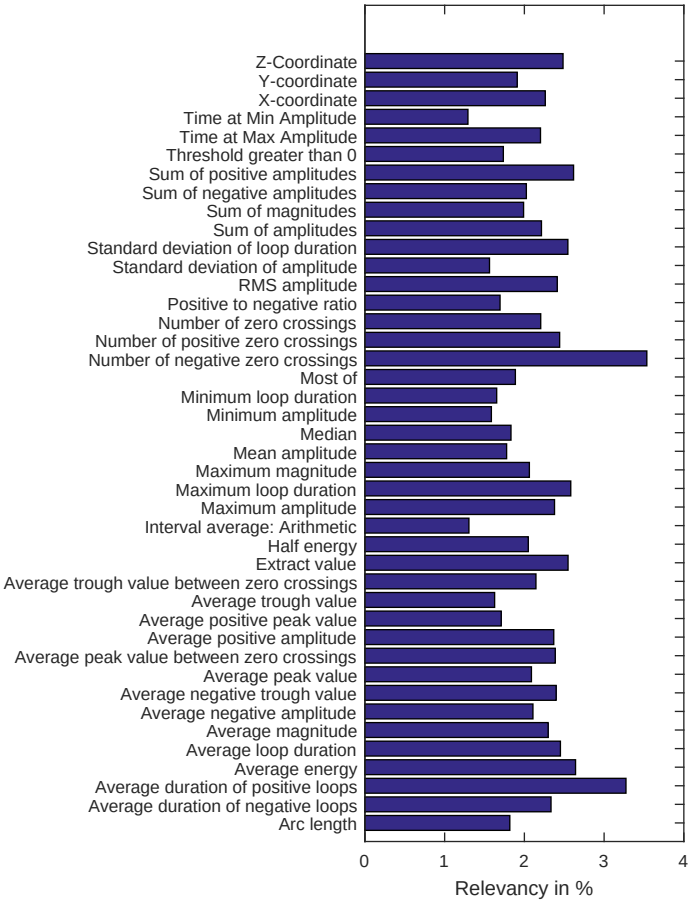

Figure 6.3. Relevancy of seismic attributes

It is evident from Figure 6.4, that seismic attributes did have a good correlation with NPHI log. The mean average testing error was found to be 4.3% out of 3 testing cases. In the above figure, the red line indicates the ANN predicted log value and blue indicates the actual log value. Y axis represents the depth in feet. Each time zone is split up into 150 average log values. Zone-1 corresponds to 1800-2200 ms. The depths corresponding to these time zones are computed using the check shot information.

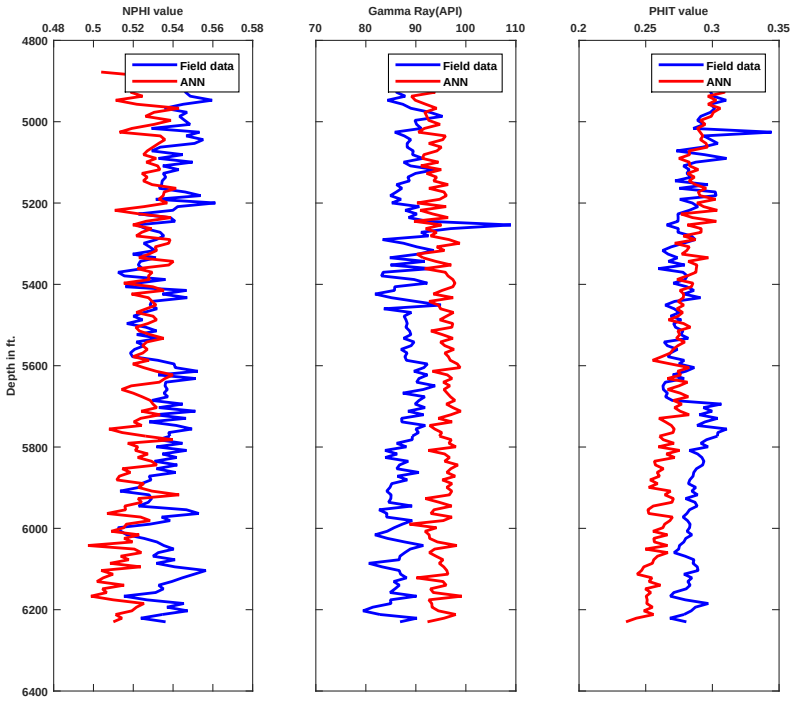

Figure 6.4. Comparison of model predicted data vs. field data for Well #13

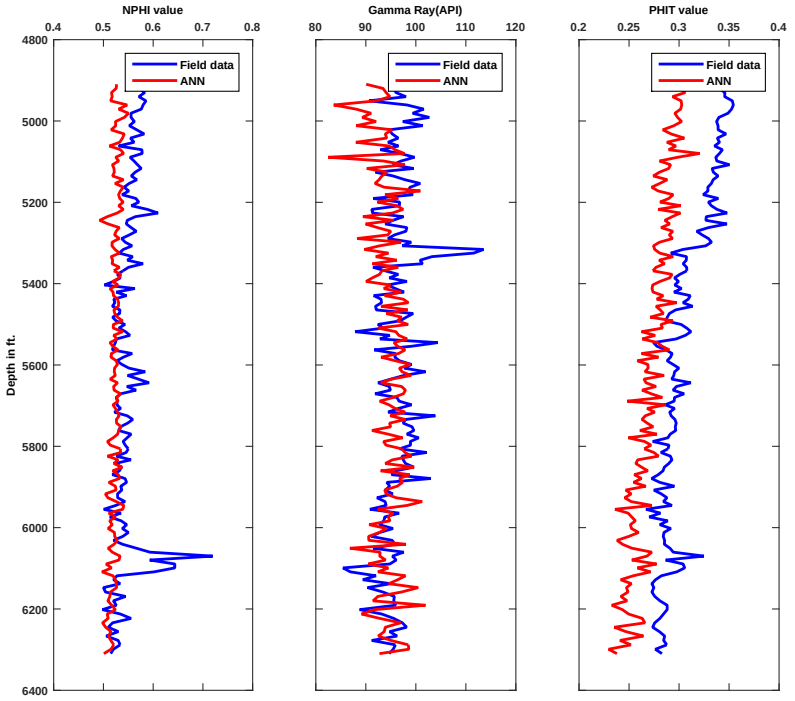

Figure 6.5. Comparison of model predicted data vs. field data for Well #18

Gamma ray log testing cases resulted in a mean testing error of 7.3%. The peaks and troughs are not completely captured, but the trend of the well log seems to be captured in the testing cases. The test cases shown in Figure 6.5 represent the median error cases. A mean average testing error of 11.7% is observed in three testing cases used for PHIT log prediction. In testing case 1(refer Figure 6.4) and testing case 3 (refer Figure 6.6, model predictions are slightly different actual field GR log data. In Well #18, model is able to capture the variation of GR log satisfactorily .

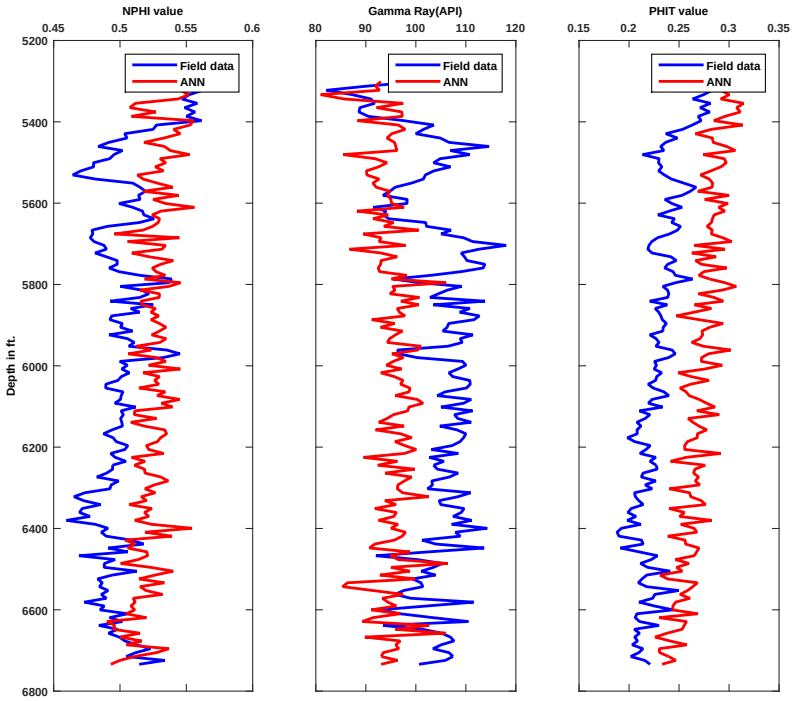

Figure 6.6. Comparison of model predicted data vs. field data for Well #36

Pruning methods have been tried with limited to no success in improving the correlations. On removing the two least relevant seismic attributes, it was found that the regression coefficients started to go below 0.9. Relevancy plots for other

five networks look very similar to the above plot with small variations. Not one seismic attribute has consistently proved to be more relevant than the others. In this field, it can be said that all the seismic attributes do contribute to the synthetic well log correlation.

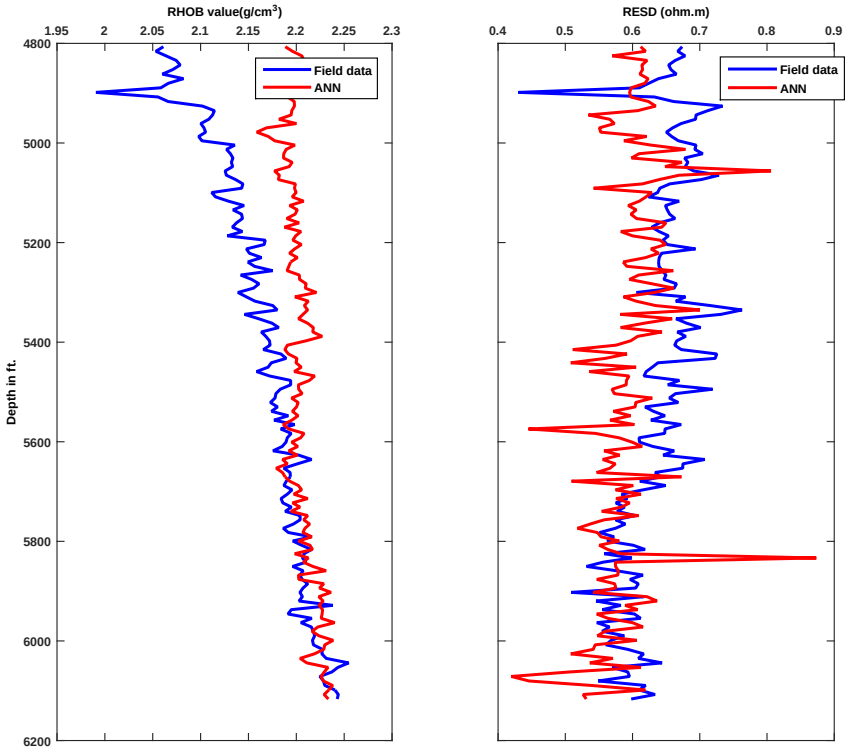

Figure 6.7. Comparison of model predicted data vs. field data for Well #2

Zone-1: RHOB RESD Network: As discussed earlier, Zone-1 bulk density log (RHOB) and deep resistivity logs (RESD) are trained together to obtain better correlations. While developing correlations to predict deep resistivity(RESD) logs, it is observed that the abnormal deviations from the regularly observed values tend to skew the correlation and therefore higher errors are observed consistently across all zones for resistivity log predictions. *Log* and *antilog* scheme was introduced to deal with the sharp variations in resistivity values, that in turn helped improve the correlations. Optimal architecture obtained for this network has four hidden

layers with *tansig*, *tansig*, *logsig* and *logsig* as the transfer functions and 257, 126, 248, 185 neurons on each of the hidden layers respectively. Schematics of the networks developed for zone one RHOB RESD network and rest of the networks are indicated in the Appendix C. Average testing error of 8.37% indicates the robustness of the correlation obtained between seismic attributes and RHOB, RESD logs for Zone-1. The schematics of the optimal network and the error percentages observed while testing these architectures is presented in Appendix C. For brevity purposes, all the subsequent network architectures, error percentages while training for optimal architectures, individual log wise blind testing errors and relevancy plots are presented in Appendix C.

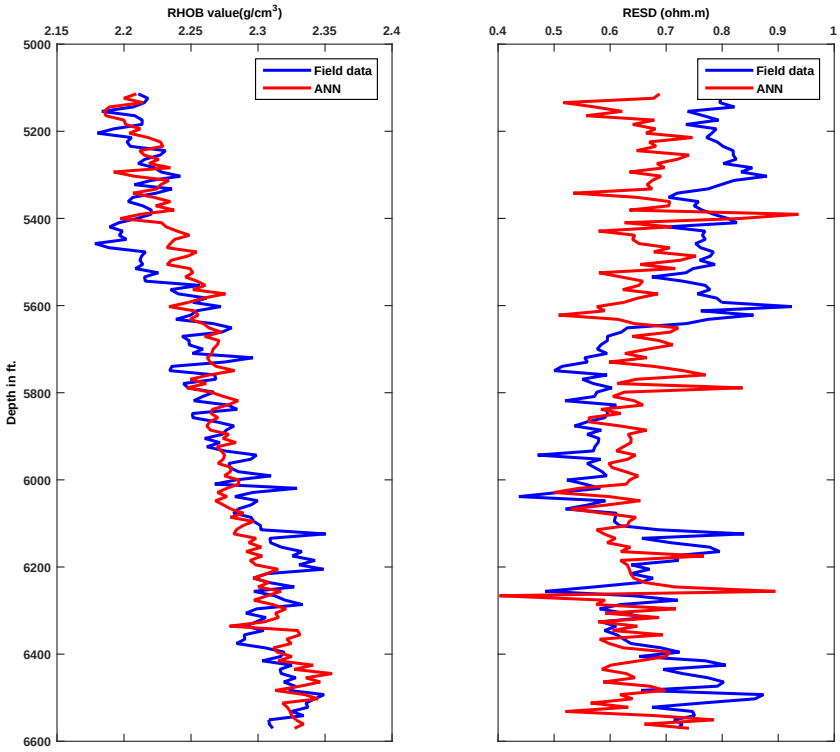

Figure 6.8. Comparison of model predicted data vs. field data for Well #7

The mean average testing error observed in the four testing cases is 8.37% for the entire network. The models RHOB trend and log value prediction seems to be

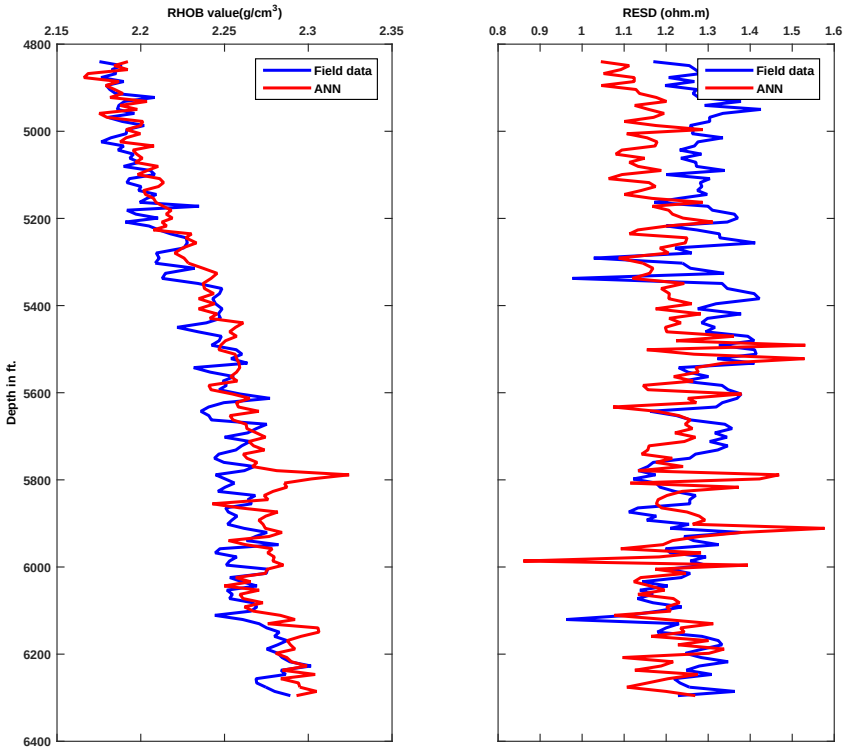

Figure 6.9. Comparison of model predicted data vs. field data for Well #21

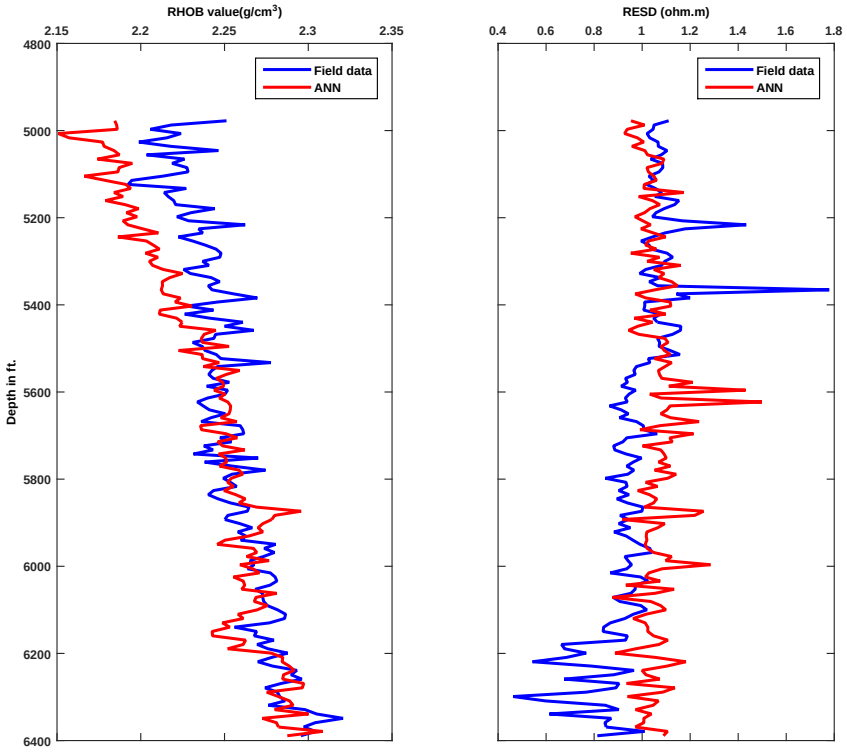

Figure 6.10. Comparison of model predicted data vs. field data for Well #22

very well captured in testing Wells #7, #21 and #22(refer Figures 6.8 to 6.10). Testing case, Well #2 seems to have unrealistic values of bulk density observed. It is interesting to note that bulk density values increase as the depth increases across all the well logs. The average testing error resulted in predicting the RHOB logs is 1.1%.

For RESD logs, a mean average testing error of 12.1% was observed amongst four testing cases. Some of the peak values could not be accurately captured in a few test cases.

Zone-2: NPHI GR PHIT network: Zone-2 in this study is defined as region between 2200-2600 ms of two way travel time. The optimal architecture established for this has four hidden layers each with a transfer function of *logsig*. Number of neurons in each hidden layers is 191, 191, 161, and 168 respectively. Functional links based on X, Y, Z coordinates are used. This network could capture the correlation well at an mean observed error of 6.05%.

The trends in prediction of NPHI log values in all the three testing wells are well captured. Sharp contrast in NPHI values as it approaches Zone-3 is evident in Wells #27 and #32 (See Figures 6.11 and 6.12, where the model is able to predict those as well.

NPHI log in Zone-2 resulted in good correlations with seismic attribute data with a mean average testing error of 5.7% over three testing cases. Amongst these testing cases, Well #35 (refer Figure 6.13) has relatively high error between predicted log value and actual NPHI value. The model predictions tend to estimate lower GR log values at locations with high shale content. The model seems to be marginally over predicting sands and under predicting the shaly layer GR values. Model predictions of PHIT values are in line with the actual field data at all the three testing wells. The sharp transition in Figure 6.13 PHIT value could be an

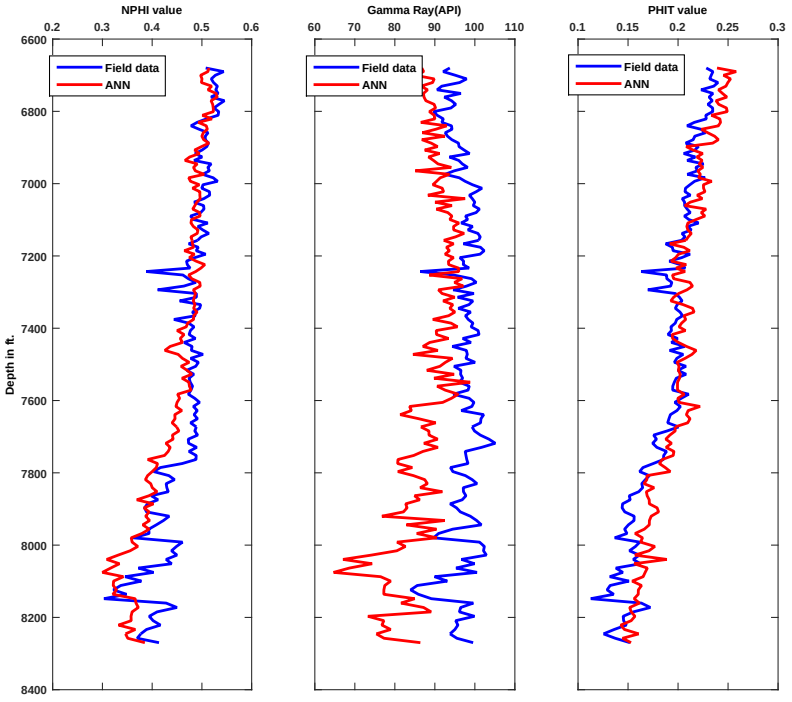

Figure 6.11. Comparison of model predicted data vs. field data for Well #27

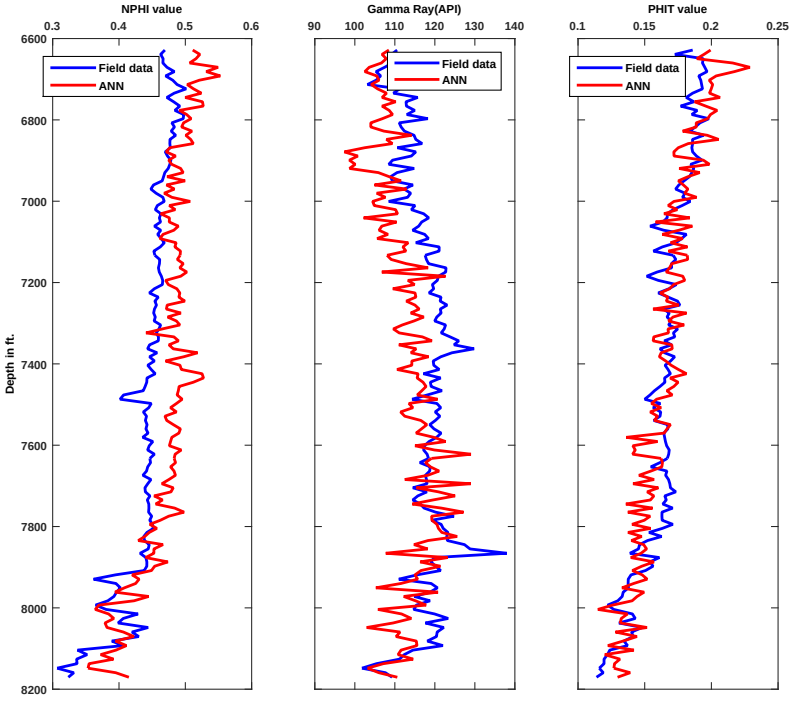

Figure 6.12. Comparison of model predicted data vs. field data for Well #32

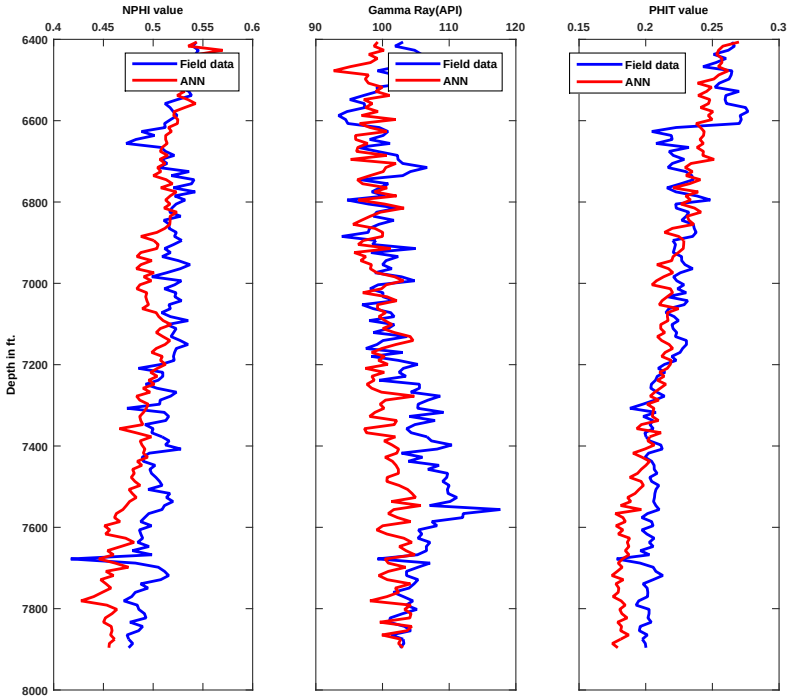

Figure 6.13. Comparison of model predicted data vs. field data for Well #35

error in the logging environment. The average testing errors for NPHI log at 5.7% , GR log at 5.9%, and PHIT log at 6.5% indicate the relatively strong correlations obtained between the seismic data and well log data in Zone-2.

Zone-2: RHOB RESD Log network: The optimal architecture established for Zone-2 RHOB RESD network has four hidden layers with 151, 281, 144, 259 neurons each. The transfer functions associated with these layers are *logsig*, *logsig*, *tansig*, *tansig*. The output layer is fed through a *purelin* transformation. The overall mean testing error observed for this entire network is 9.5%.

Bulk density log correlated well with seismic data in zone two resulting in a mean average testing error of less than 1%. All four blind testing cases for bulk density are predicted very well as shown in Figure 6.14 through Figure 6.17.

The peak values of over 5 *ohm-m* could not be accurately predicted by the network. The resistivity log trends for Well #21 and Well #24 are captured satisfactorily by the network. However in Well #15 and Well #30, the peak values

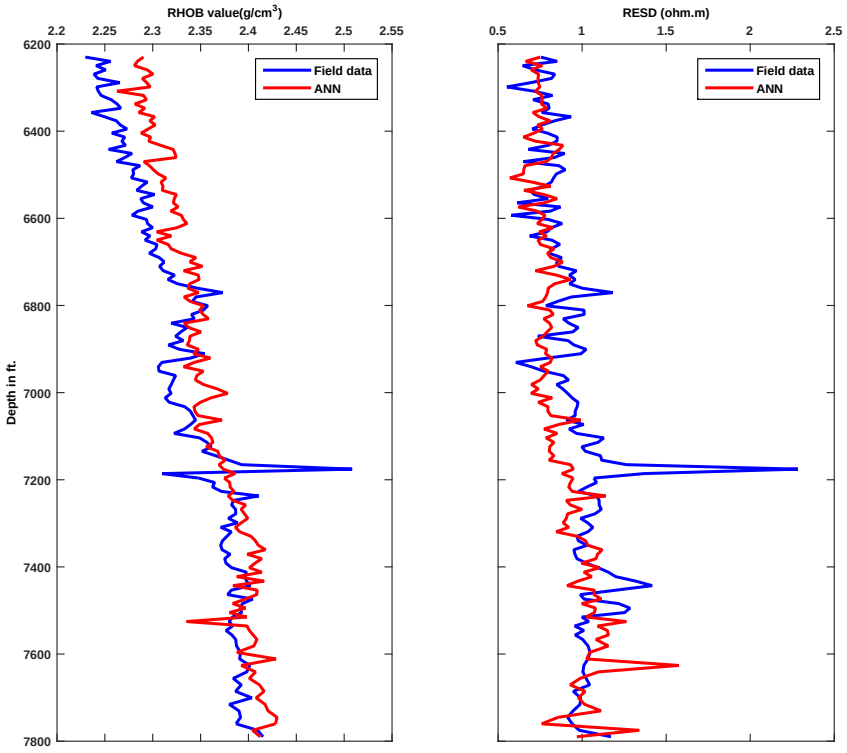

Figure 6.14. Comparison of model predicted data vs. field data for Well #15

of over 10 *ohm-m* could not be accurately predicted. The mean average testing error observed over four blind testing cases is 13.1%. The model predictions are in line with actual field data for RESD log from Well #24 as seen in Figure 6.16.

Zone-3: NPHI GR PHIT Log network: The three log network optimal architecture is found to have four hidden layers with 162, 154, 239, 177 neurons each with *tansig*, *logsig*, *tansig*, *logsig* as their respective transfer functions. Output layer has *purelin* as the transfer function. The mean average testing error for the network is at 21%.

Figure 6.18 highlights model's ability to capture sand bodies that exist within the layers by predicting the gamma ray log accurately. NPHI log correlations show

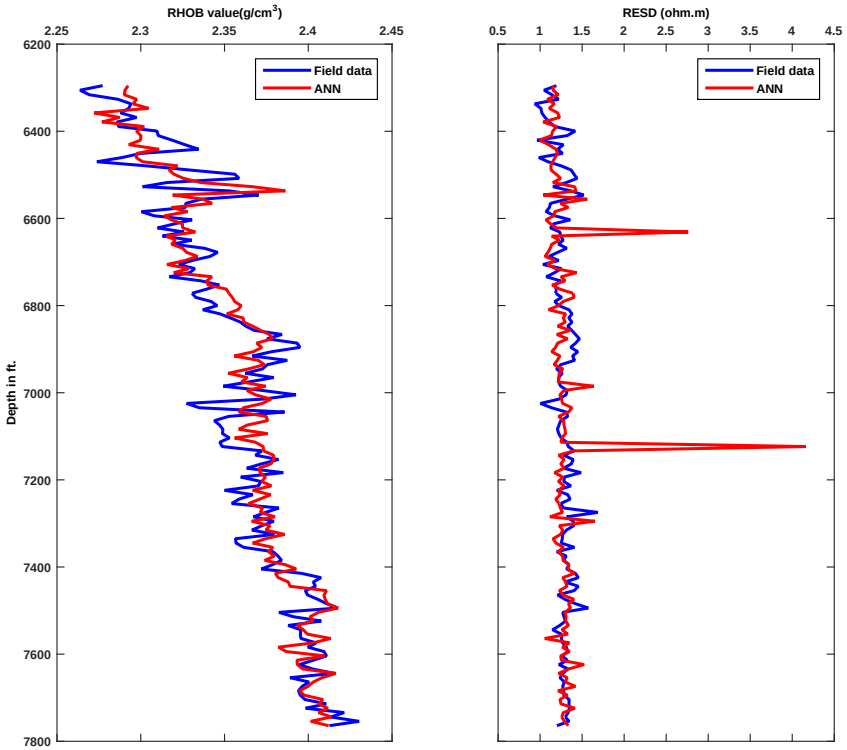

Figure 6.15. Comparison of model predicted data vs. field data for Well #21

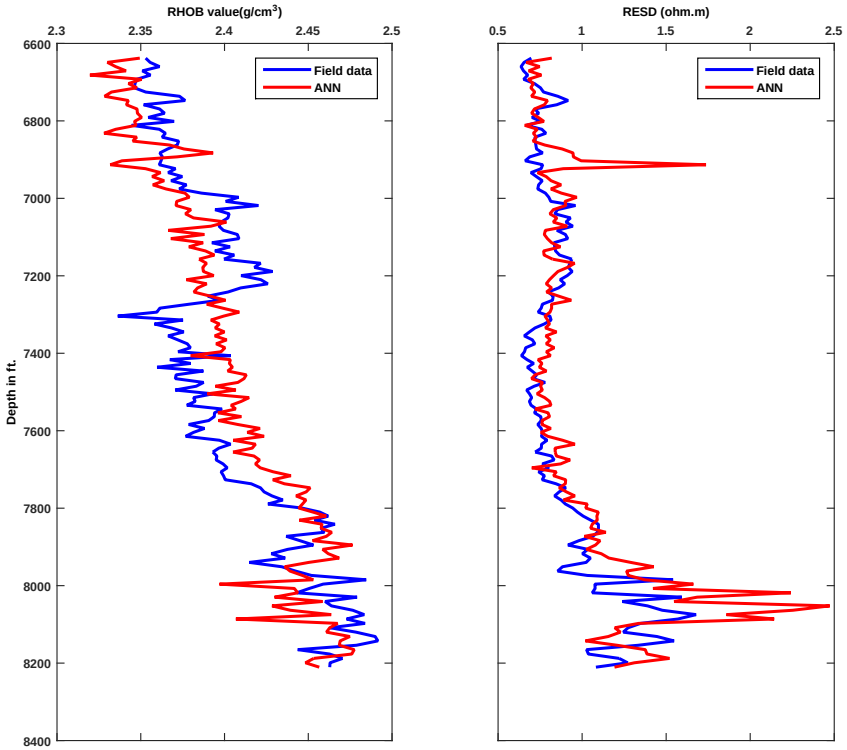

Figure 6.16. Comparison of model predicted data vs. field data for Well #24

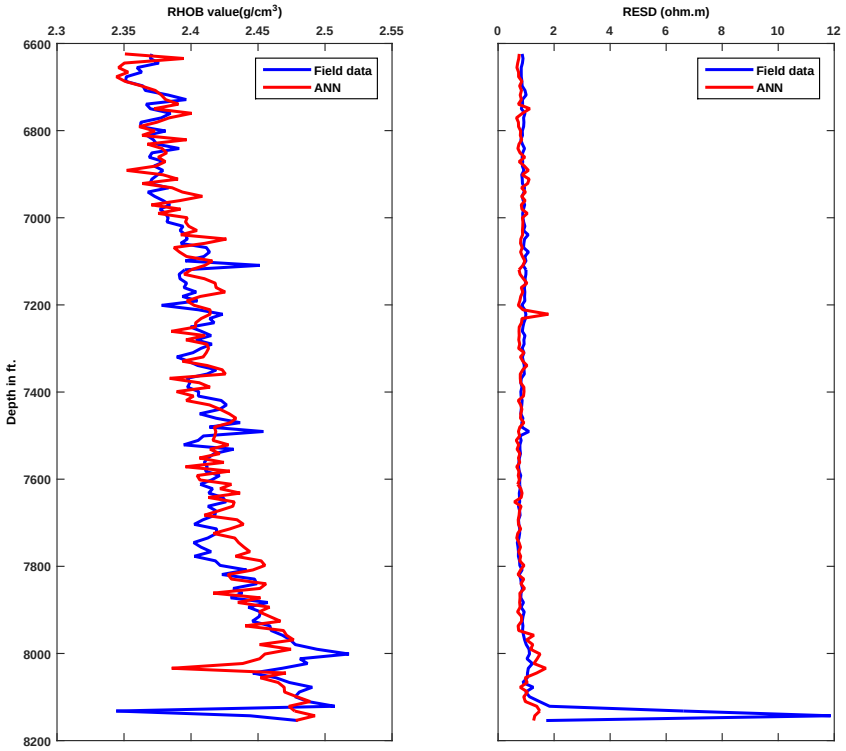

Figure 6.17. Comparison of model predicted data vs. field data for Well #30

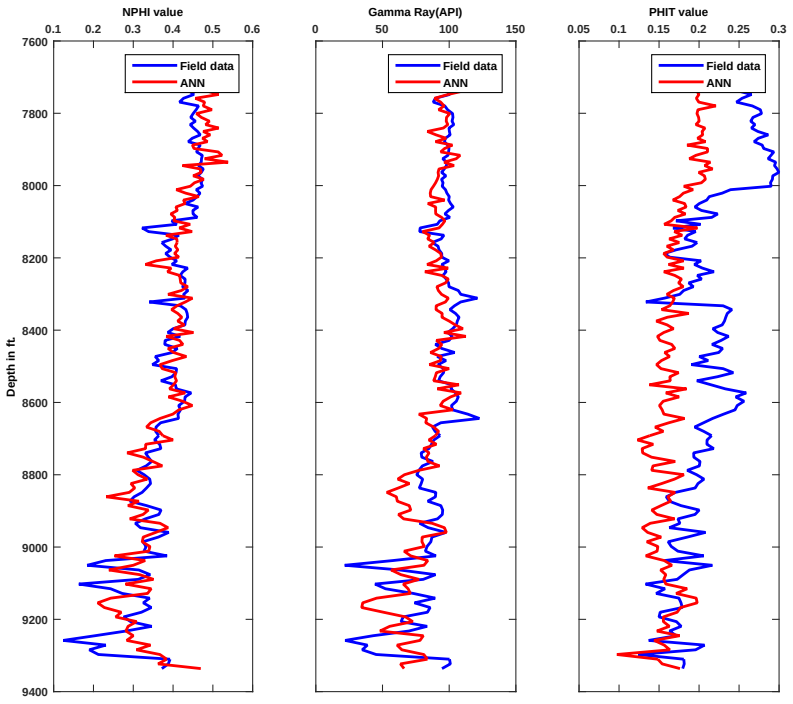

Figure 6.18. Comparison of model predicted data vs. field data for Well #1

promise with an observed error less than 2% in this case. PHIT log variations are well captured in Figures 6.19 to 6.21.

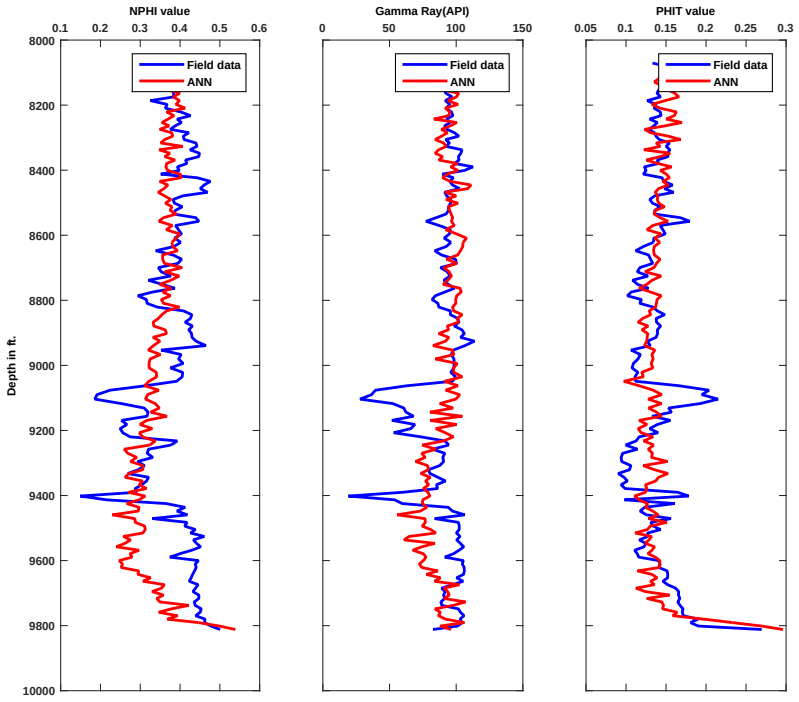

Figure 6.19. Comparison of model predicted data vs. field data for Well #8

A mean average testing error of 22% is observed in NPHI log predictions for Zone-3. For predicting GR log, the model resulted with an average error of 25.7%. PHIT logs are predicted with an average testing error of 18.4%. NPHI and GR trends are predicted in line with field data for the Well #1 as indicated in Figure 6.18. PHIT log trends as bottom of the 3000 ms is approached are predicted accurately. In some instances, low GR troughs could not be satisfactorily captured.

The model is having difficulty to predict the log values below 40 *API* on a few occasions. Lower *API* values indicate the presence of sand in the lithographic section. Higher *API* values indicated the presence of shale.

Zone-3: RHOB RESD log network: Zone-3 correlations were more difficult to establish owing to the sharp variations of log values. RHOB log is converted to

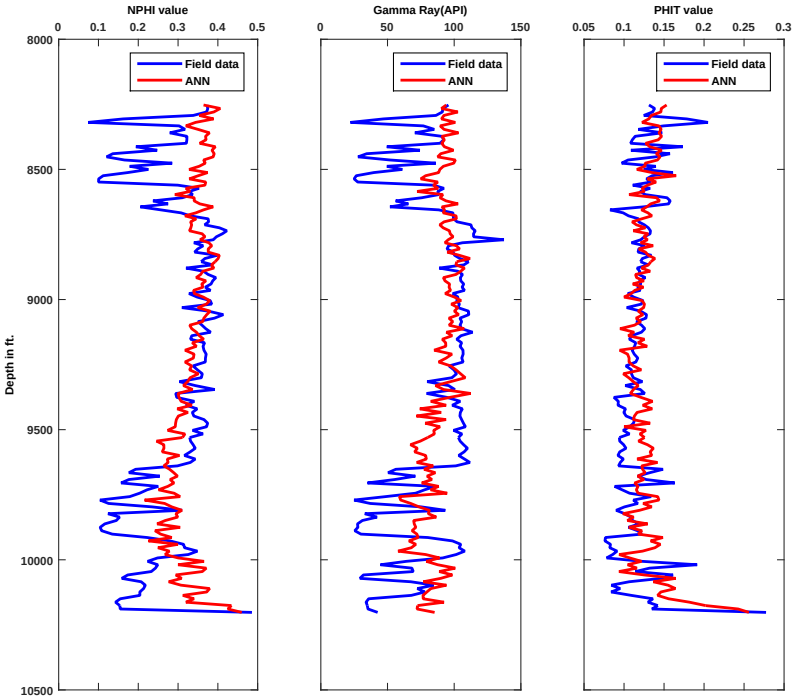

Figure 6.20. Comparison of model predicted data vs. field data for Well #26

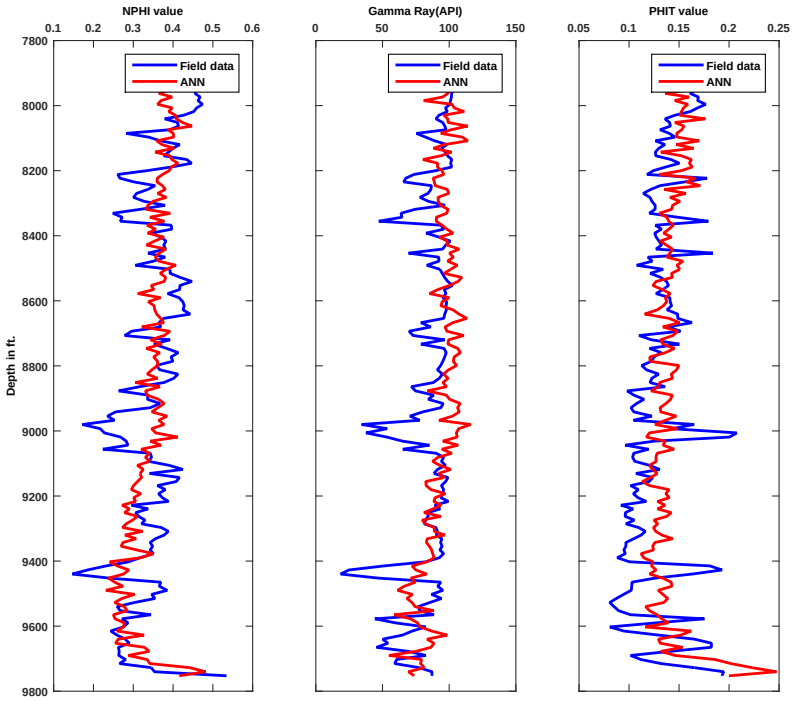

Figure 6.21. Comparison of model predicted data vs. field data for Well #34

a pseudo porosity log via density porosity equation and then used as a target data for generating the correlation. This process has resulted in significant reduction of error while predicting RHOB log. *Log* and *anti-log* schemes have helped in reducing the errors in the process of establishing RESD log correlation. Zone-3 optimal networks have four hidden layers with 294, 214, 272, and 115 each. The transfer functions between the hidden layers are *logsig*, *tansig*, *logsig*, *logsig* and *purelin* for the output layer. The overall mean testing error for the entire network is observed to be 26.2%. The three blind test cases are displayed in Figures 6.22 to 6.24.

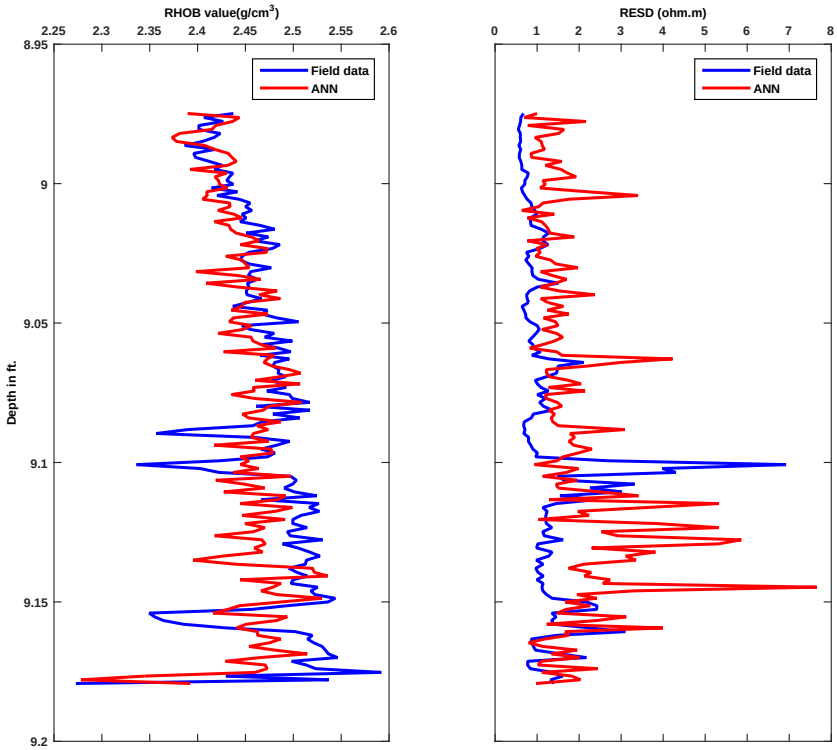

Figure 6.22. Comparison of model predicted data vs. field data for Well #4

RHOB logs consistently correlate well with the seismic data across all the zones. In zone three, the mean average testing error is found to be 1.5% and the network is able to capture the variation in the bulk density for the testing cases. Some of the peaks are not captured completely through ANN predictions, but the trends

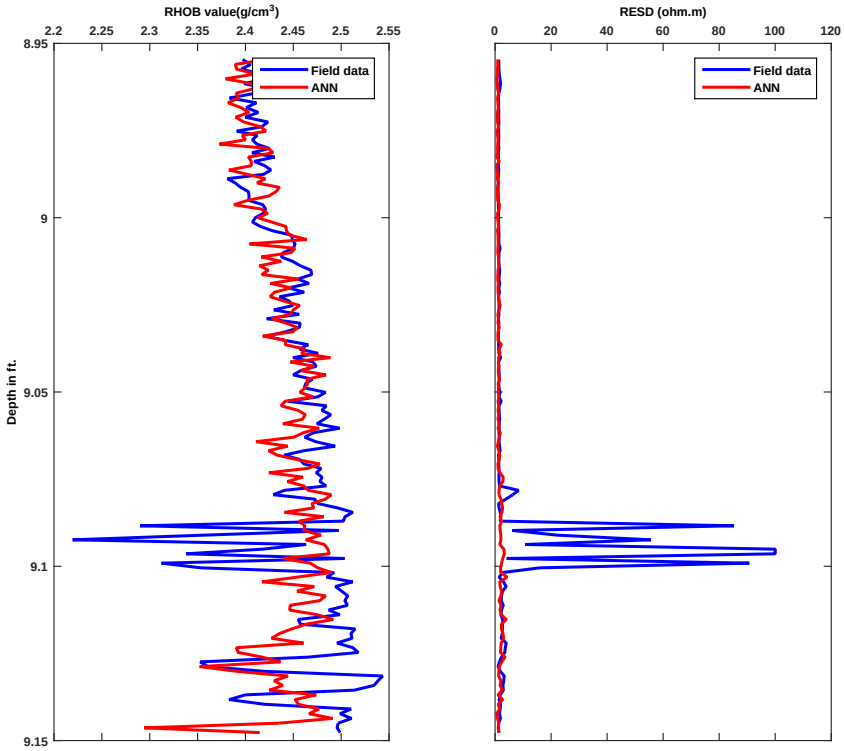

Figure 6.23. Comparison of model predicted data vs. field data for Well #5

are in line with the actual logs. The RHOB values do not seem to increase with depth as observed in Zone-2. This phenomenon could be attributed to the presence of hydrocarbon in Zone-3 which alters the bulk density values significantly.

Zone-3 log predictions had the highest error amongst all zones. This is due to sharp variations in the properties of the zone along the depth. This zone is believed to be the prolific production zone because of which the resistivity variations are large. Hence, the mean average testing error observed for resistivity logs is around 35%. The RHOB logs consistently performed better than the rest of the logs. This is due to their relationship to seismic amplitudes through impedance. Impedance log is generated through combining bulk density log with sonic log. It is then used to construct seismic well ties throughout the field to validate the velocity model. The errors observed during prediction of RHOB logs are lower than 2% in any given zone

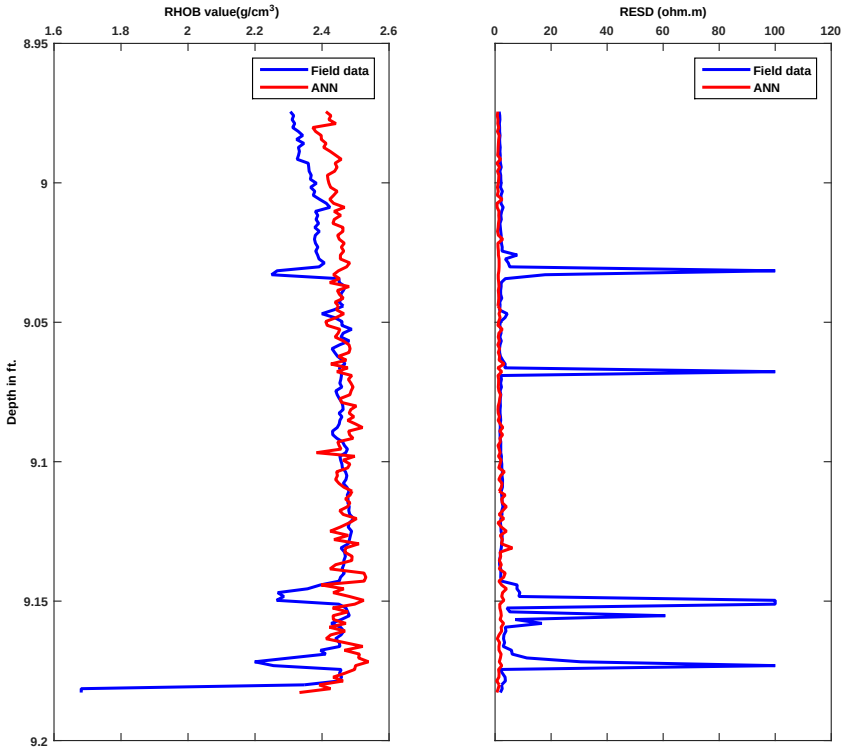

Figure 6.24. Comparison of model predicted data vs. field data for Well #23

due to the fact that they correlate well with seismic amplitudes. The correlation coefficient values R^2 observed in generating synthetic well log correlation fall in the range of 0.7-0.95. Higher correlation coefficient values indicate a high degree of accuracy. Attempts to train the entire length of well log in one model has resulted in lower correlation coefficients, thus indicating different zones of the log do carry unique information in this field. With the help of these synthetic well log networks, log cubes are created with all the five logs at every location seismic data is available. Average GR, NPHI, PHIT and RHOB logs generated from Zone-1 logs is displayed in Figure 6.25. These plots clearly indicate that the sands are deposited along the north to south direction with high porosity channels that could be potential flow channels. From the average PHIT logs it is evident that high porosity channels run from north to south. RHOB logs indicate that the eastern part of the field

could be having lower porosity. But the density porosity calculations are performed according to lithology. The south east region is known to be closer to oil water contact, that is one of the reasons why the density porosity logs indicate a higher values, that translate to lower effective porosity values. The generation of these log surfaces aided in understanding the complex lithology patterns exhibited by this field. These synthetic logs can be populated back to static model for better informing the facies model at the highest possible resolution. With these synthetic log networks described above, model is able to generate well log suite for undrilled wells of any directional configuration.

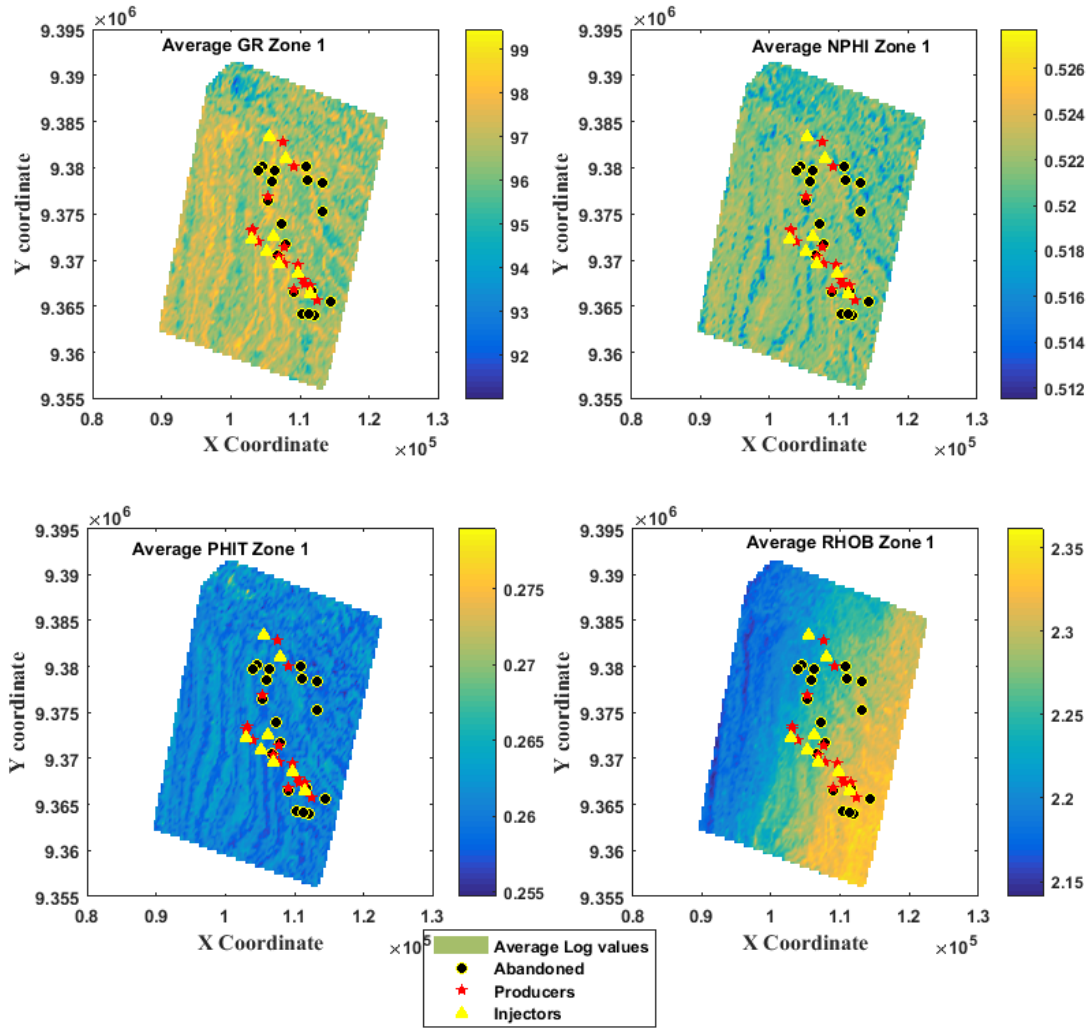

Figure 6.25. Average logs generated from log cubes for Zone-1

6.1.1 Washed out log predictions

Synthetic well log module can aid in completing the log suite at any given location. For instance in Figure 6.26: PHIT log is washed out in zones one and two. Using the network the log can be reconstructed as indicated by the ANN based prediction outline by red curve.

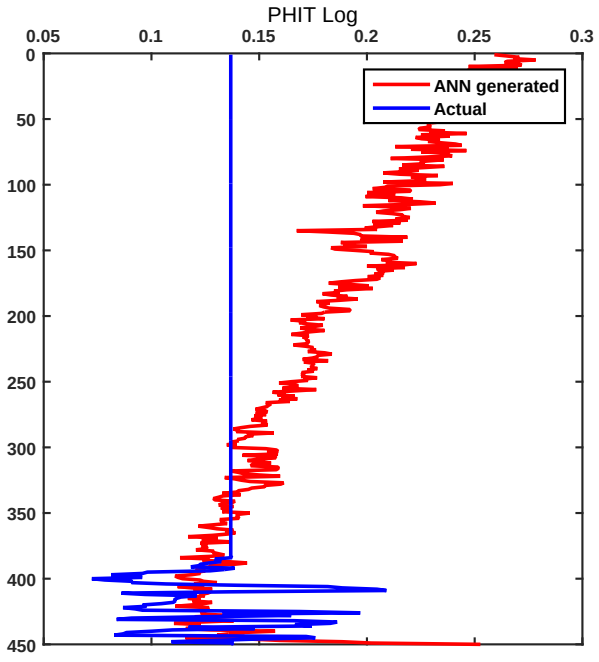

Figure 6.26. Well #28 washed out log reconstructed using synthetic log network

The complete log suite for all the 38 wells is completed using the synthetic well log network module. All the 157,348 points of seismic trace data are used to develop synthetic well logs assuming a vertical well passing through each of these points with well head at X, Y coordinate of these seismic traces. These synthetic logs are further used to predict production profiles with a hypothetical well at each of these location to result in spatial oil, gas and water distribution maps that is discussed in Section 6.3

6.2 Monte Carlo Simulations

The goal of net pay determination is to eliminate nonproductive hydrocarbon rock intervals, and calculations provide a solid basis for quality 3D reservoir characterization with quantitative hydrocarbons in place.

Oil in place calculations require accurate estimation or determination of net pay which could be obtained by point by point summation of the producing reservoir

rocks on the basis of core descriptions and log characteristics. Typical approach includes determining net pay by applying cut offs to gamma ray, porosity and resistivity logs. Other approaches are mobility or permeability based cutoff that allows a reservoir engineer define net pay by applying a fluid flow cutoff. These mobility based calculations are different based on the reservoir fluid being produced. For oil reservoirs these cutoffs generally tend to be higher than gas reservoirs. The choice however also depends on the relative permeability effects and interwell connectivity. For this study, gamma ray, and resistivity are used to establish net pay, since permeability logs are not being predicted. An assumption pertaining the logs used in building synthetic well log architectures are normalized is made. The net pay cutoff calculations are verified with the exiting well net pay summaries. Gamma ray cutoff of 50 API along with resistivity cutoff of 4 ohm-m is established as a norm for this field.

In order to accurately estimate the reserves in place, one needs to account for all the uncertainties that exist within the data being used. A Monte Carlo simulation is a stochastic way of estimating a parameter given the variables used in prediction has uncertainty. Probability density functions (PDFs) are computed for each of the variables and are fed to the Monte Carlo simulation algorithm for obtaining the cumulative distribution function for original oil in place ($OOIP$) at each of the locations present in the field. $OOIP$ is calculated with the help of following equation 6.1:

$$OOIP(bbls) = 7758 \times A(acres) \times netpay(ft) \times \phi \times \frac{1 - S_{wi}}{B_{oi}(RB/STB)} \tag{6.1}$$

$$OOIP(\frac{bbls}{acre - ft}) = 7758 \times \phi \times \frac{1 - S_{wi}}{B_{oi}(RB/STB)} \tag{6.2}$$

To calculate *OOIP* per unit *acre-ft*, porosity ϕ, initial water saturation S_{wi} and initial volume formation factor B_{oi} values need to be estimated. Using the synthetic logs developed earlier, it is possible to estimate these parameters for the layers contributing to net pay.

Porosity, ϕ is computed from the PHIT log, initial water saturation, S_{wi} is calculated using the Archie equation as described in equation below:

$$S_w = \frac{a}{\phi^m}\left(\frac{R_w}{RESD}\right)^{1/n} \tag{6.3}$$

where, S_w - water saturation, ϕ - porosity, R_w - formation water resistivity, assumed as 0.2 for this field, RESD -observed bulk resistivity, a-a constant (considered 0.81 in this case), m- cementation factor (assumed to be 2), n- saturation exponent (assumed to be 2). Initial oil volume formation factor B_{oi} is calculated based on the average pressure of the pay zone assuming a constant pressure gradient of 0.42 *psi/ft*.

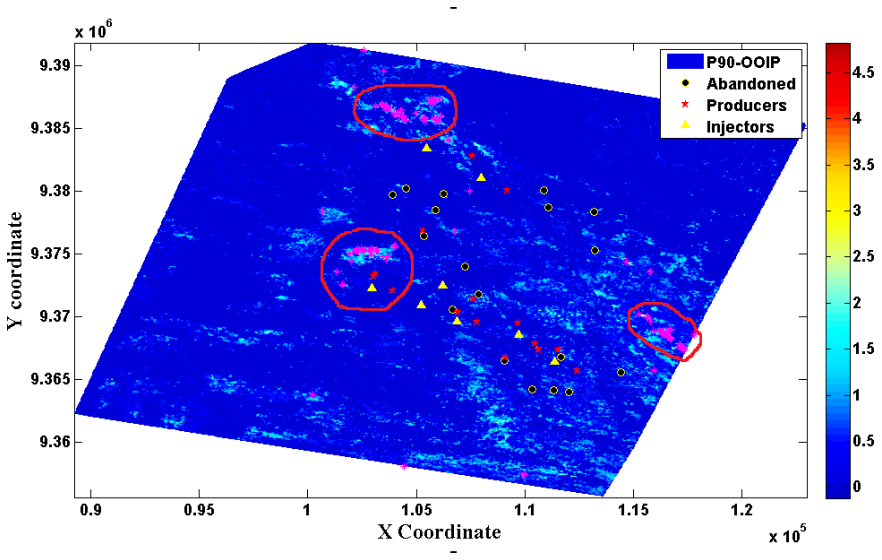

Figure 6.27. Top 100 locations based on normalized P90 OOIP overlaid with net pay maps

P90 (Probability of finding this value is 90%) *OOIP* maps are overlaid with net pay maps to estimate the top 100 locations for potential drilling are indicated in Figure 6.27(Normalized values). Therefore in a given field, if one has to estimate the best location for drilling, it needs to be based on oil in place estimates. Hence the results generated from this exercise are used in finding the optimal locations to drill the infill wells. The locations chosen based on *OOIP* maps generated from this exercise are then evaluated based on various well trajectories to develop the infill well paths. NPV module is used in evaluating the proposed well paths to identify the optimal locations and paths based on five-year production trends.

6.3 Production performance networks

Production performance networks are trained to correlate production data to seismic data and well log data observed at a well location. Seismic data, well log data long with schedule of production have been provided as the input parameters to the network. In the past, most researchers attempted to correlate production data directly with seismic data or well log data independently. In this current work, synthetic well logs provide the additional information required for the model to understand the petro-physical characteristics of a chosen location along with the geophysical data from seismic attributes. Predicting production data through monthly average data points(from 78 months) is attempted. Figure 6.28 shows a good match between model predictions and actual field data. The errors vary between 30-80%. In addition to high errors, this way of correlating might not be able to predict production rates beyond 78 month time period.

The instantaneous flow rate profiles are erratic, hence could not result in a confident fit with any one particular model. The wells in this field are undergoing

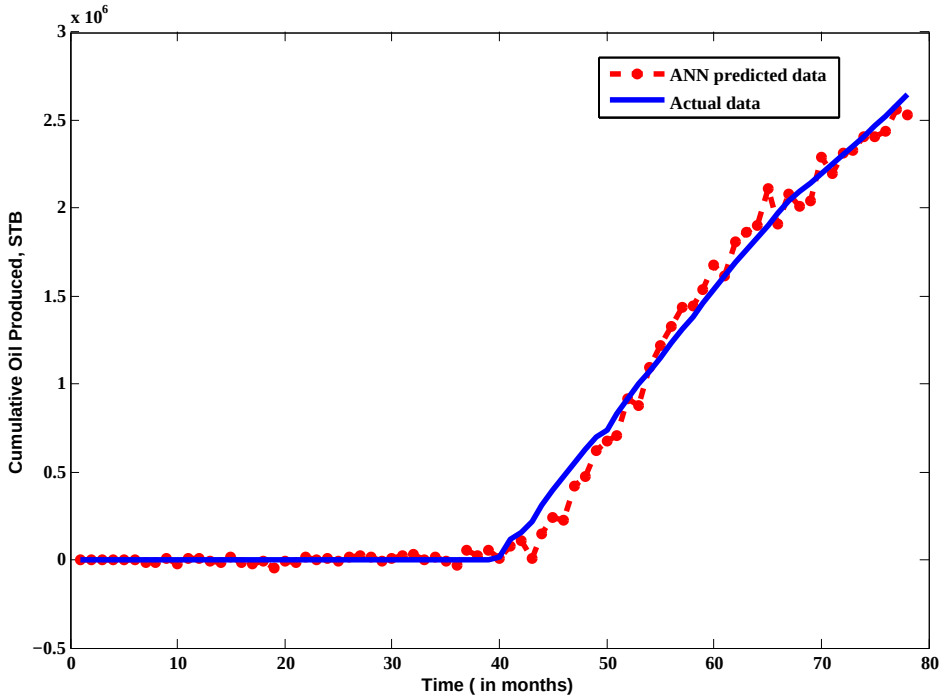

Figure 6.28. Predicting cumulative oil production via monthly rates for Well #27

work-over operations, and injectors simultaneously starting around the producers, hence fitting a flow rate profile lead to erroneous and false estimations of the instantaneous flow rates. Hence cumulative flow rates are subjected to curve fit models to generate appropriate parameters. The model used to fit the flow rates has already been presented in Chapter 5. This process has not only resulted in improved correlations, but also the ability of model to forecast oil, water, gas productions. It is essential to incorporate the input parameters that have an influence on fluid flow from a given well. On iterating, it was found that the following parameters listed as network inputs below have resulted in the optimal correlations established as a part of production performance module.

Network inputs:

- Seismic attribute data for all the three zones

- Well log data for the three zone and five log types
- Production schedule with a binary values of one and zero indicating the activity status of the well in any given month starting 2006 until 2012.
- Production well interference from the nearby wells: This is computed at each month with the Equation 6.4

$$Interference_{j^{th}well} = \sum_{i=1}^{Numberofproducers} q_{cumoil-i^{th}well}/d_{ij} \tag{6.4}$$

  where, d_{ij} is the distance between wells i, and j

- Injection well interference from the nearby wells: This is computed at each month with the Equation 6.5

$$Interference_{j^{th}well} = \sum_{i=1}^{Numberofinjectors} q_{cumwater-i^{th}well}/d_{ij} \tag{6.5}$$

  where, d_{ij} is the distance between wells i, and j

- Completion parameters

  Completion parameters include the following items listed in Table 6.1

Table 6.1. Completion parameters used

S.no	parameter	units
1	Total length of perforated interval	ft.
2	First perforation measured depth	ft.
3	First perforation TVD SubSea	ft.
4	Bottom perforation measure depth	ft.
5	Bottom perforation TVD SubSea	ft.
6	Net reservoir	ft.
7	Net pay	ft.
8	Total depth	ft.
9	KB	ft.

There are 78 inputs each from production and injection well interference terms that correspond to number of months of total production in the field.

Network outputs: Parameters a, b, c assuming the cumulative oil production follows a trend of $q_{cum} = at^b + c$ (where t is in days, q_{cum} is in STB)

The following Figure 6.29 provides a schematic for oil and gas production performance networks built in this work. For water production performance, 12 months of production data is predicted instead of curve fit parameters. Further explanation provided in section 6.3.3.

6.3.1 Oil production performance network

Fourteen of the 20 wells consistently had all the data and made up the sample data set. Out of which 12 are used for training, 1 for validation and 1 for testing in a given numerical trial. The zero flow rate part as indicated in the plots is given as

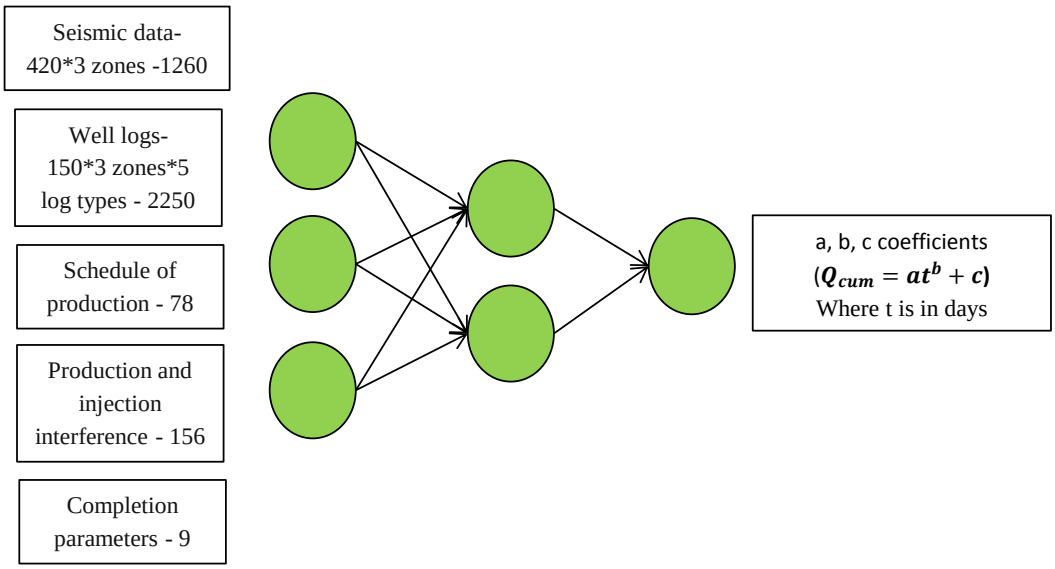

Figure 6.29. Schematic for the production performance networks

an input parameter. The comparison is only made for the time period after the wells are subject to production. In the input functional links, production schedule with binary parameters of 1 or 0 are provided for informing the network of well's operating conditions. The red curve in these plots indicate the curve generated through the model predicted parameters *a*, *b*, *c*. The blue curve depicts the actual field oil production observed.

Mean average testing error of 21% is observed between the ANN cumulative oil predicted and observed cumulative oil produced in the field. On the contrary, if the monthly cumulative oil rates were predicted, the optimal architecture resulted had an average blind test error of 30%. The output parameters used in building the optimal architecture are curve fit parameters *a*, *b*, *c*. Magnitude of errors in prediction of parameters do not directly correlate with the magnitude of deviation in oil cumulative flow rates. Hence, error in the cumulative oil prediction is used to

find the optimal network architecture. The negative flow rate values observed is an artifact of the error in prediction of parameter 'c'. In trials, where the error in parameter prediction was used as a metric in establishing optimal architectures, it was found small errors in parameter b had a significant impact on the blind test errors on comparison with parameters a and c. So in order to constrain the output vector, mean monthly production is used as a functional link in outputs.

The summary of the best architecture is outlined in Figure 6.30. Four hidden layers with 47, 33, 46 and 34 neurons with transfer functions *tansig*, *tansig*, *tansig* and *logsig* was found to be the optimal architecture. The blind testing errors observed while testing the optimal architecture is indicated in Figure 6.31. Most of the error contribution has consistently been coming from parameter 'c' because of which some of the test cases indicate a negative production at the first month due to the nature of curve fit parameters.

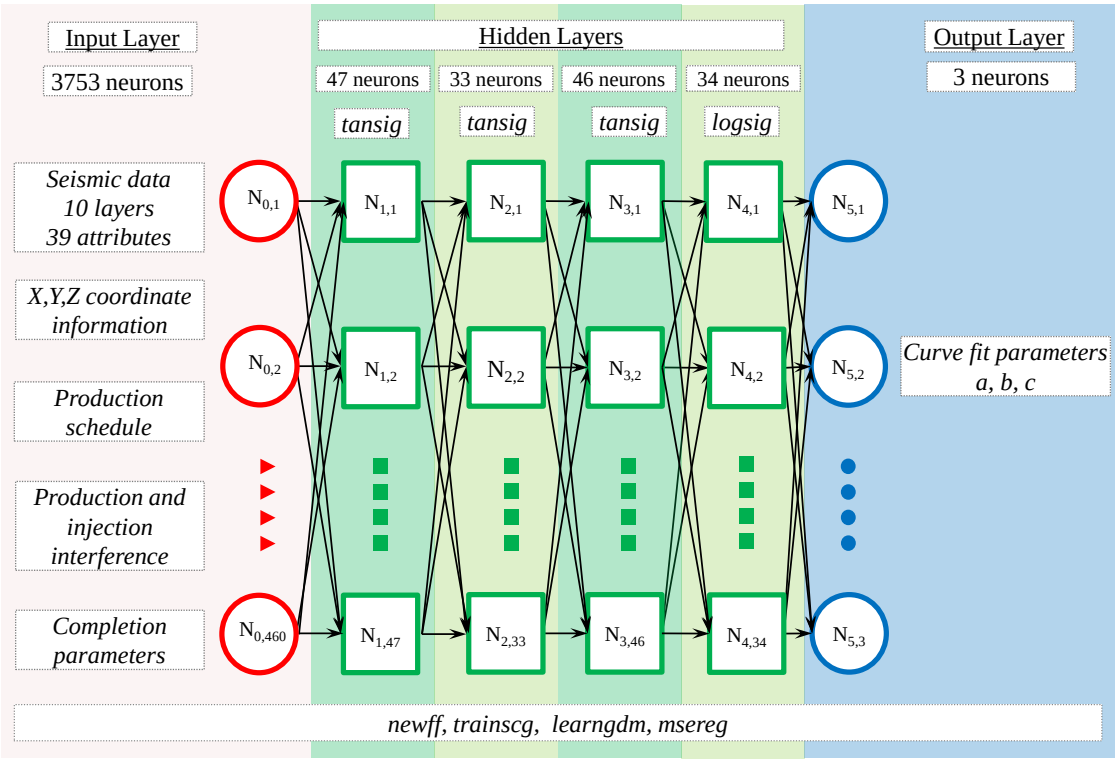

Figure 6.30. Cumulative oil production performance network architecture

The testing errors ranged between 5% to 35% (see Figure 6.31) while generating the optimal architecture for predicting cumulative oil production.

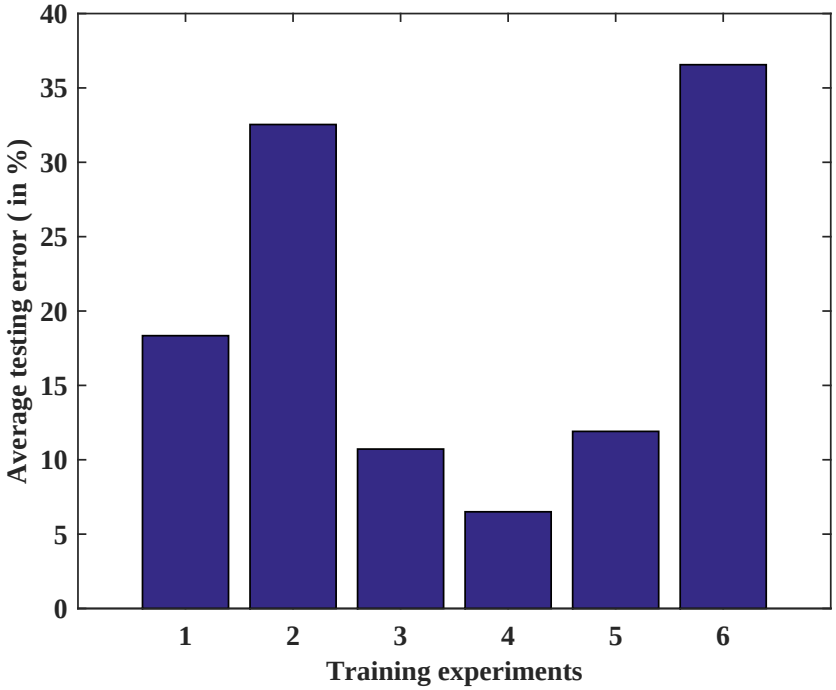

Figure 6.31. Blind testing errors observed for oil production network

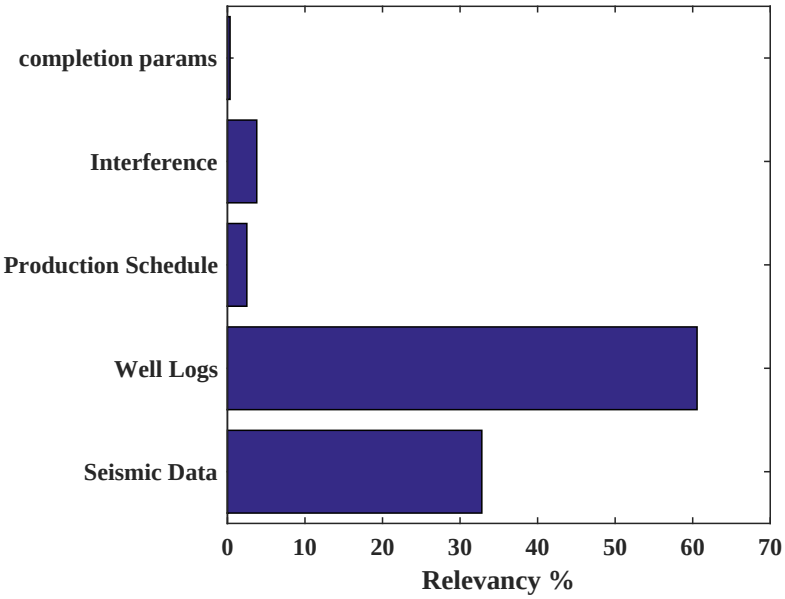

Figure 6.32. Relevancy of input attributes

From Figure 6.32, it is evident that well logs have a significant contribution to the oil production performance. They are found to be 60% relevant, seismic data is second most relevant input attribute at 32%.

Gamma ray log as indicated in Figure 6.33 is about 13.5% relevant in predicting cumulative oil production. This is intuitive due to the fact that information on geology informing the network of sand/shale presence is crucial in predicting the oil production.

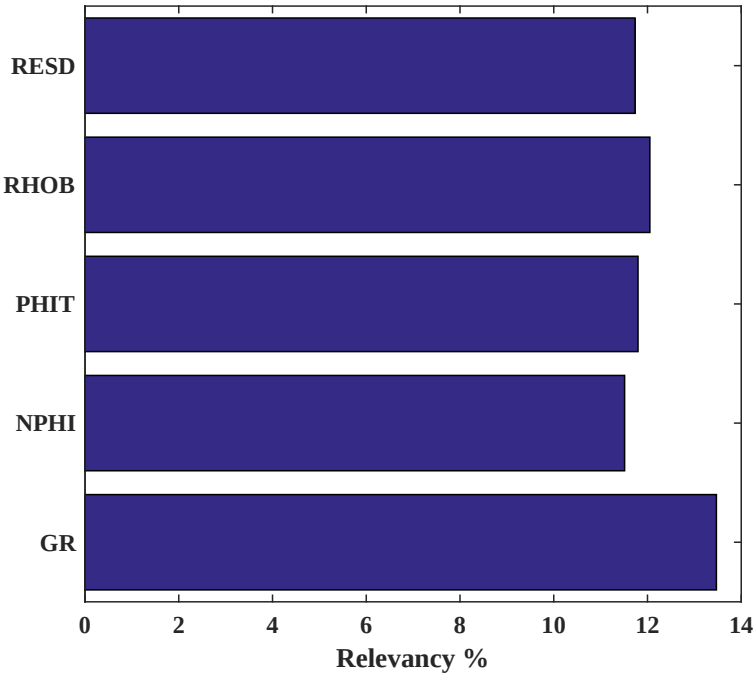

Figure 6.33. Relevancy of well logs

The best case, worst case, and median error case are indicated in Figures 6.34 through 6.36. In Figure 6.34, zero flow rate till end of month 51 is provided via the schedule in inputs. Curve fit parameters a, b, c are predicted through the expert system based on network inputs as discussed earlier. Using those curve fit parameters, red curve is generated for the active production months 52 till 78. Blue curve indicates the cumulative oil production data observed in the field.

Cumulative oil produced in STB is compared in the given plot. Well #5 resulted in least error while testing for optimal architecture. Instantaneous error computed at each month is displayed in Figures C.16 to C.18.

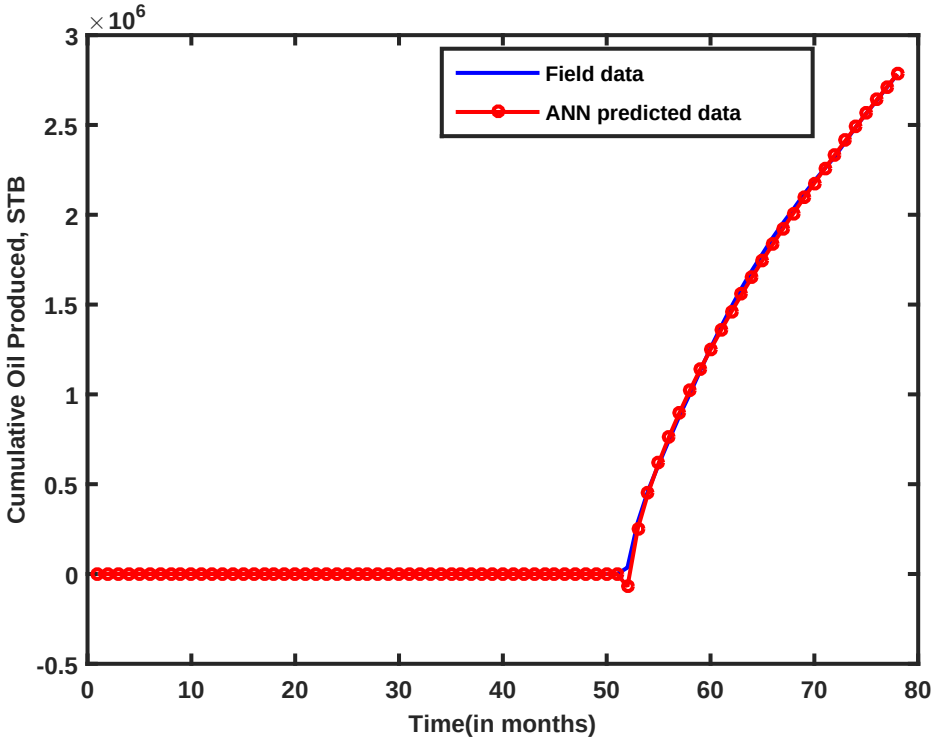

Figure 6.34. Well #5 blind testing best case - an error of 8% is observed

Well# 5 has been the best blind testing case. An average error of 8% is observed in predicting the cumulative oil production through model. A large contribution to the error comes from the first month production data, since the prediction is made through curve fit parameters. This well has been operating steadily with no major interventions, hence the model could accurately capture the production characteristics at this well location through seismic data, and well log data along with other functional links.

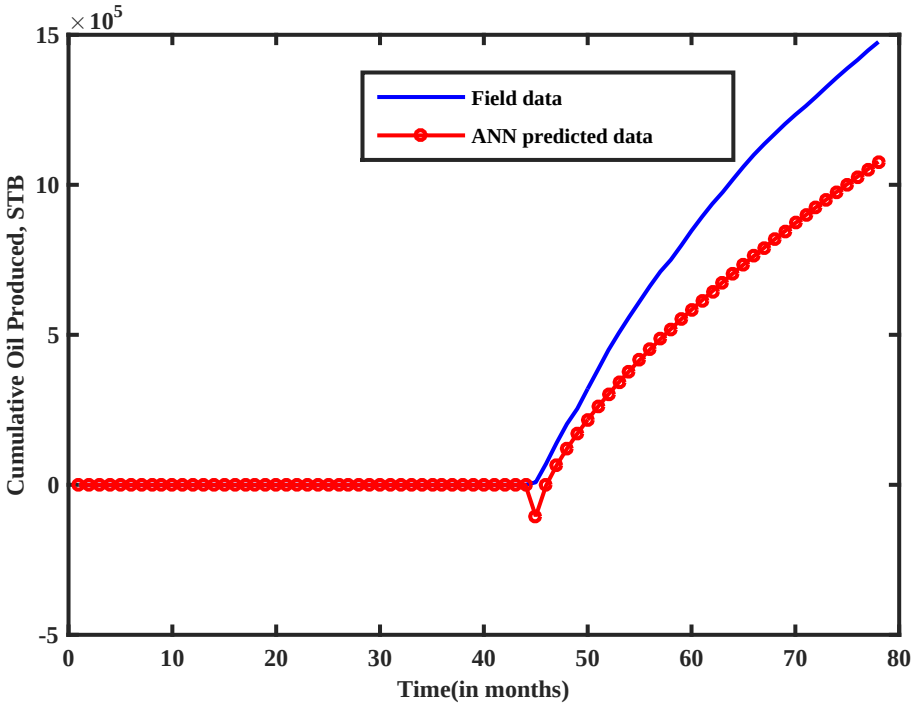

Figure 6.35. Well #17 blind testing worst case - an error of 45% is observed

For Well #17 (refer Figure 6.35), the model has under predicted the production data by about 45%. This location has an unusually high gas oil ratio. That probably could mean that this is producing from a different reservoir than its neighboring wells. With time, model predictions deviate from actual field data owing to smaller 'b' value predicted by model. The deviation is highest at the first two data points post production, where the model predicted extremely low values that resulted in large errors. In case of Well #27 (refer Figure 6.36), the model has over predicted the production data by about 32%. This can be attributed to two reasons, first is that a work-over operation that happened three months after the start of production and secondly, the interference effects of nearby injection well may not be well understood by the model. This well is at the bottom most fringe of reservoir and is the southernmost of all the wells in the existing dataset. In the later part of the well, an additional zone was re-completed. All these conditions

add to the complexity of the resultant production profile. One of the assumptions made in building the model was that all perforations are available to flow at all times. It is possible because of the assumption made in model building process, the expert system has consistently over predicted the cumulative oil production in this case. By adding new wells to the existing data sets, the model can be improved by having supplemental information.

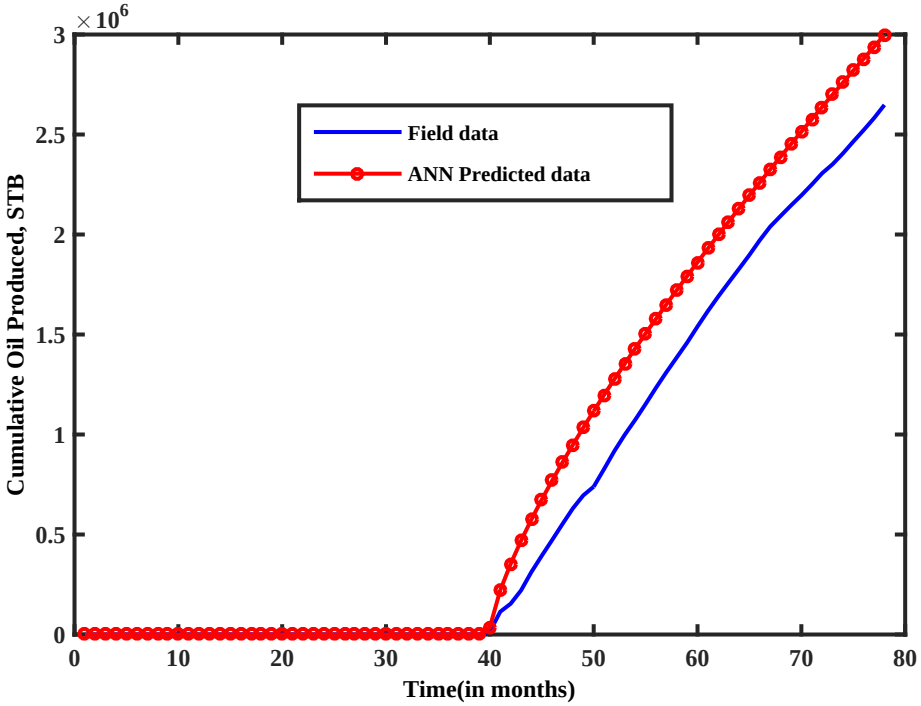

Figure 6.36. Well #27 blind testing median case - an error of 32% is observed

Rest of the cases are presented in Appendix D.

6.3.2 Gas production performance network

The optimal architecture found for cumulative gas production performance network is outlined in Figure 6.37. Four hidden layers with 42, 37, 44 and 26 neurons each and *logsig*, *tansig*, *logsig*, *logsig* were the respective transfer functions

associated with these layers. Output layer has *purelin* function as the transfer function. The zero flow rate part as indicated in the plots is given as an input parameter. Mean average error from blind testing results is at 32%.

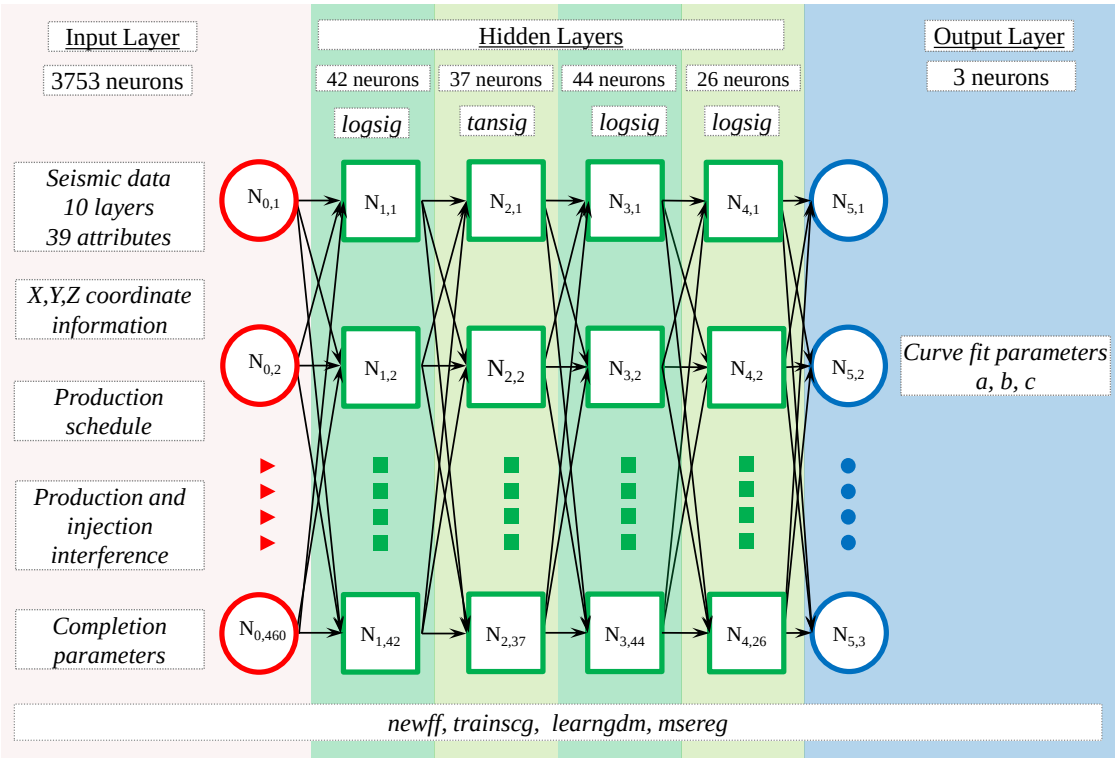

Figure 6.37. Cumulative gas production performance network architecture

The errors encountered while testing the optimal architecture are displayed in Figure 6.38. The testing errors ranged between 6% to 55%. The relevancy of the input attributes is shown in Figures 6.39 and 6.40. Well logs remained to be the most important input attribute while correlating cumulative gas production with seismic data, well logs, interference and completion parameters. All five well logs together have 61.5% relevancy as indicated by the weights of the input neurons. Seismic data at 33.1% is the second more relevant input attribute. Interference attributes contributed to approximately 3.5% of the input neuron weights.

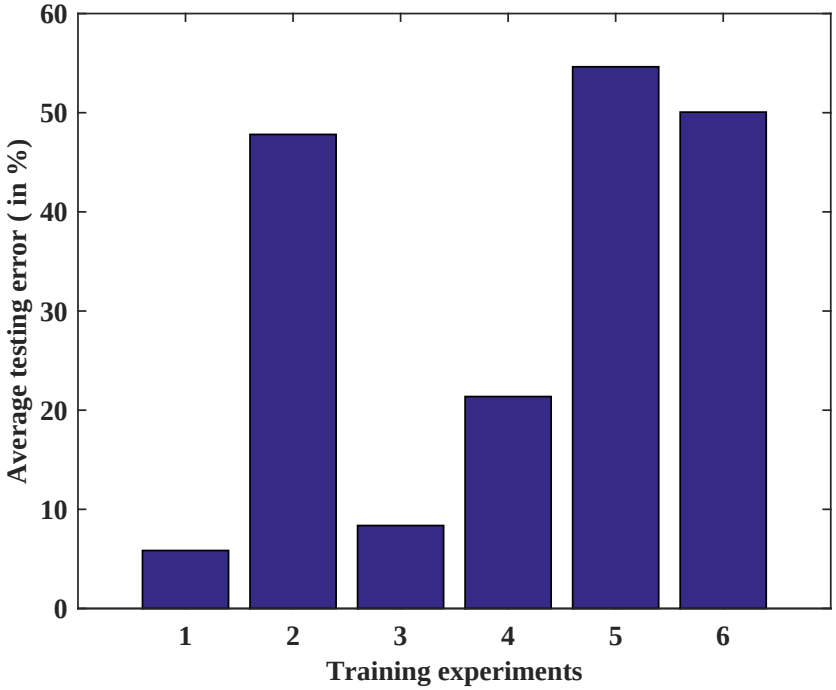

Figure 6.38. Blind testing errors observed for gas production network

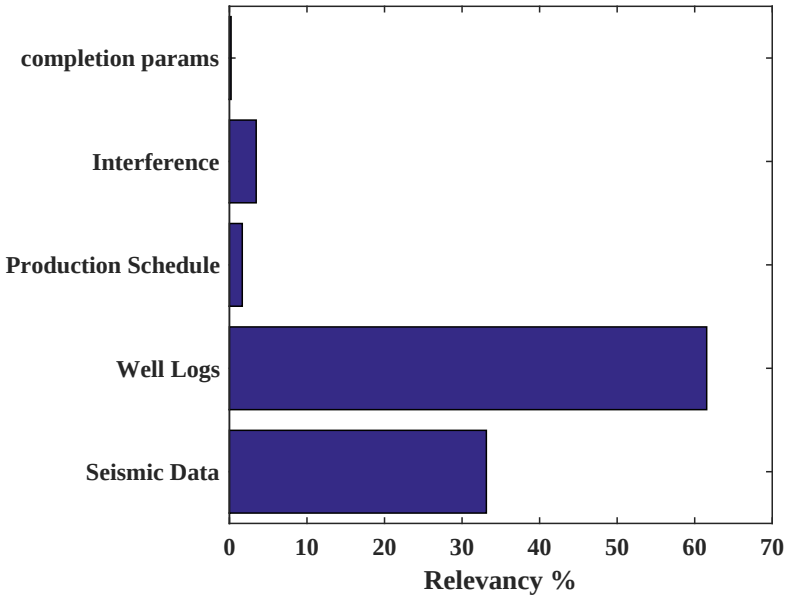

Figure 6.39. Relevancy of input attributes

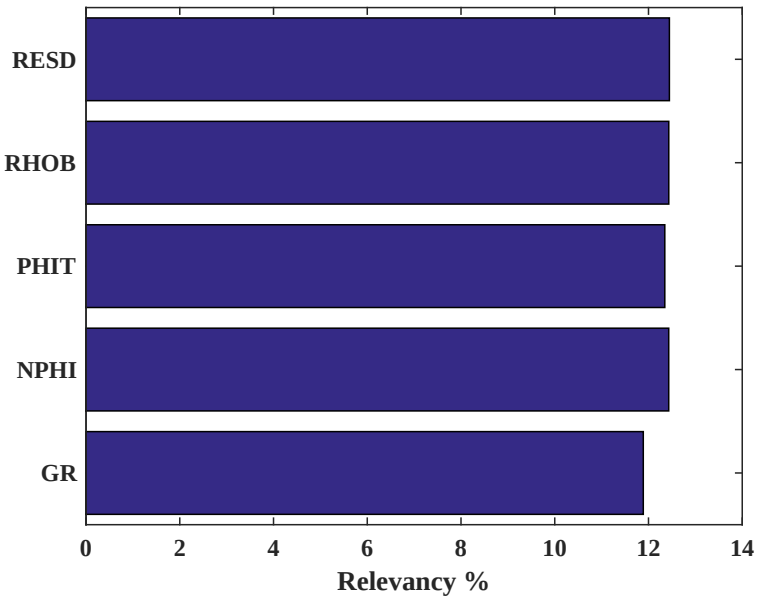

Figure 6.40. Relevancy of well logs

The best, worst and median blind testing cases are indicated in Figures 6.41 to 6.43. It is noteworthy to see the good correlations obtained in predicting cumulative gas production inspite of varying gas oil ratio throughout the field. In case of Well#17, the bottomhole pressure at the end of 15 months of production has dropped to less than bubble point pressure. Owing to the two phase region, more gas is being produced at the later stages of production. There has been an intial decrease in GOR in this region from 9,000 *SCF/STB* to 7,000 *SCF/STB* and in later times, it has increased to values greater than 10,000 *SCF/STB*. Instantaneous error plots computed at each month for all the test cases are shown in Figures C.19 to C.21.

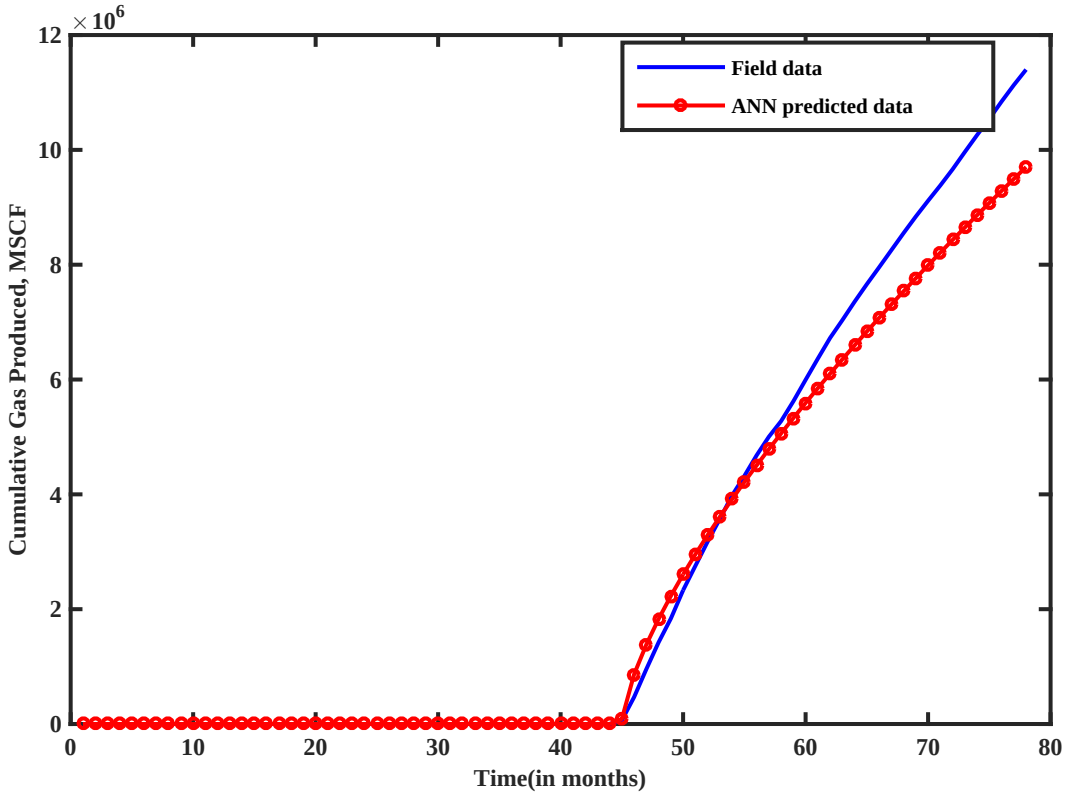

Figure 6.41. Well #17 blind testing best case - an error of 14% is observed

The worst blind test case as displayed in Figure 6.42 is observed in predicting cumulative gas production from Well #21. Well # 21 has declining GOR from 2,000 *SCF/STB* to 800 *SCF/STB* at the later times of production. The network was not able to capture the decline in GOR, due to which model predicted higher gas production at later times for this well.

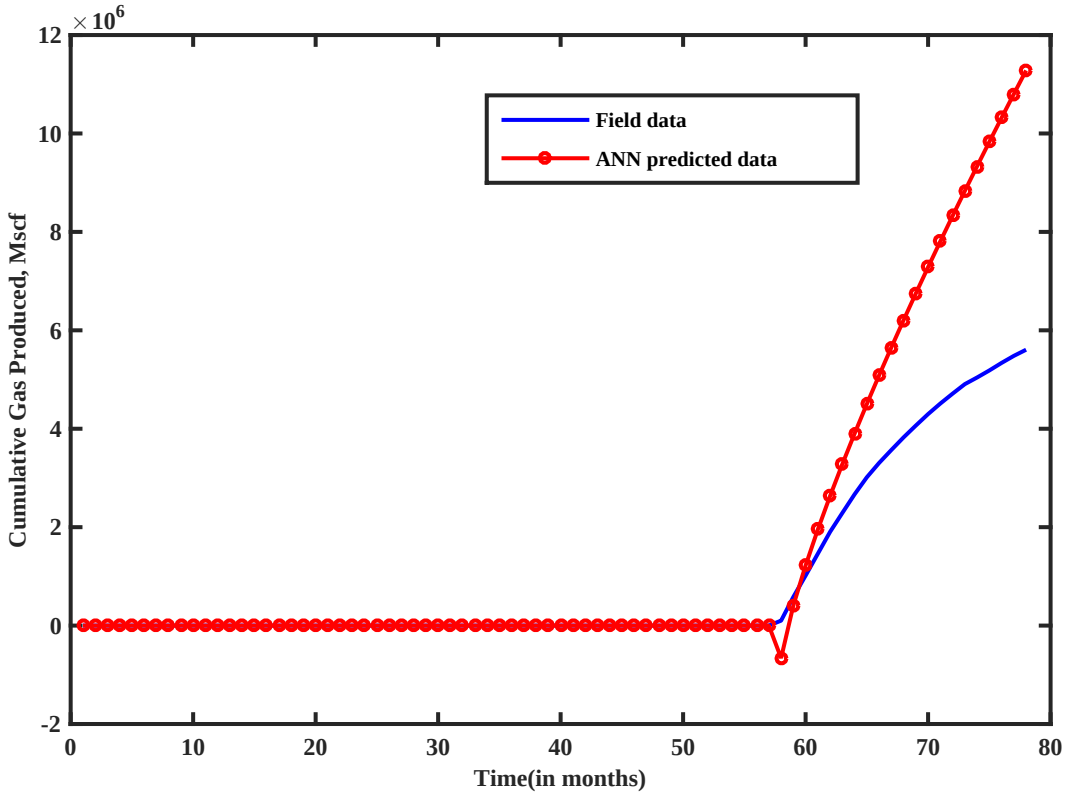

Figure 6.42. Well #21 blind testing worst case - an error of 90% is observed

The median blind test case is cumulative gas production from Well# 27. An average error of 20% was observed while predicting the cumulative gas rates. Errors are mostly from the initial part and later parts of the production. The initial error is due to the parameter 'c' being under-predicted. The gas oil ratio has been highly fluctuating in this region owing to interference from neighboring injectors and producers.

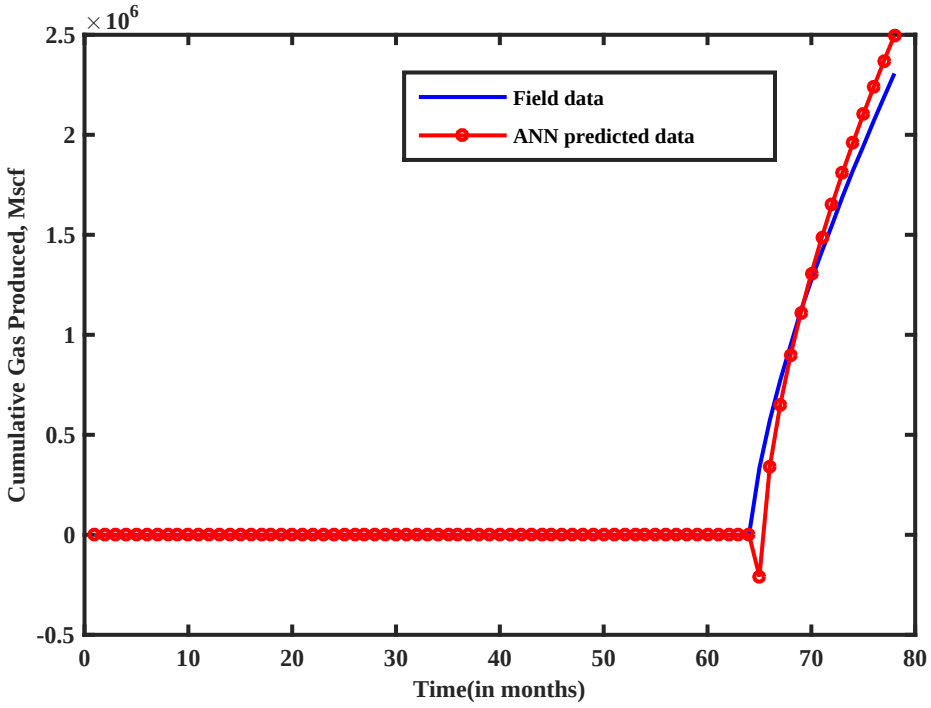

Figure 6.43. Well #27 blind testing median case - an error of 20% is observed

6.3.3 Water production performance network

The curve fit parameters even though have obtained a good correlation coefficient, the parameters a, b, c have a large range because of which the ANN model could not capture the coefficients effectively. Errors consistently higher than 200% were found while trying to establish an architecture. Water cut behavior has been influenced by nearness of a given well to oil water contact and the injectors interference. The water cut behavior of the production wells is indicated in Figures D.3 to D.6(in Appendix D. They clearly indicate how water production has been erratic with time. So fitting it through a curve fit procedure did not yield satisfactory results. Hence 12 months of water production data was used as the target data set for training water production performance networks.

The optimal architecture correlating cumulative water production consists of five hidden layers with 15, 50, 10, 47, and 11 neurons and transfer functions *logsig*, *logsig*, *tansig*, *tansig* and logsig associated with them. The output layer with 12 hidden neurons is fed through *purelin* transformation.

The errors obtained while testing this architecture are given in Figure 6.44:

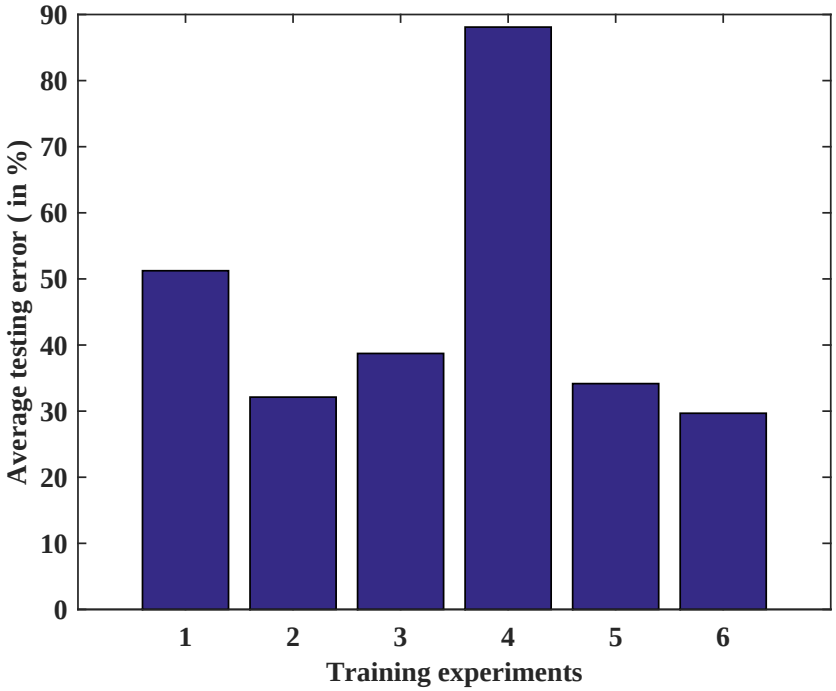

Figure 6.44. Blind testing errors observed for water production network

The input attribute relevancy plots indicated in Figure 6.45 show that well log data is consistently the most important attribute in the production performance networks. Gamma ray log is slightly the more relevant log compared to other logs in this network.

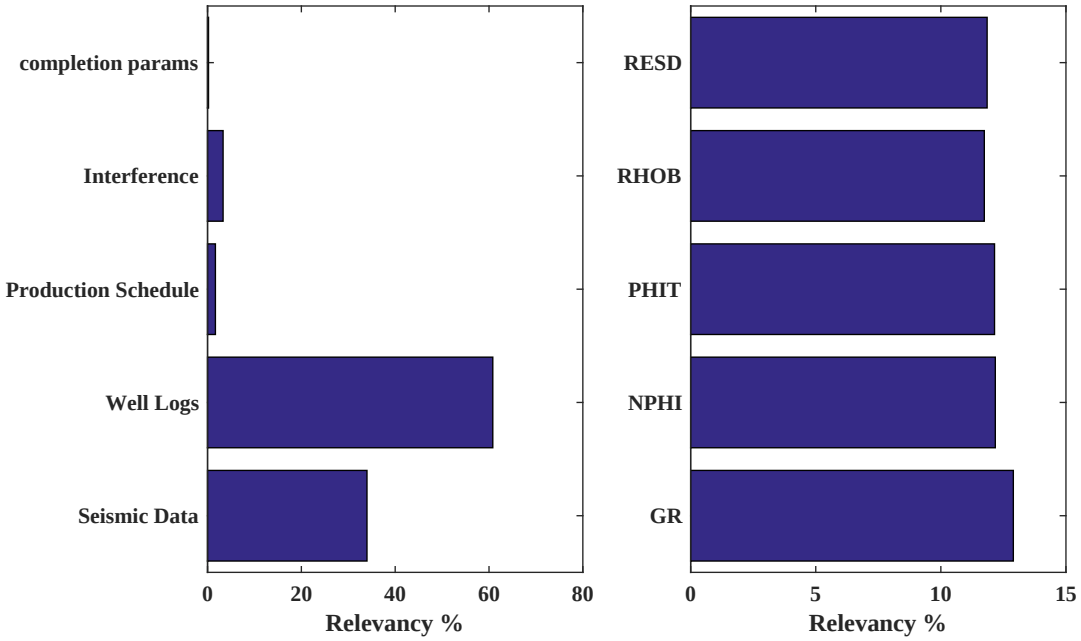

Figure 6.45. Relevancy of input attributes for water network

Well#30 has been re-completed to a different reservoir after one year. That could be one of the reasons for error in predicting water production. First reservoir produced at almost twice the amount of water oil ratio(WOR) as compared to the second reservoir. That partly explains the reason for consistently higher predictions of water by the model. Instantaneous error plots showing error at each month for all the test cases are displayed in Figures C.22 to C.24.

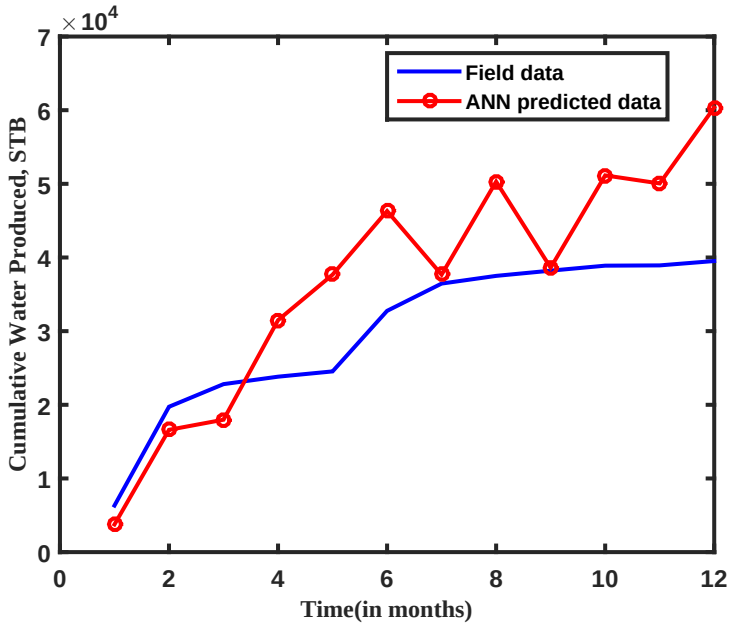

Figure 6.46. Well #30 blind testing best case - an error of 30% is observed

The worst case blind test comes from Well #31. Extremely high water production has been predicted for this well as shown in Figure 6.47. The results can still be improved. This well has an unusually low water production compared to the neighboring wells. This is the southernmost well in the field. The model could not accurately capture the extremely low water cut in this well.

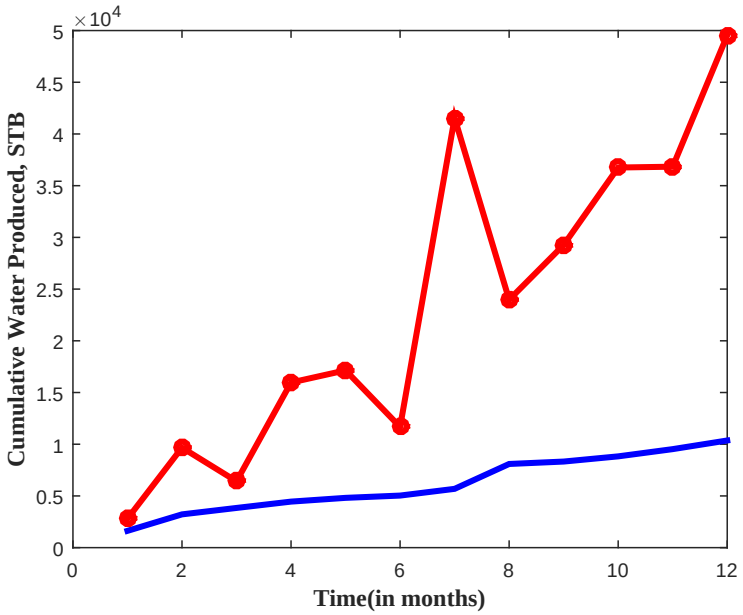

Figure 6.47. Well #31 blind testing worst case - an error of 70% is observed

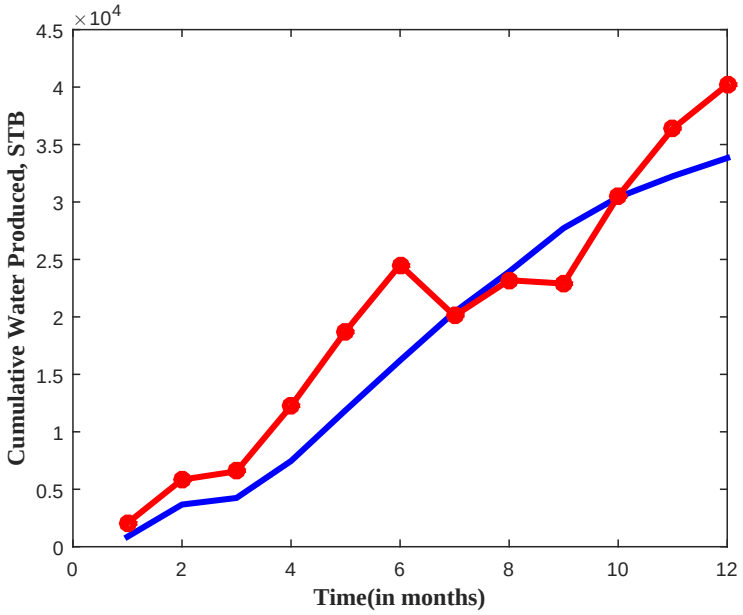

Figure 6.48. Well #21 blind testing median case - an error of 40% is observed

The decrease in cumulative flow rate is not a physical solution. This is a statistical artifact of predicting each month's production by the network. Additional

trials are underway to improve the water production performance module to reduce the blind test errors. Innovative ways of incorporating injection effects are being studied.

6.4 Directional well log generation

One of the principal objectives of the work is to map directional(horizontal) well logs to their corresponding seismic attributes and be able to correlate with them. With the use of synthetic well log module, the correlation is established as discussed in section 6.1. Once a user provides a trajectory to the tool developed in this work, the work flow as demonstrated in Figure 6.49 is adopted in generating the directional log signatures. Well log values from each of the vertical wells drilled at the X, Y locations are used as input logs which are further resampled at the ellipses indicated in the Figure 6.49 to obtain the directional well log suite.

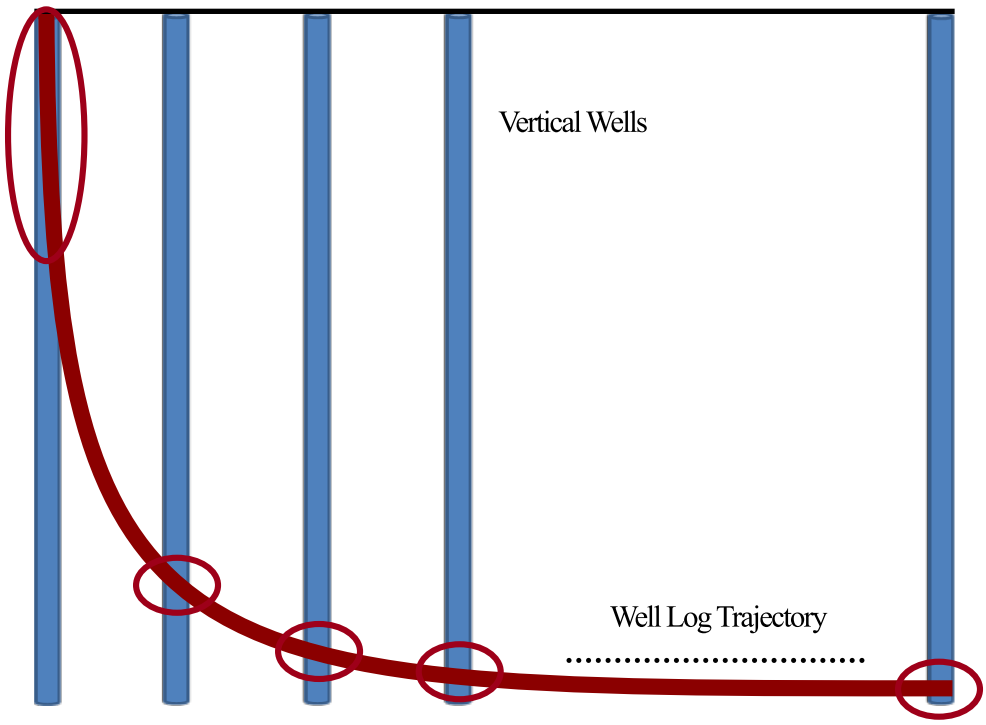

Figure 6.49. Horizontal well log generation workflow

For each zone, X, Y coordinates for 150 points along the trajectory are computed, and vertical synthetic well logs are generated. Based on the depth vector, the directional log values are picked from the vertical well log sections. This ensures the highest resolution of log to be generated using the workflow.

There are multiple ways of specifying a trajectory for a wellbore. In this work, the acceptable inputs are well top, kick off point and end of lateral X, Y, Z coordinates. Once the kick off point is specified the trajectory of wellbore is automatically computed using biggest arc that can be fit to minimize the length of curved part of the wellbore.

Once the location is identified as indicated in Figure 6.50, various directional well log architectures indicated in plot on the right are tested for evaluating the best production profile. As observed from Figure 6.51,the best trajectory at the

given location is given by profile four. Once all the potential well locations are identified, NPV analysis is performed to optimize the drilling schedule.

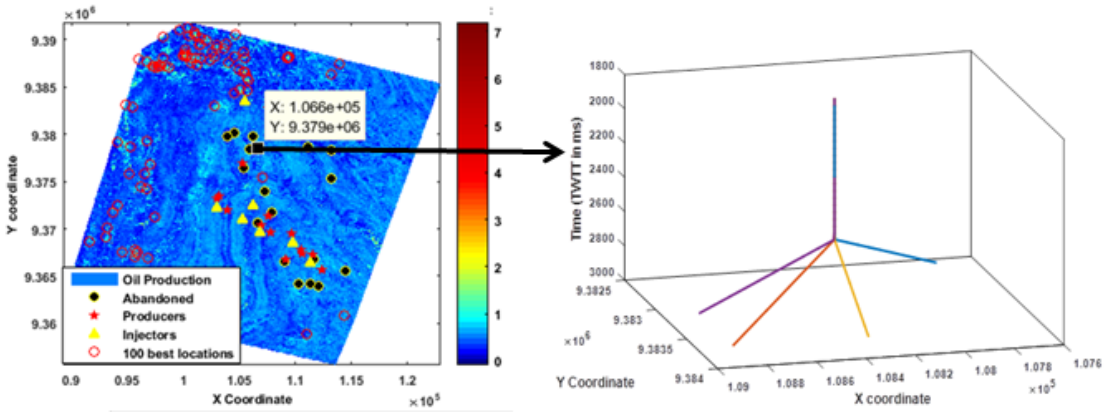

Figure 6.50. Horizontal well log evaluation

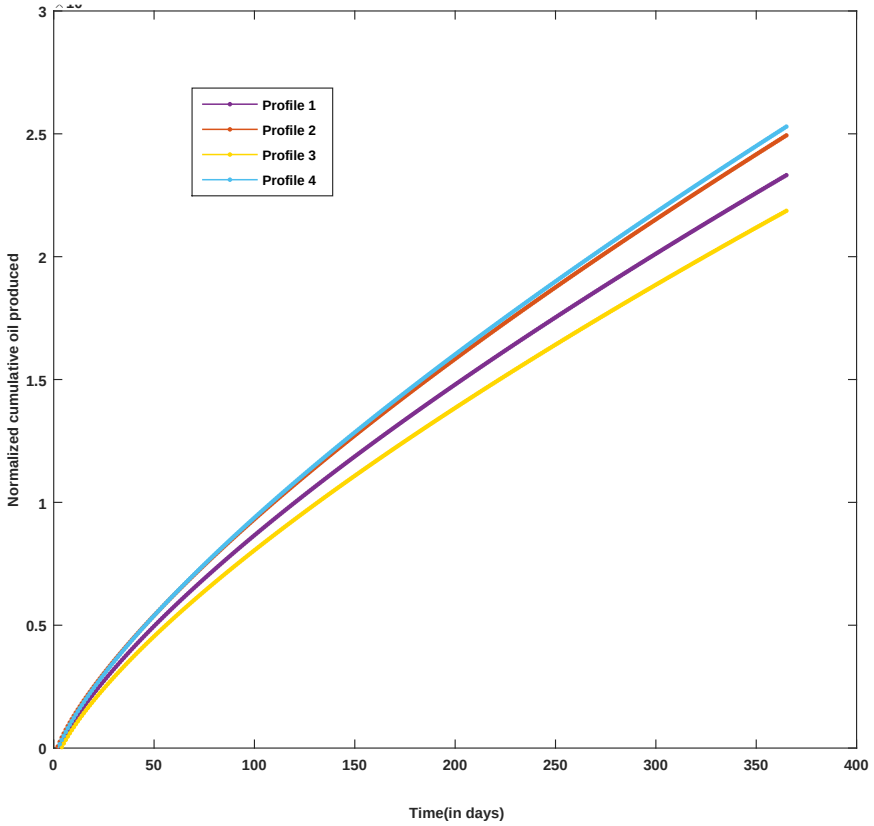

Figure 6.51. Production profiles of chosen well log trajectories

6.5 Net present value (NPV) analysis

NPV is net present value calculated by adjusting revenue with discounted cash flows. In calculating flow rate from the horizontal wells, the production performance module predictions are used rather than considering wellbore flow dynamics and related factors that affect the fluid flow performance. The minimum and maximum lengths of the horizontal well are considered from the history of the field. Minimum total drilled depth for a directional well in this field is 13,388 *ft* and maximum is 19,583 *ft*. Therefore, the range of the lateral length explored is 3,000 *ft* to 9,000 *ft* for evaluating the NPV of the well to be drilled. There are other factors that determine the economics of the horizontal well as follows:

- Drainage area
- Friction loss
- Productivity index
- Early time production increase
- Reserves increase

But in this work, only the increase in revenue based of oil production is considered. Well construction costs can be estimated either through *JAS* method or *MRI* method (Syed, 2014).

Models to estimate well cost: There are several ways of estimating the drilling cost of a directional well in deep water environments. Mechanical risk index (*MRI*) was first developed in late 1980s by Conoco engineers to compare offset drilling data for a collection of offshore wells in Gulf of Mexico (Kaiser, 2007). In mid 1990's, Dodson modified the MRI using key drilling factors. Through time, this method

has undergone changes to incorporate new factors into qualitative indicators. This model is defined in terms of four component factors and a weighted composite key drilling factor. The component factors are described in terms of six primary variables and key drilling factor represents composite impact of 14 qualitative indicators. Six primary variables of the MRI include the total measured depth (TD), vertical depth (VD), horizontal displacement (HD), water depth (WD), number of casing string (NS), and mud weight at total depth (MW). All distances are measured in feet. Mud weight is reported in pounds per gallon (PPG). Casing is one of the more important factors that can cost up to 10-20% of a completed well.

$$\begin{aligned}
\varphi_1 &= (\frac{TD+WD}{1000})^2, \\
\varphi_2 &= (\frac{VD}{1000})^2.\frac{TD+HD}{VD}, \\
\varphi_3 &= (MW)^2.\frac{WD+VD}{VD}, \\
\varphi_4 &= \varphi_1.\sqrt{NS+\frac{MW}{NS^2}}.
\end{aligned} \tag{6.6}$$

The units of φ_1 and φ_2 are ft^2; the unit of φ_3 is ppg^2 ; the unit of φ_4 is $ftppg^{0.5}$. Each component factor is nonlinear in the primary variables.

Key drilling factors are defined to capture drilling characteristics that are encountered or are expected to be encountered, but not described by the component factors. The key drilling factors are user-defined qualitative variables φ_i that are assigned an integer-valued weight $\varphi_i(w)$ according to the occurrence of the condition and degree of complexity. The composite key drilling factor is determined by the sum of the drilling factor weights:

$$\psi = \sum_{i=1}^{14} \psi_i(w) \tag{6.7}$$

where the variables and corresponding weights are as follows:

ψ_1= horizontal section ($\psi_1(w) = 3$),

ψ_2= J-curve directional($\psi_2(w) = 3$),

ψ_3= S-curve directional($\psi_3(w) = 2$),

ψ_4= subsea well installed($\psi_4(w) = 2$),

ψ_5= H2S/CO2 environment($\psi_5(w) = 1$),

ψ_6= hydrate environment($\psi_6(w) = 1$),

ψ_7 = depleted sand section($\psi_7(w) = 1$),

ψ_8 = salt section($\psi_8(w) = 1$),

ψ_9 = slimhole($\psi_9(w) = 1$),

ψ_{10} = mudline suspension system installed($\psi_{10}(w) = 1$),

ψ_{11} = coring($\psi_{11}(w) = 1$),

ψ_{12} = shallow water flow Drilling Cost and Complexity Estimation Models 11 potential($\psi_1 2(w) = 1$),

ψ_{13} = riser less mud to drill shallow water flows($\psi_{13}(w) = 1$),

ψ_{14} = loop current($\psi_{14}(w) = 1$).

$$MRI = (1 + \frac{\psi}{10}).\sum_{i=1}^{4} \varphi_i \tag{6.8}$$

The protocol followed is illustrated with the example given below:

1. Specify the well characteristics encountered/expected: e.g., TD=15,000 ft, WD =150 ft, VD=13,800 ft, HD =2500 ft, MW=16 ppg, NS=6

   Specify the risk factors encountered/expected ; e.g., : ψ_1= horizontal section, ψ_3 = S-curve directional, ψ_7 = depleted sand section, ψ_9 = slimhole, ψ_{12} = shallow water flow potential

2. Compute component factors and key drilling factors: :$\varphi_1 = 229.5$, $\varphi_2 = 241.5$, $\varphi_3 = 258.5$, $\varphi_4 = 582.6$, $\psi = 8$.

3. Compute MRI:

$$MRI = (1 + \frac{\psi}{10}).\sum_{i=1}^{4} \varphi_i = 2,362 \tag{6.9}$$

There are other factors like directional difficulty index, proposed by Schlumberger that could be incorporated to further refine the model and obtain precise estimates. These calculations are possible and feasible given the cost of existing wells is known. In this work, since the actual cost of the wells is not known, an alternate approach of revenues generated through five year production is used to compare the well trajectories. Following parameters are used in estimating NPV:

Parameter	Value
Oil cost, in $/per barrel	50
Well cost, in $/per foot	3500
Discount rate, in %	7
Time period, in years	5

The four well trajectories analyzed in horizontal well section are analyzed with respect to the NPV generated by each of the scenarios. The revenues from gas production and costs associated with water disposal is assumed to be zero for a simplified analysis. Construction and capital costs are included in the cost of well per foot. Taxes are assumed to be 10%. Royalty costs are ignored. Revenue thus generated is by sales of oil produced. The fourth log profile has the highest NPV

of 340 million dollars.

$$\sum NetCashFlow = \sum Revenue - \sum Operatingcost - \sum Overhead - \sum ConstructionCost - \sum Captialcost - \sum taxes \tag{6.10}$$

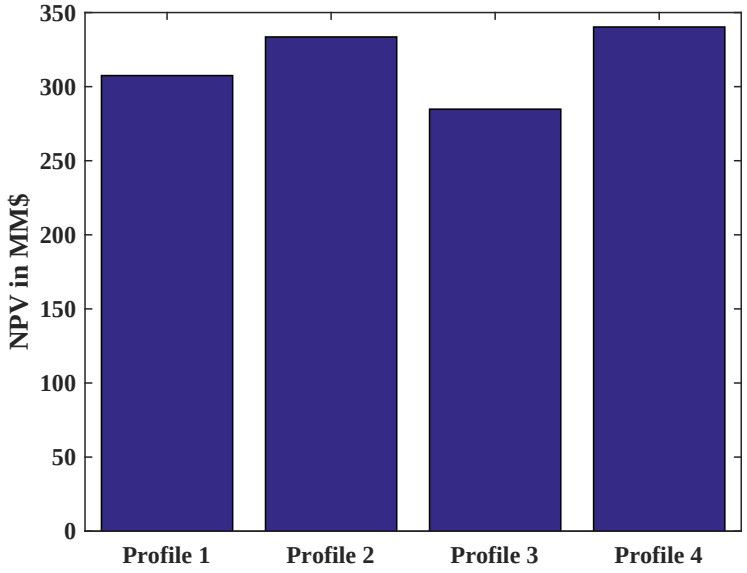

Figure 6.52. NPV value in MMUSD for the four log profiles considered

6.6 Sensitivity analysis

To check the sensitivity of the input parameters with production rates, the following input parametric sensitivities are conducted. Since oil production is of prime importance in the current study, all of the sensitivities are tested with respect to the oil production. Learnings from this study were incorporated to improve the gas production and water production networks. Input parameters constitute:

- Seismic attribute data alone

  Seismic attributes from full angle stack data (mean error − 27%)

  Seismic attributes from full angle stack data and inversion products (mean error − 32%)

- Well log data alone

  50 average log values (mean error − 26%)

  350 average log values (mean error − 25%)

- Both seismic data and well log data together (mean error − 21%)

Sensitivity analysis of input parameters has suggested the use of both seismic data along with well log data for better correlations. Seismic data together with well log data have resulted in the best performing network architecture with mean average testing error of less than 21%. Seismic data alone resulted with an architecture that performs with an error of 27%. Well log data alone when used to predict the production parameter a, b, c has resulted in mean average testing error of 25%. Therefore for the optimal architecture both seismic data and well log data are used together.

6.7 Production surface maps

Using the cumulative oil production performance module, surface maps are generated assuming a vertical well drilled at each of the seismic data point, following production surface maps as shown in Figure 6.53 are created. The plot on the left indicates normalized end of year one production and plot of the right indicates the end of year two production surface. The production maps clearly indicate

permeability channels that exist within the field. The lighter green channels indicate the pathways where the oil could have been trapped. The best well in the field (highest cumulative oil observed in field) is in the northern most region of the field.

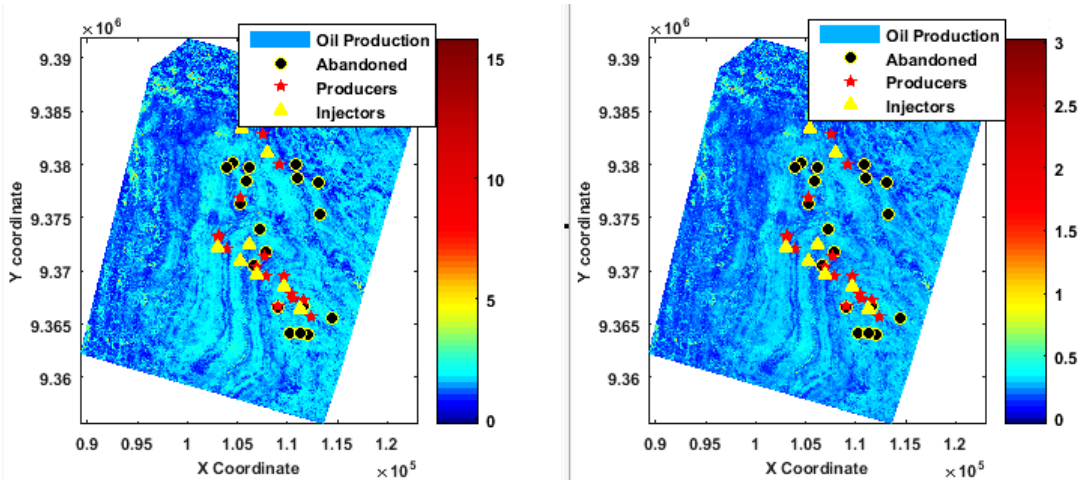

Figure 6.53. Oil production surface maps at the end of year one(Left) and two(Right)

Similarly using the gas production performance module, surface maps are generated assuming vertical wells drilled all over the area where seismic data is present. Maps of end of year one and year two productions are indicated in Figure 6.54. Figure 6.54 exhibits an interesting trend of expected gas production profiles. On detailed examination it was found that the areas of northen region, namely Landana is prolific in gas production. Towards the southern part of the field, the gas production tends to be lower. This prediction is inline with the observed gas production in the southern region of the field with each well producing around 5 *Bcf* on average in first two years of production.

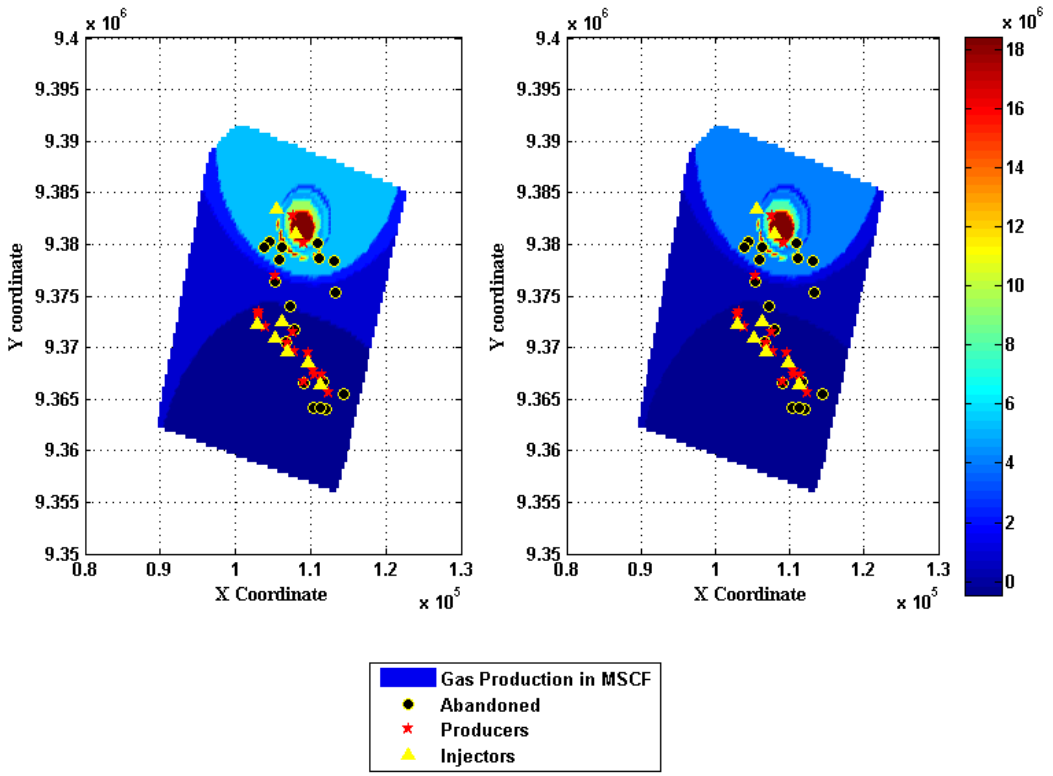

Figure 6.54. Gas production surface maps at the end of year one(Left) and two(Right)

Water production networks enable generation of 12 months cumulative water production data at a chosen location.

Chapter 7

Conclusions

A novel methodology of mapping a well log suite from directional wells with seismic data is developed. In this work, an artificial neural network based tool is successfully developed to map the seismic attributes to well logs that can generate synthetic gamma ray, neutron porosity, total porosity, bulk density, deep resistivity logs. Production performance networks established correlation between seismic data, well log data completion data, and production data. The tool has two modules, first module generates synthetic logs, and the second module generates the production profiles for a chosen location. Results indicate that the best performance was obtained while training logs in conjunction than isolation. Two sets of synthetic well log modules are developed, first one predicting NPHI, GR, and PHIT together and second set predicting RHOB and RESD. Robustness of the results indicate the capabilities of ANN technology to successfully map the correlations that exist within complex reservoirs. This workflow enables generation of synthetic log suites at all the locations where seismic data is available, and also predict expected oil, gas and water flow rates at any undrilled location. Monte Carlo simulations help

Table 7.1. Summary of synthetic well log networks

		Hidden layer neurons	Transfer functions	Average error
Zone 1	NPHI,GR,PHIT	369, 398, 99	logsig, tansig, logsig, purelin	7.7% (4.3, 7.3, 11.7)
	RHOB,RESD	257, 126, 248, 185	tansig, tansig, logsig, logsig, purelin	8.37% (1.1, 12.1)
Zone 2	NPHI,GR,PHIT	191, 191, 161, 168	logsig, logsig, logsig, logsig, purelin	6.05% (5.7, 5.9, 6.5)
	RHOB,RESD	151, 281, 144, 259	logsig, logsig, tansig, tansig, purelin	9.52% (0.8, 13.1)
Zone 3	NPHI,GR,PHIT	162, 154, 239, 177	tansig, logsig, tansig, logsig, purelin	21.04% (22, 25.7, 18.4)
	RHOB,RESD	294, 214, 272, 115	logsig, tansig, logsig, logsig, purlein	33.1% (1.9, 45)

in estimating the risk associated with reserve estimation by providing probabilistic estimates.

The proposed method do not involve any horizons or horizon based seismic attributes, thereby reducing the uncertainty associated with geophysical interpretation of horizons. This method can potentially reduce the interpretation time significantly, providing a quick estimate of production potential of a given zone.

Overall mean testing error of the chosen synthetic well log networks is less than 20%. The Table 7.1 presents a summary of the synthetic well log networks created in this work. The errors indicated in the parentheses indicate the individual errors corresponding to each of the logs. For example, for Zone-1, mean error in blind testing for NPHI logs resulted in 4.3% error, GR logs in 7.3% error, and PHIT logs 11.7% error.

Table 7.2. Summary of production performance networks

	Parameters	Hidden layer neurons	Transfer functions	Average error
Oil	a, b, c	47, 33, 46, 34	tansig, tansig, tansig, logsig, purelin	21%
Gas	a, b, c	42, 37, 44, 26	logsig, tansig, logsig, logsig, purelin	32%
Water	12 months production	15, 50, 10, 47, 11	logsig, logsig, tansig, tansig, logsig, purelin	46%

Table 7.2 presents a summary of the production performance networks. The production data of oil could be correlated with the seismic attributes, well log data, and production schedule with a mean testing error of less than 21%. Gas production is highly variable in this field due to altering bottomhole conditions; and bottomhole pressure's proximity to bubble point. Well bottomhole pressures staying close to bubble point pressure at reservoir conditions create uncertainties in oil and gas production rates. Gas oil ratio varies over a wide range in the given field, since different reservoirs are producing at different conditions. Cumulative gas production prediction module resulted in 32% testing errors while obtaining the optimal architecture. Water production however could not be correlated well with the chosen input attributes. Water production is highly variable in this field owing to varying OWC in the field and changing injection conditions are some of the reasons. The interwell connectivity could not be completely established in this study. Further work needs to be done to investigate the injection effects on water cut behavior. Summary of production performance networks is indicated in Table 7.2:

Water production networks correlations are slightly poorer compared to oil and gas production. This is due to the effect of injection wells and continuously changing bottomhole conditions at the wellbore. These changes have resulted in a dataset that has quite a large number of variations in the flow rates and sharp transition of water cut performance. Using MC simulations, P90 OOIP maps are analyzed for areas with high production potential. Synthetic logs together with production performance module characterize the reservoir and aid in field development planning. It is observed that these networks work for specific field, upon following the methodology, this work can be extended to wide varieties of reservoirs and fields. A graphic user interface(GUI) has been created as a part of this study to aid a user in predicting the well logs,and oil, water, gas production profiles at any given location. Additionally a user can specify the trajectory of the well bore and the tool would be able to generate a well log along the trajectory of the well bore along with the production forecasts. Surface maps indicating production potentials of oil and gas can be generated with the help of developed GUI. This methodology serves as an alternative form of effective reservoir characterization for complex reservoirs that are often misunderstood through simplified reservoir models.

7.1 Future Work

- Integration of this model with a high fidelity economic forecast model(that includes MRI method of directional well cost evaluation) and predict infill drilling strategies.
- Use genetic algorithms to evaluate the optimal horizontal well trajectories.

- Include additional well data to retrain and improve the performance of production networks
- Globalize the network generation process to incorporate variety of operating conditions and well logs to make it a universal expert system.

References

Al-Kaabl, A.-A. U., McVay, D. A., Lee, J. W., et al. (1990). Using an expert system to identify a well-test-interpretation model. *Journal of Petroleum Technology*, 42(05):654–661.

Aminzadeh, F., Barhen, J., Glover, C., and Toomarian, N. (2000). Reservoir parameter estimation using a hybrid neural network. *Computers & Geosciences*, 26(8):869–875.

Aminzadeh, F., Ross, C., de Groot, P., and Brouwer, F. (2005). Hydrocarbon probability index based on ann and prestack attributes: 67 th annual conference and ehibition, eage. In *Extended Abstracts F*, volume 1.

Archie, G. E. et al. (1942). The electrical resistivity log as an aid in determining some reservoir characteristics. *Transactions of the AIME*, 146(01):54–62.

Artun, E., Mohaghegh, S., Joanthan, T., Wilson, T., and Sanchez, A. (2005). Reservoir characterisation using intelligent seismic inversion. In *SPE*, Morgantown, WV.

Athichanagorn, S., Horne, R. N., et al. (1995). Automatic parameter estimation from well test data using artificial neural network. In *SPE Annual Technical Conference and Exhibition*. Society of Petroleum Engineers.

Baldwin, J. L., Otte, D. N., Whealtley, C., et al. (1989). Computer emulation of human mental processes: Application of neural network simulators to problems in well log interpretation. In *SPE Annual Technical Conference and Exhibition*. Society of Petroleum Engineers.

Bansal, Y., Ertekin, T., Karpyn, Z., Ayala, L. F., Nejad, A., Suleen, F., Balogun, O., Liebmann, D., Sun, Q., et al. (2013). Forecasting well performance in a discontinuous tight oil reservoir using artificial neural networks. In *SPE Unconventional Resources Conference-USA*. Society of Petroleum Engineers.

Berger, B. and Anderson, K. (1981). *Modern petroleum: a basic primer of the industry*. Penn Well Books, Tulsa, OK.

Bois, P. (1984). Fuzzy seismic interpretation. *Geoscience and Remote Sensing, IEEE Transactions on*, 6(6):692–697.

Bravo, C. E., Saputelli, L., Rivas, F., Pérez, A. G., Nickolaou, M., Zangl, G., De Guzmán, N., Mohaghegh, S. D., Nunez, G., et al. (2014). State of the art of artificial intelligence and predictive analytics in the e&p industry: A technology survey. *SPE Journal*, 19(04):547–563.

Brown, A. R. (2001). Understanding seismic attributes. *Geophysics*, 66(1):47–48.

Cuddy, S. et al. (2000). Litho-facies and permeability prediction from electrical logs using fuzzy logic. *SPE Reservoir Evaluation & Engineering*, 3(04):319–324.

De Groot, P. and Bril, A. (1996). The use of pseudo-wells in seismic interpretation studies. In *58th EAGE Conference and Exhibition*.

Ershaghi, I., Li, X., Hassibi, M., Shikari, Y., et al. (1993). A robust neural network model for pattern recognition of pressure transient test data. In *SPE Annual Technical Conference and Exhibition*. Society of Petroleum Engineers.

Gharbi, R., Elsharkawy, A. M., et al. (1997). Neural network model for estimating the pvt properties of middle east crude oils. In *Middle East Oil Show and Conference*. Society of Petroleum Engineers.

Gharehlo, A. M. (2012). *Development of Artificial Expert Reservoir Characterization tools for Unconventional Reservoirs*. PhD thesis, The Pennsylvania State University.

Hart, B. S., Pearson, R., and Rawling, G. C. (2002). 3-d seismic horizon-based approaches to fracture-swarm sweet spot definition in tight-gas reservoirs. *The Leading Edge*, 21(1):28–35.

Hecht-Nielsen, R. (1987). Kolmogorov's mapping neural network existence theorem. In *Proceedings of the international conference on Neural Networks*, volume 3, pages 11–14. New York: IEEE Press.

Higgs, W., Domingos, F., Isaac, R., Redwine, R., Benoit, P., et al. (2005). Benguela belize-lobito tomboco development, block 14: Angola's next deepwater hub. In *18th World Petroleum Congress*. World Petroleum Congress.

Hopfield, J. J. (1982). Neural networks and physical systems with emergent collective computational abilities. *Proceedings of the national academy of sciences*, 79(8):2554–2558.

Kaiser, M. J. (2007). A survey of drilling cost and complexity estimation models. *International Journal of Petroleum Science and Technology*, 1(1):1–22.

Kalam, M., Al-Alawi, S., Al-Mukheini, M., et al. (1996). Assessment of formation damage using artificial neural networks. In *SPE Formation Damage Control Symposium*. Society of Petroleum Engineers.

Kohonen, T. (1982). Self-organized formation of topologically correct feature maps. *Biological cybernetics*, 43(1):59–69.

Koning, T. (2014). Angola's oil industry - a century of progress in exploration and production. *Search and Discovery*, 70174(1).

Lim, J.-S., Kim, J., et al. (2004). Reservoir porosity and permeability estimation from well logs using fuzzy logic and neural networks. In *SPE Asia Pacific Oil and Gas Conference and Exhibition*. Society of Petroleum Engineers.

Mapsofworld (2014). Where is angola | location map of angola.

McCormack, M. D., Zaucha, D. E., and Dushek, D. W. (1993). First-break refraction event picking and seismic data trace editing using neural networks. *Geophysics*, 58(1):67–78.

McCulloch, W. S. and Pitts, W. (1943). A logical calculus of the ideas immanent in nervous activity. *The bulletin of mathematical biophysics*, 5(4):115–133.

Metropolis, N. and Ulam, S. (1949). The monte carlo method. *Journal of the American statistical association*, 44(247):335–341.

Mohaghegh, S., Arefi, R., Ameri, S., Aminiand, K., and Nutter, R. (1996). Petroleum reservoir characterization with the aid of artificial neural networks. *Journal of Petroleum Science and Engineering*, 16(4):263–274.

Mohaghegh, S., Arefi, R., Ameri, S., Rose, D., et al. (1995). Design and development of an artificial neural network for estimation of formation permeability. *SPE Computer Applications*, 7(06):151–154.

Mohaghegh, S. et al. (2000). Virtual-intelligence applications in petroleum engineering: Part 1âĂŤartificial neural networks. *Journal of Petroleum Technology*, 52(09):64–73.

Murtha, J. A. et al. (1994). Incorporating historical data into monte carlo simulation. *SPE Computer Applications*, 6(02):11–17.

Nikravesh, M. and Aminzadeh, F. (2001). Past, present and future intelligent reservoir characterization trends. *Journal of Petroleum Science and Engineering*, 31(2):67–79.

Nikravesh, M. et al. (1998a). Neural network knowledge-based modeling of rock properties based on well log databases. In *SPE Western Regional Meeting*. Society of Petroleum Engineers.

Nikravesh, M. et al. (1998b). Neural network knowledge-based modeling of rock properties based on well log databases. In *SPE Western Regional Meeting*. Society of Petroleum Engineers.

Nordlund, U. (1996). Formalizing geological knowledge–with an example of modeling stratigraphy using fuzzy logic. *Journal of Sedimentary Research*, 66(4).

Oloso, M. A., Khoukhi, A., Abdulraheem, A., and Elshafei, M. (2009). Prediction of crude oil viscosity and gas/oil ratio curves using advances to neural networks. 2009 spe. In *EAGE Reservoir Characterization and Simulation Conference*, pages 19–21.

Osman, E., Abdel-Wahhab, O., Al-Marhoun, M., et al. (2001). Prediction of oil pvt properties using neural networks. In *SPE Middle East Oil Show*. Society of Petroleum Engineers.

Ouenes, A., Chawathe, A., and Weiss, W. (1997). A new approach to integrate seismic and production data in reservoir models. Technical report, BDM Corp., Bartlesville, OK (United States); American Association Petroleum Geologists, Tulsa, OK (United States).

Rolon, L., Mohaghegh, S. D., Ameri, S., Gaskari, R., and McDaniel, B. (2009). Using artificial neural networks to generate synthetic well logs. *Journal of Natural Gas Science and Engineering*, 1(4):118–133.

Rosenblatt, F. (1958). The perceptron: a probabilistic model for information storage and organization in the brain. *Psychological review*, 65(6):386.

Roth, G. and Tarantoia, A. (1992). Inversion of seismic waveforms using neural networks. In *1992 SEG Annual Meeting*.

Sadiq, T., Nashawi, I., et al. (2000). Using neural networks for prediction of formation fracture gradient. In *SPE/CIM International Conference on Horizontal Well Technology*. Society of Petroleum Engineers.

Shahkarami, A., Mohaghegh, S. D., Gholami, V., Haghighat, S. A., et al. (2014). Artificial intelligence (ai) assisted history matching. In *SPE Western North American and Rocky Mountain Joint Meeting*. Society of Petroleum Engineers.

Singh, K., Holditch, S. A., and Ayers, W. B. (2008). Basin analog investigations answer characterization challenges of unconventional gas potential in frontier basins. *Journal of Energy Resources Technology*, 130(4):043202.

Sultan, M. A., Al-Kaabi, A. U., et al. (2002). Application of neural network to the determination of well-test interpretation model for horizontal wells. In *SPE Asia Pacific Oil and Gas Conference and Exhibition*. Society of Petroleum Engineers.

Syed, A. (2014). *Horizontal well length optimization considering wellbore hydraulics*. PhD thesis, Institutt for petroleumsteknologi og anvendt geofysikk.

Taner, M., Walls, J., Smith, M., Taylor, G., Carr, M., Dumas, D., et al. (2001). Reservoir characterization by calibration of self-organized map clusters. *SEG/San Antonio*.

Thararoop, P., Karpyn, Z., Gitman, A., and Ertekin, T. (2008). Integration of seismic attributes and production data for infill drilling strategies - a virtual intelligence approach. *Journal of Petroleum Science and Engineering*, 63(1):43–52.

Wong, P., Aminzadeh, F., and Nikravesh, M. (2002). Intelligent reservoir characterization. In *Soft Computing for reservoir Characterization and Modeling*, pages 3–12. Springer.

Yang, F.-M., Huang, K.-Y., et al. (1991). Multilayer perceptron for detection of seismic anomalies. In *1991 SEG Annual Meeting*. Society of Exploration Geophysicists.

Yegnanarayana, B. (2009). *Artificial neural networks*. PHI Learning Pvt. Ltd.

Yilmaz, Ö. (2001). *Seismic data analysis*, volume 1. Society of exploration geophysicists Tulsa, OK.

Zadeh, L. A. (1965). Fuzzy sets. *Information and control*, 8(3):338–353.

Zhou, C.-D., Wu, S.-L., Zhang, C. M., Zhu, D. H., Zhang, V. X., et al. (1994). Direct identification of hydrocarbon from well logs: A neural network interpretation approach. In *Annual Technical Meeting*. Petroleum Society of Canada.

Appendix A

Graphic User Interface

A graphic user interface has been created in MATLAB to enable a user to generate synthetic well logs and predict oil, water, gas production at any desired location. The tool will also be able to generate horizontal well log profiles as per the user specification as indicated in Figure A.1. Well logs could be generated along the trajectory of the given well configuration. Well logs are created at every point of X, Y space using the synthetic well log module and then 150 points are re sampled according to their respective X coordinate and Y coordinate. The user could click on any location within the boundaries indicated by blue dots. On clicking the pushbutton vertical well, log suite comprising of GR, NPHI, PHIT, RHOB, and RESD logs will be computed and displayed on the right side panel. The user will also be able provide with a wellbore trajectory and the GUI will be able to generate well logs along the trajectory of the directional well. For demonstration purposes, two configurations as indicated in Figure A.3 are provided with push buttons horizontal well 1 and horizontal well 2.

On clicking the location corresponding X and Y coordinates are read through and populated into the X Coord Y Coord static boxes. Then user has an option of generating a vertical well log profile or two types of horizontal well log profiles. On selecting the option for horizontal wells, another pop up window appears indicating the progress of log generation as indicated in Figure A.2.

The push-buttons oil, water and gas will enable generation of production profiles. Figure A.4 displays a sample prediction of cumulative oil produced at the chosen location. Gas and water productions can be obtained via pushbuttons gas, and water.

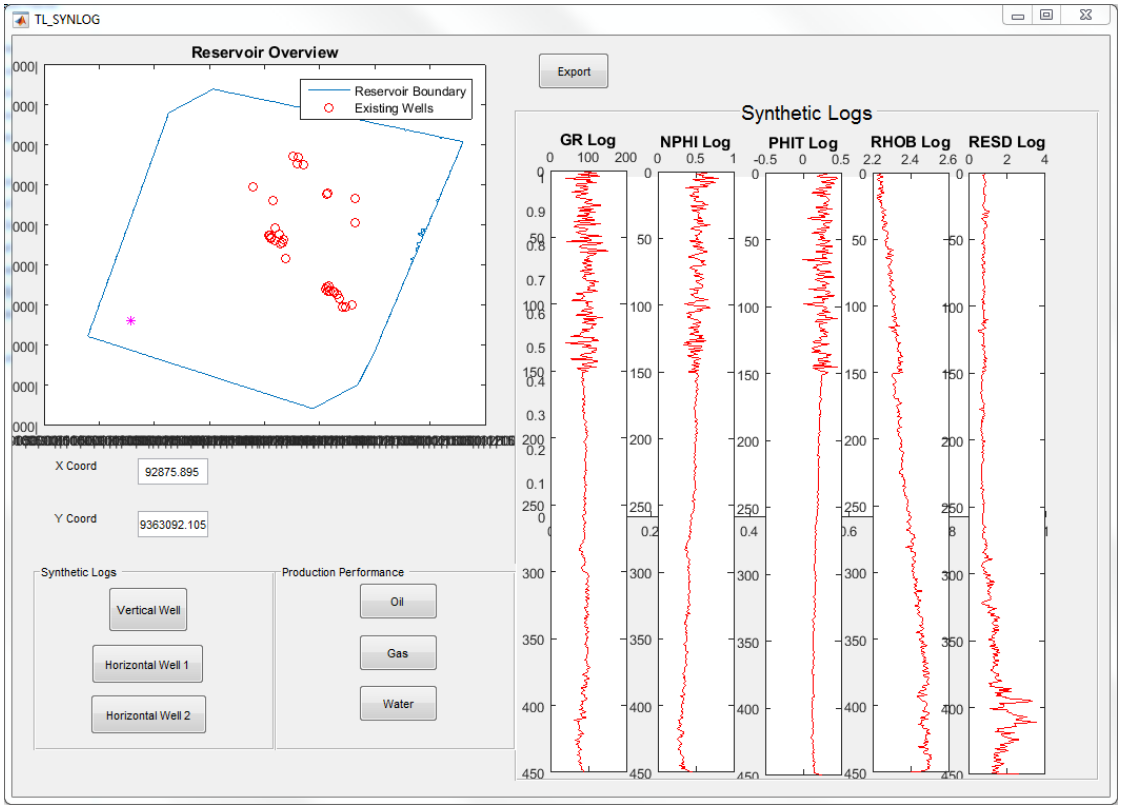

Figure A.1. Graphical User Interface

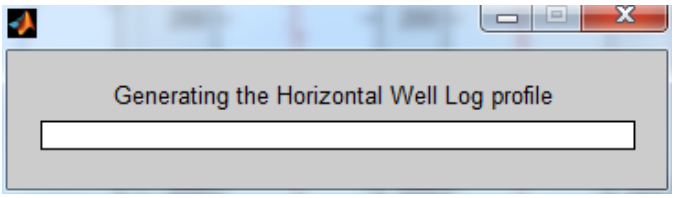

Figure A.2. Pop up window indicating the progress of synthetic log generation

This GUI also enables a user to predict surface maps at the end of n'th year as well as view the cross sections of well log surfaces at any desired locations.

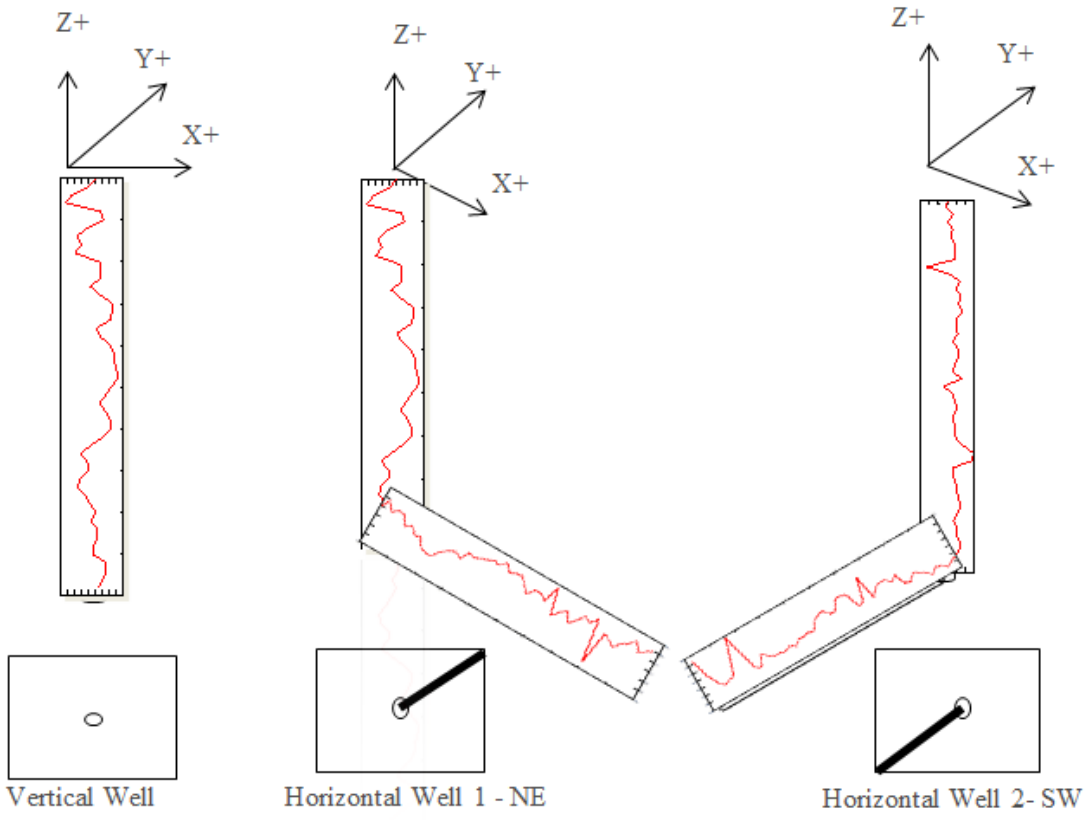

Figure A.3. Sample directional well log configurations

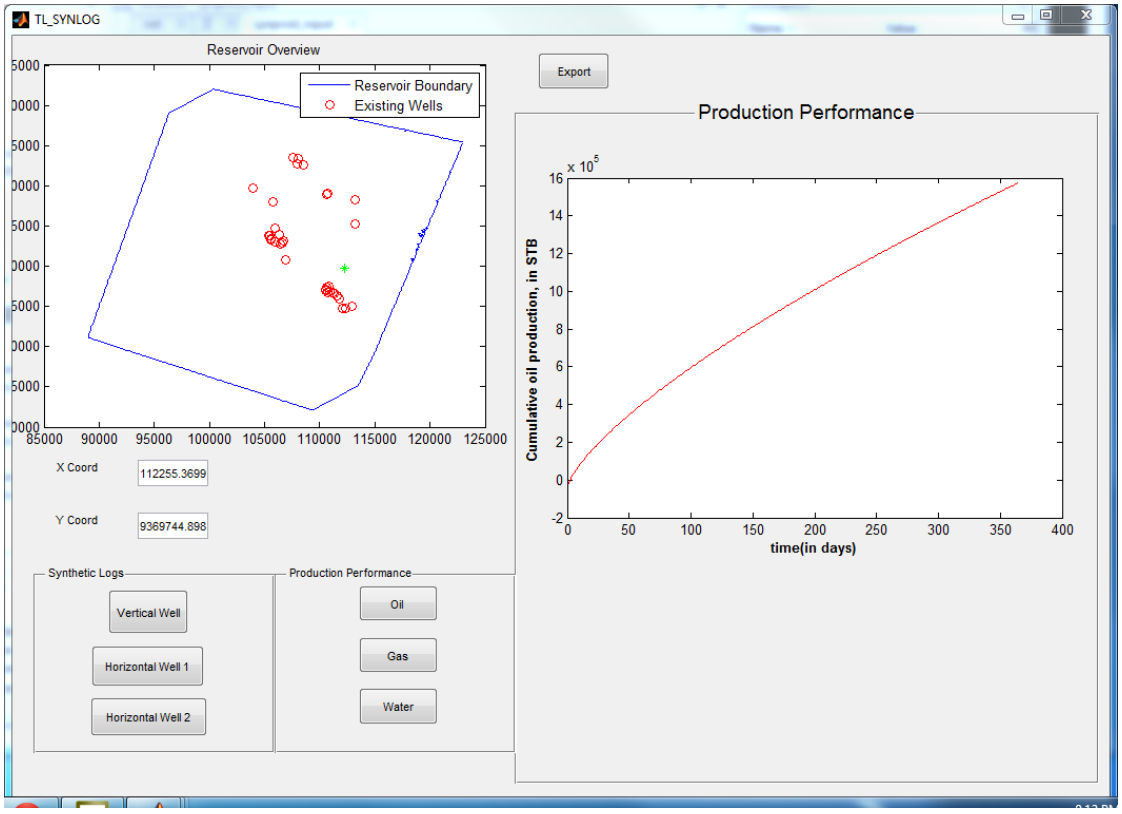

Figure A.4. Cumulative oil production forecast

Appendix B

Petrel Work-flows Used

This appendix includes the workflows used in generating seismic attributes.

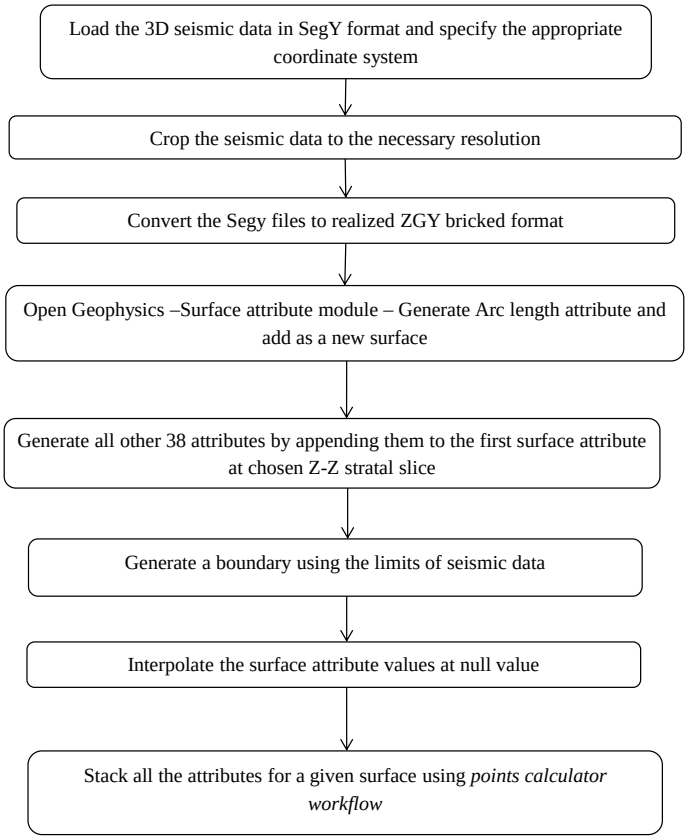

Figure B.1. Workflow used in petrel to create seismic attribute data set

Vertical Resolution: All the attributes are extracted at default settings of petrel based on z-z approach every 40 ms.

Areal Resolution: The original resolution of seismic data is 12.5m × 12.5m. A reduced resolution of 62.5m × 62.5m is used in generating the realized cropped volume. The volume is cropped to 1800ms - 3000 ms as the region of interest lies in between. Points calculator workflow: For appending points with attributes, automated workflow in Petrel[2] is created and is as follows:

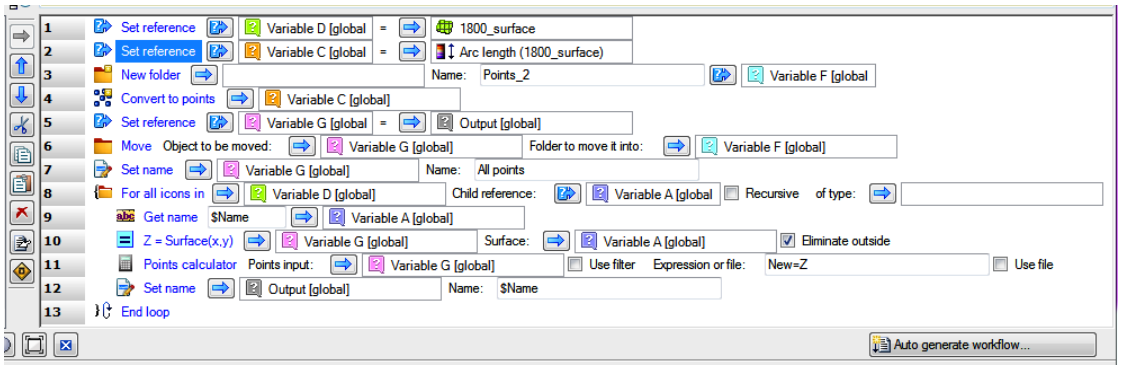

Figure B.2. Points calculator workflow in Petrel

Detailed workflow steps:

Line 1: User drop in folder of surfaces that need to be converted to points

Line 2: User drops in one surface from the list of surfaces from the folder. This surface will be the one that is converted to points and used as the main points object. The X, Y points will be taken from this surface so it may be useful if the user drops in the largest surface here.

Line 3: A folder is created to store the points (Optional)

Line 4: The surface provided in line 2 is converted to points.

Line 5: A reference is set to the points so that we can refer to these points later on in the workflow

Line 6: The points are moved into the Points 2 folder (Optional)

Line 7: The name of the main point set is changed to 'All points'

Line 8: All of the surfaces are extracted from the folder supplied in Line 1.

Line 9: The name of the surface is extracted in order to rename the attributes later.

Line 10: The points are set to the same Z values as the surface. The point set will change Z value many times throughout the workflow and it current Z position will be recorded as an attribute. For example, the first run will set the point equal to

Arc length-the Z value is then extracted as an attribute called 'Arc length'.
Line 11: An attribute 'New' is created to record the current Z value of the points - this will change every time the workflow loops around to the next surface
Line 12: The name of the attribute is set to the name of the surface.
Line 13: The loop ends and moves on to the next surface if one exists.
Conclusion: This workflow results in a folder that contains a single point set with an attribute that represents each surface at each XY -coordinate.
The subsequently generated point set if contains null values at a few locations; those locations can be appended with attributes via convergent interpolation in Petrel[2]. This above process is repeated for all the 30 surfaces extracted between 1800ms - 3000ms at every 40ms.
The subsequently generated point set if contains null values at a few locations; those locations can be appended with attributes via convergent interpolation in Petrel[2]. This above process is repeated for all the 30 surfaces extracted between 1800ms - 3000ms at every 40ms.

Appendix C

Summary of Network Architectures

The summary of the network architectures built for synthetic logs are as follows:

Zone-1 blind testing results for two log architectures

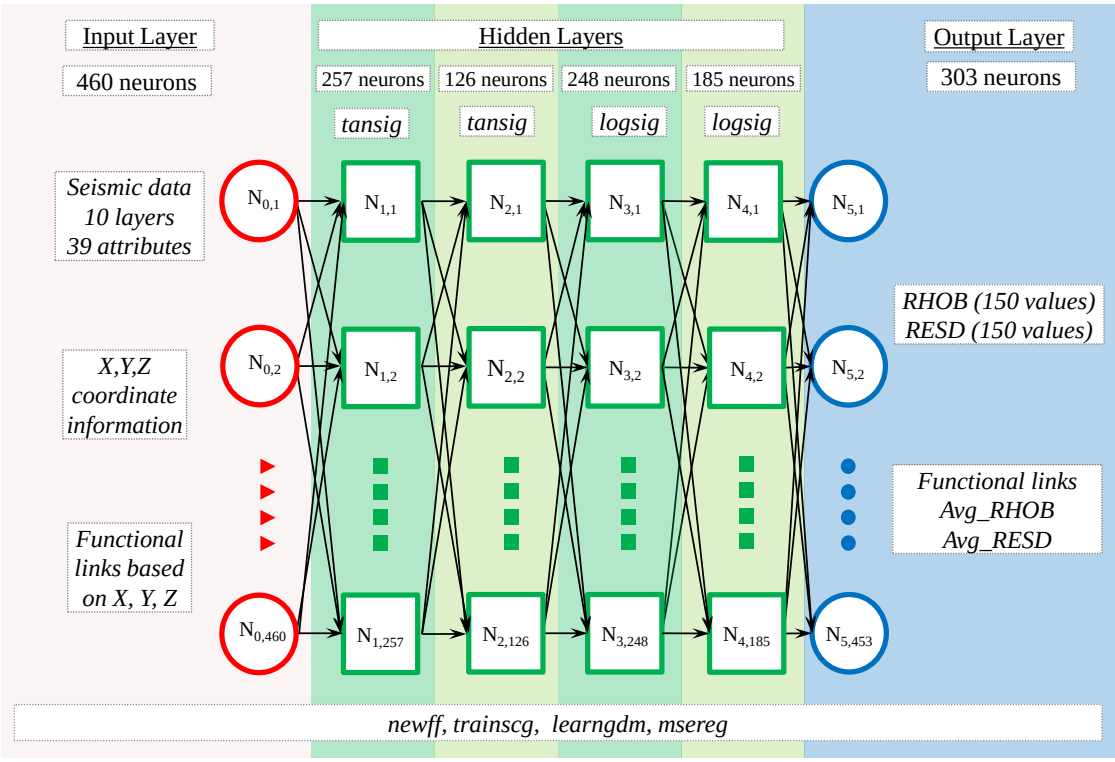

Figure C.1. Zone-1 - Two log architecture

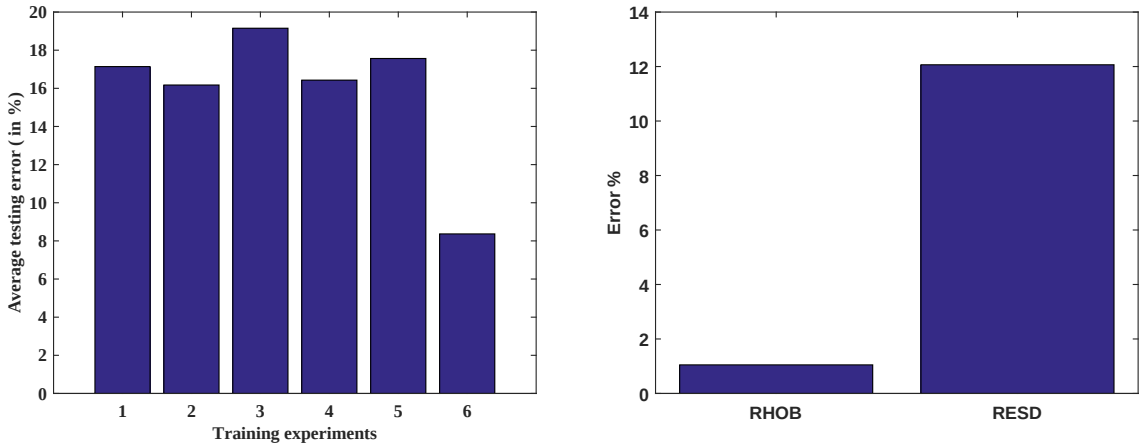

(a) Blind testing errors observed during numerical experiments

(b) For two different logs, Errors observed in blind testing

Figure C.2. Blind testing errors observed

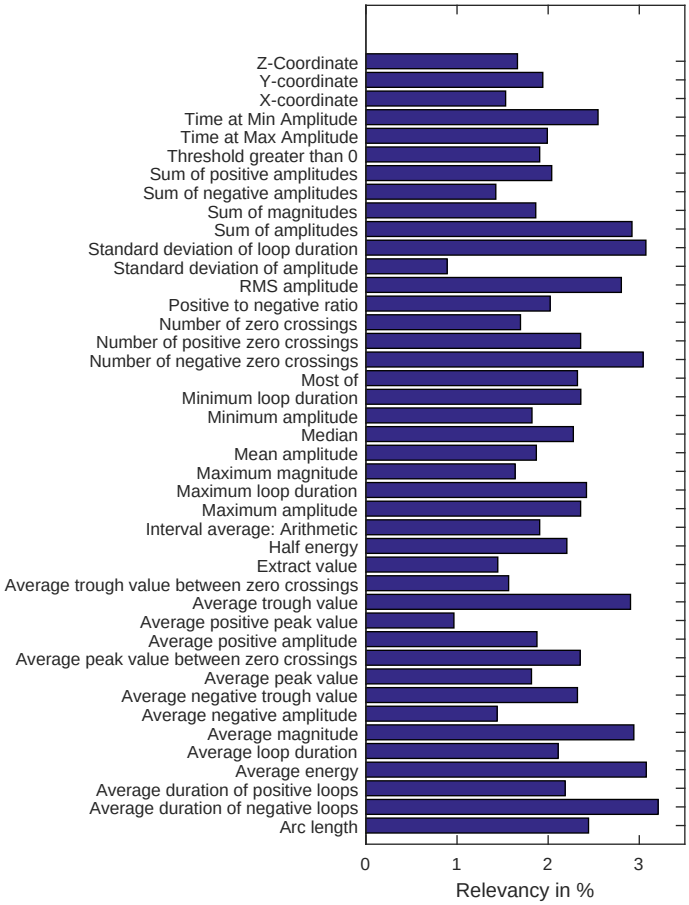

Figure C.3. Relevancy of seismic attributes

Zone-2 blind testing results for three log architecture

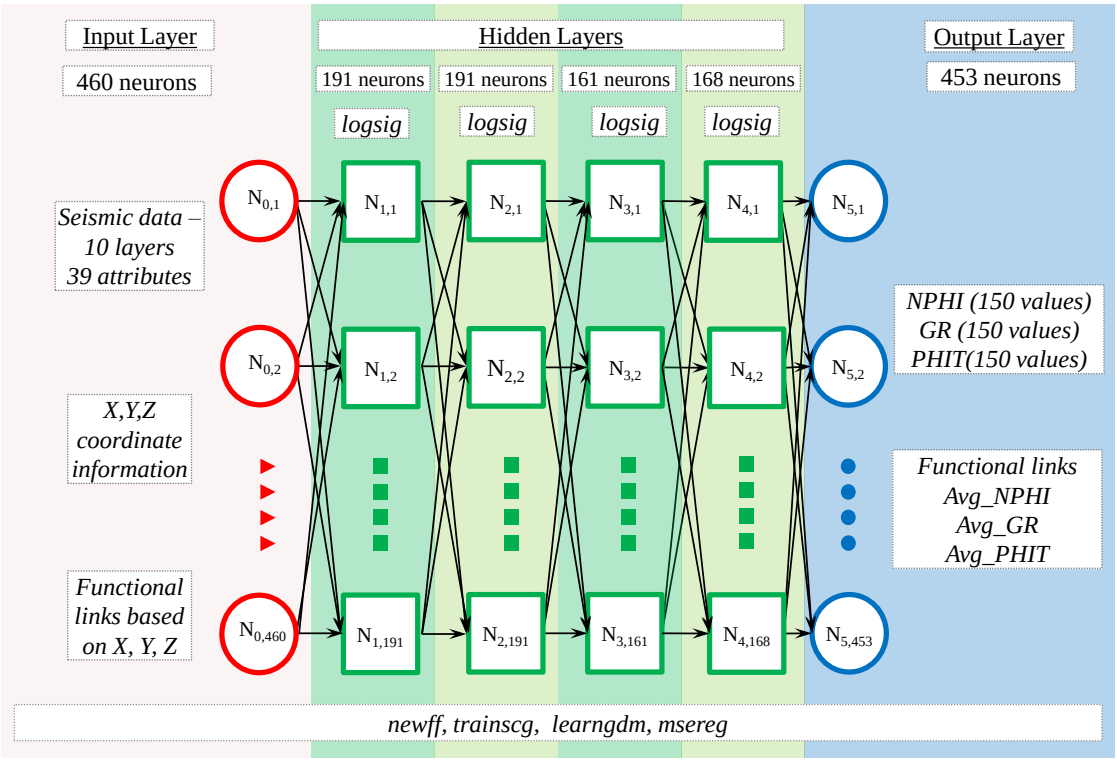

Figure C.4. Zone-2 - Three log architecture

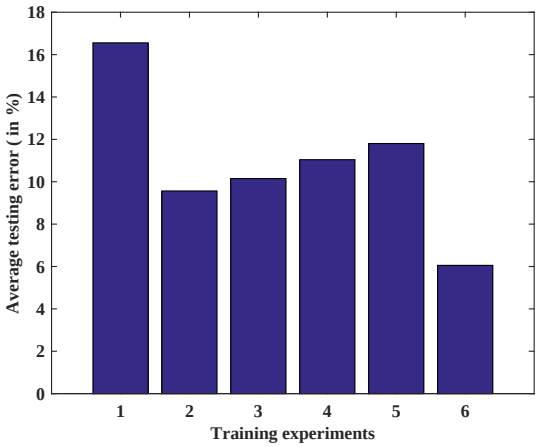

(a) Blind testing errors observed during numerical experiments

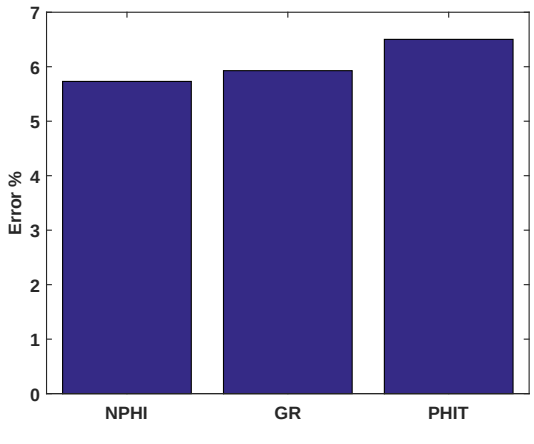

(b) For three different logs, Errors observed in blind testing

Figure C.5. Blind testing errors observed

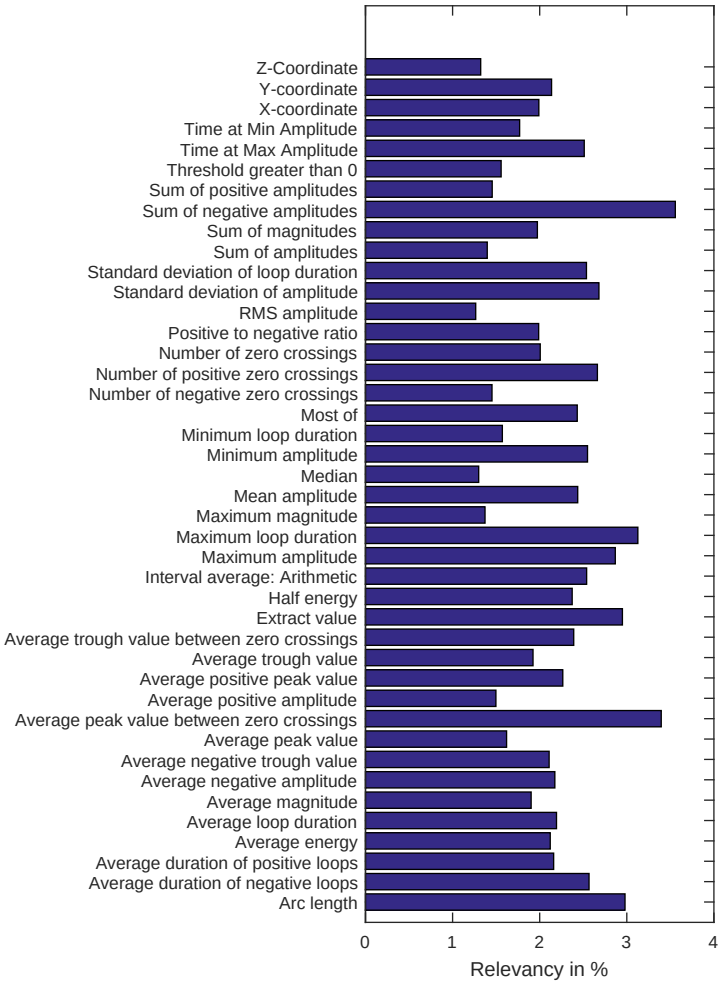

Figure C.6. Relevancy of seismic attributes

Zone-2 blind testing results for two log architectures

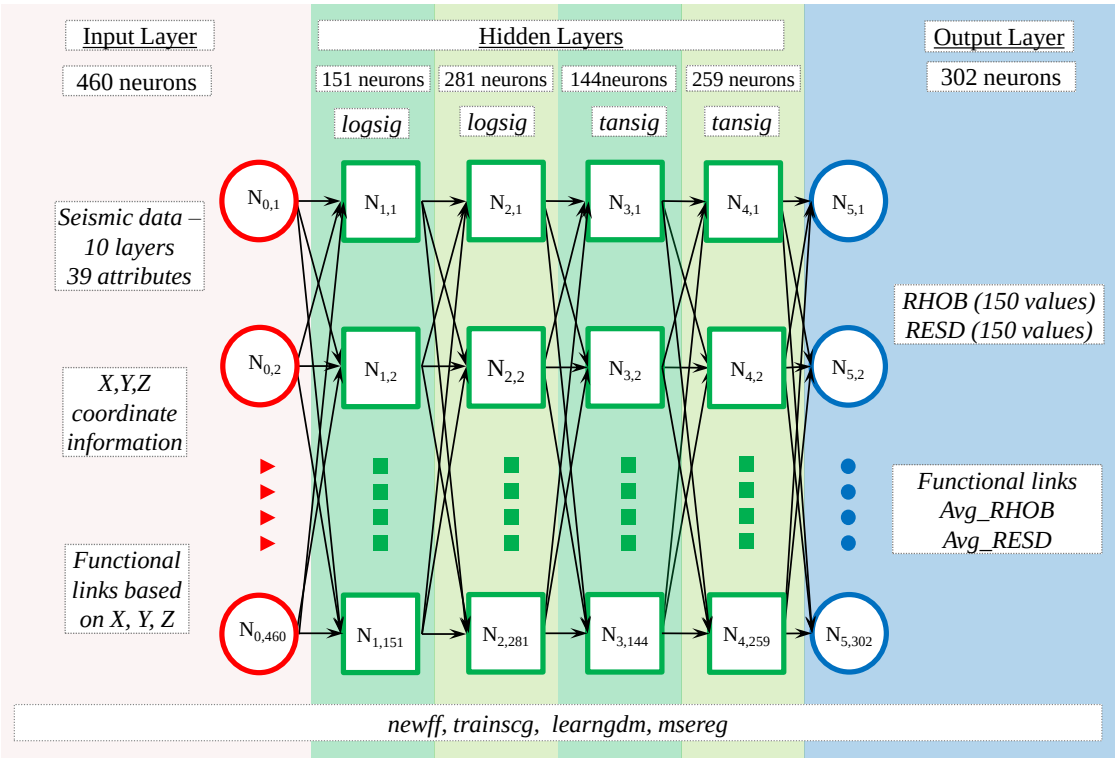

Figure C.7. Zone-2 - Two log architecture

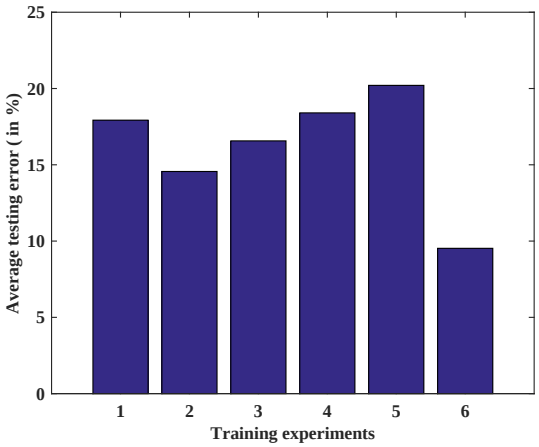

(a) Blind testing errors observed during numerical experiments

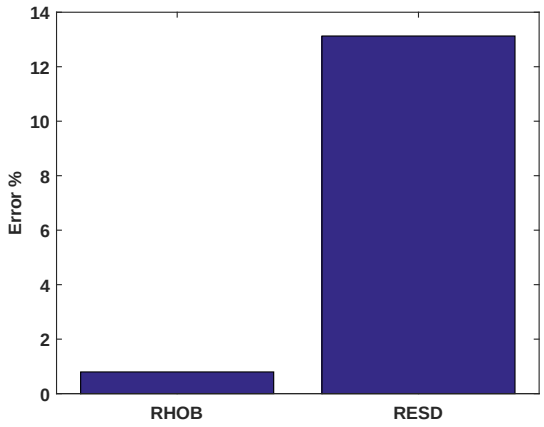

(b) For two different logs, Errors observed in blind testing

Figure C.8. Blind testing errors observed

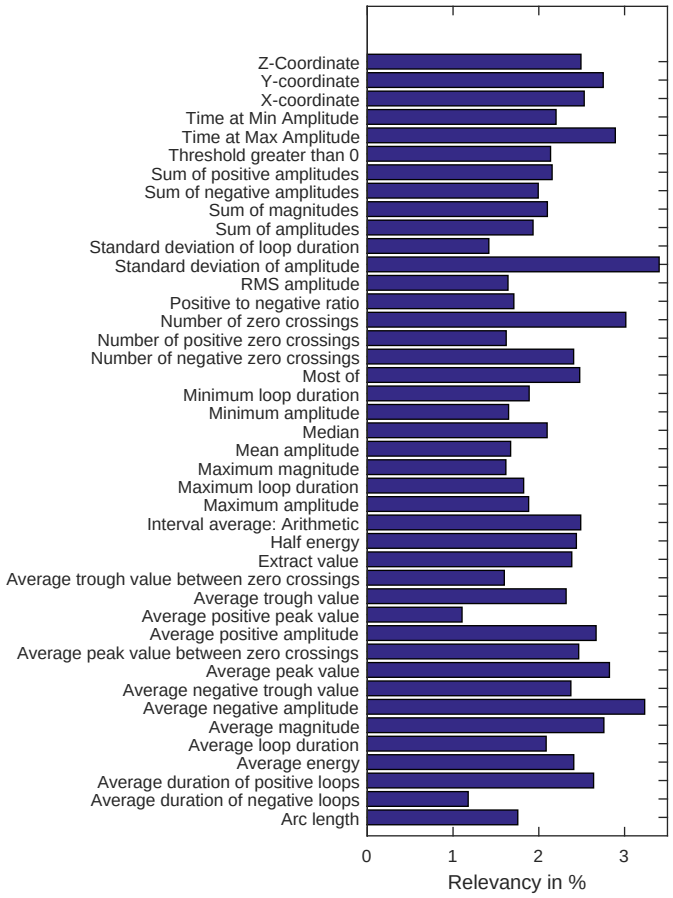

Figure C.9. Relevancy of seismic attributes

Zone-3 blind testing results for three log architecture

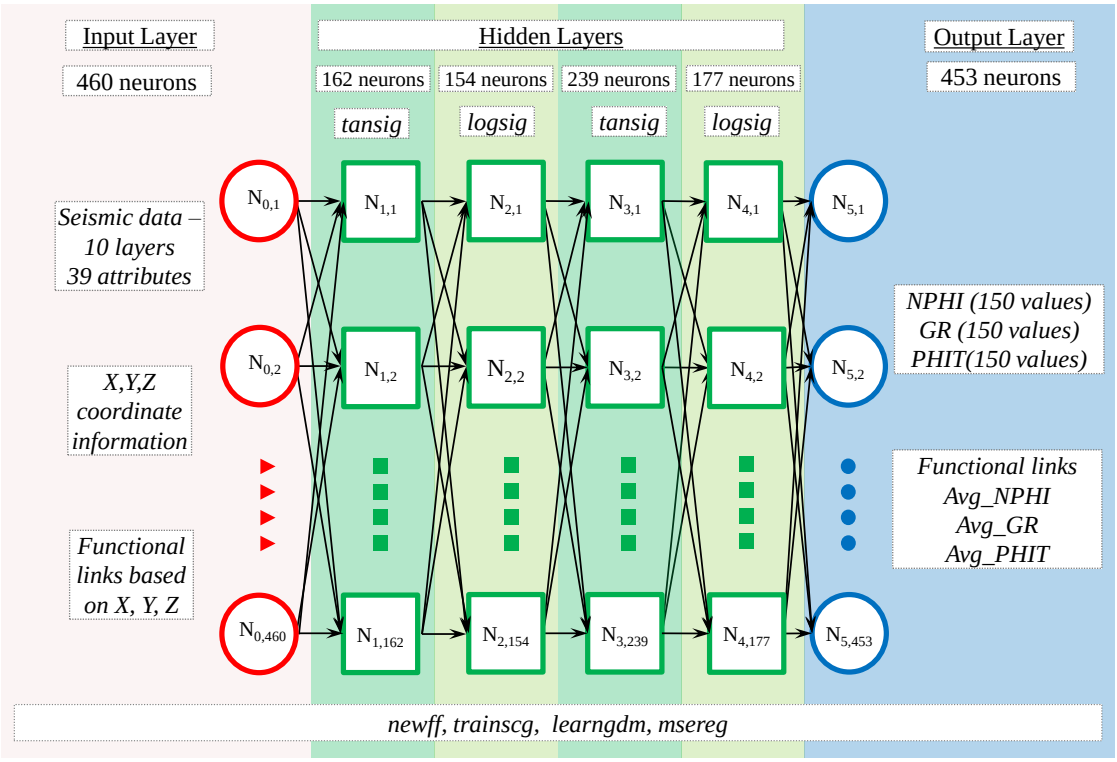

Figure C.10. Zone-3 - Three log architecture

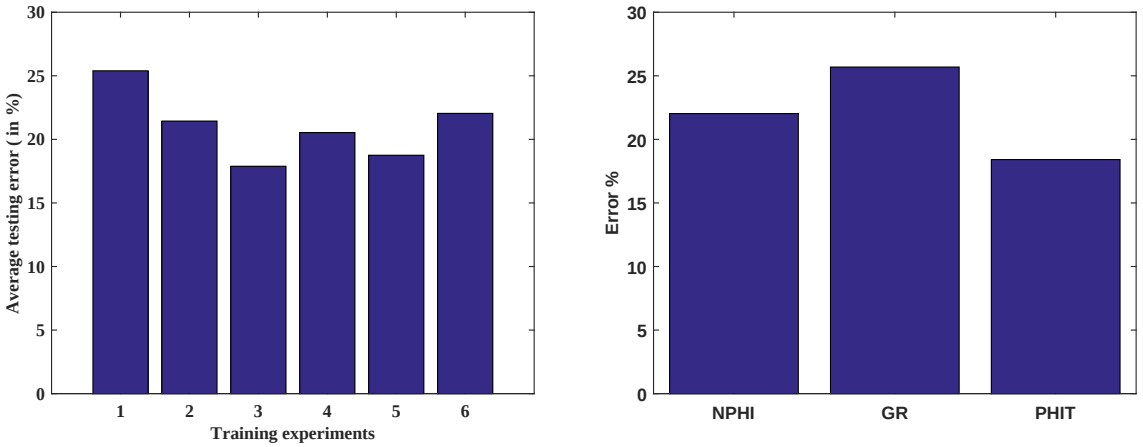

(a) Blind testing errors observed during numerical experiments

(b) For three different logs, Errors observed in blind testing

Figure C.11. Blind testing errors observed

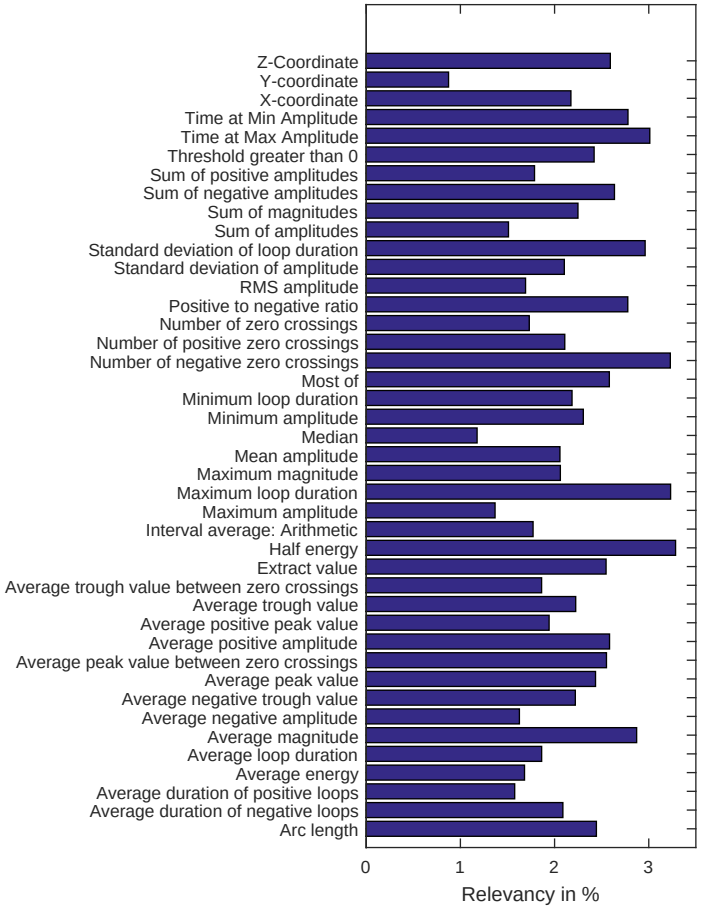

Figure C.12. Relevancy of seismic attributes

Zone-3 blind testing results for two log architectures

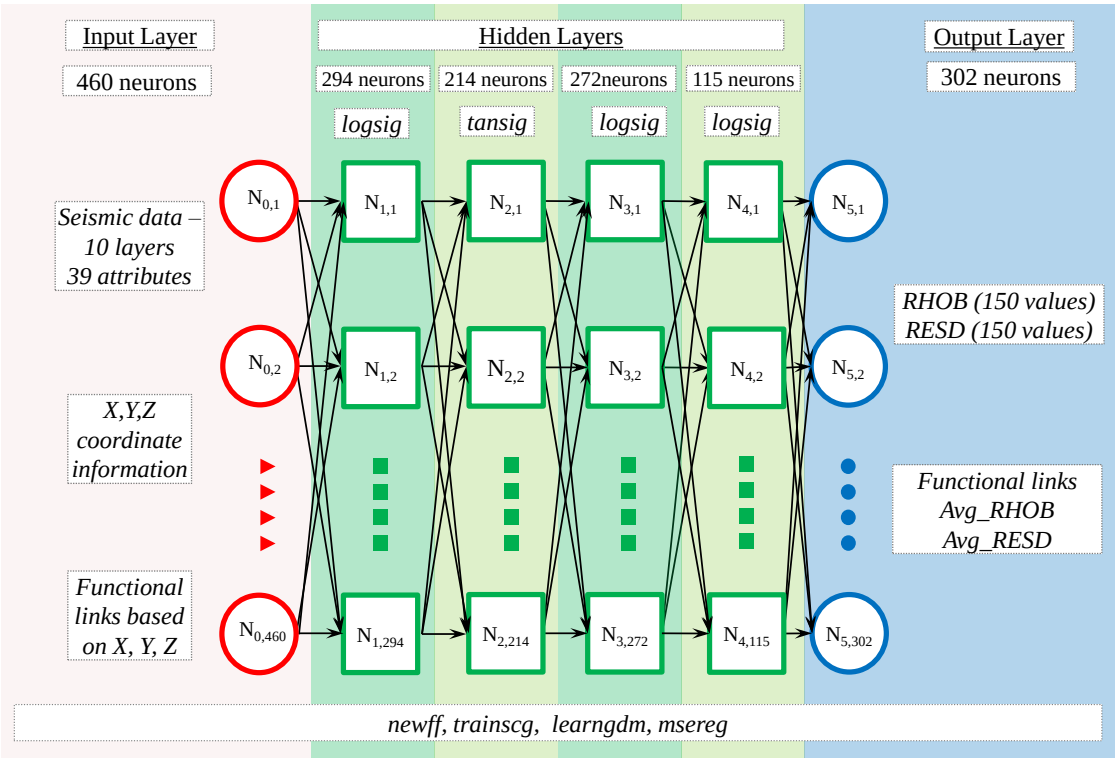

Figure C.13. Zone-3 - Two log architecture

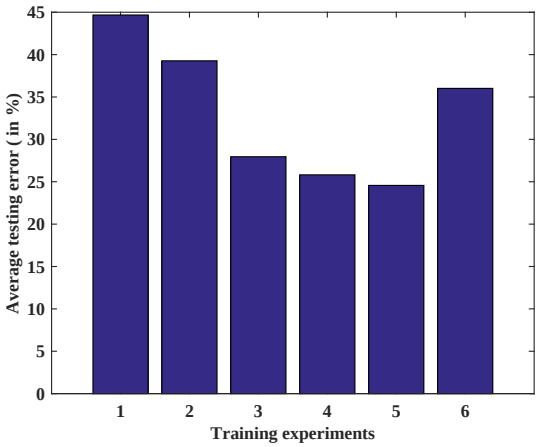

(a) Blind testing errors observed during numerical experiments

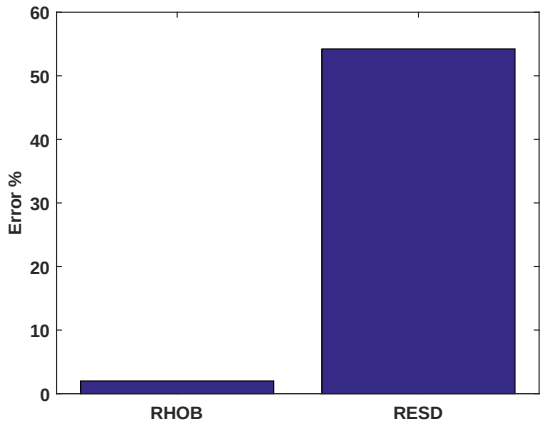

(b) For two different logs, Errors observed in blind testing

Figure C.14. Blind testing errors observed

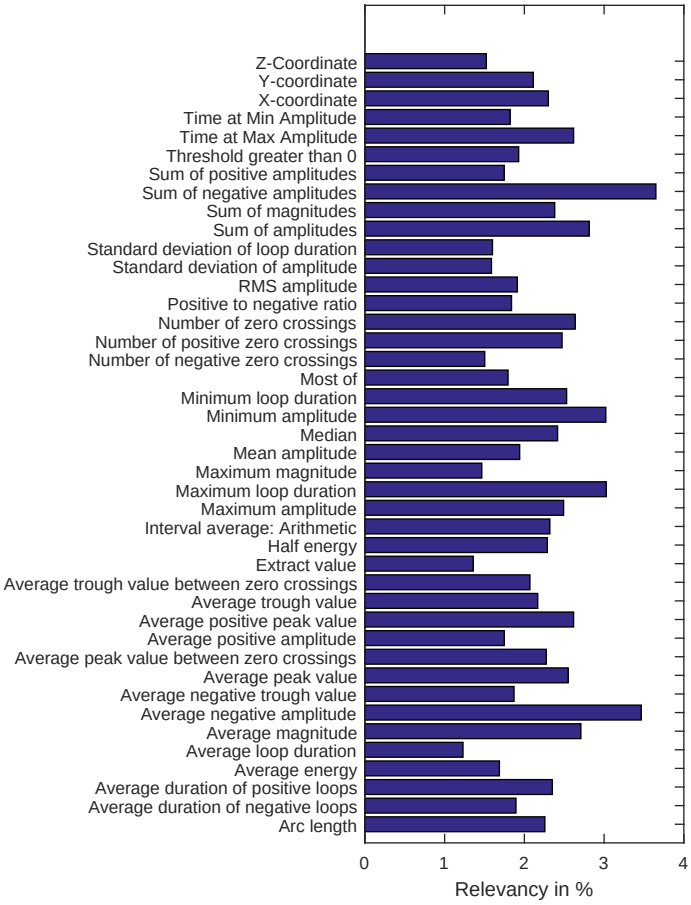

Figure C.15. Relevancy of seismic attributes

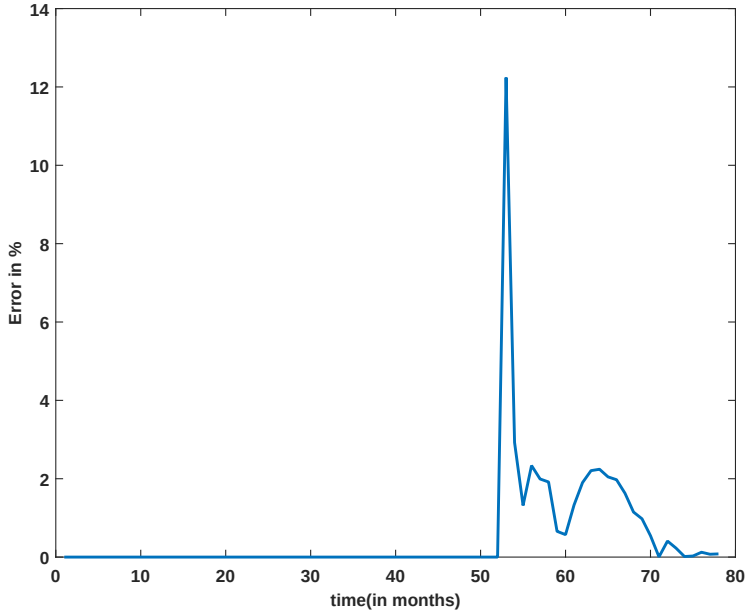

Figure C.16. Monthly cumulative oil flow rate error observed at Well #5

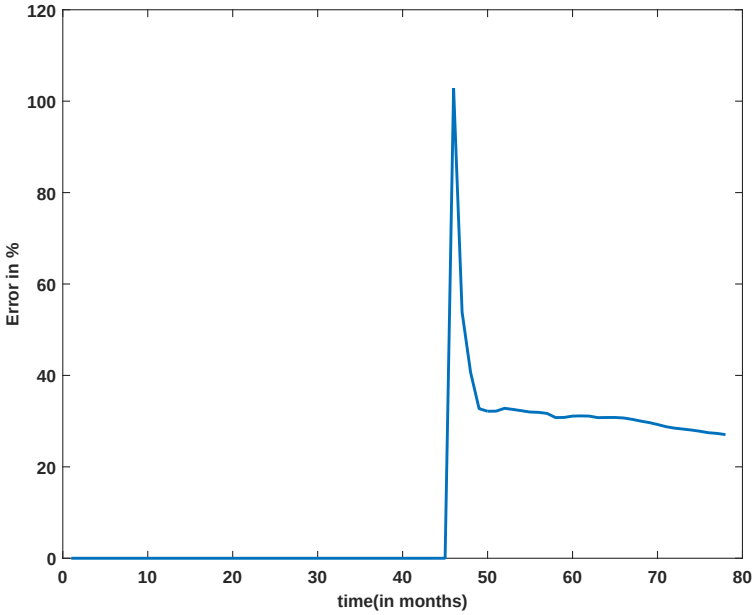

Figure C.17. Monthly cumulative oil flow rate error observed at Well #17

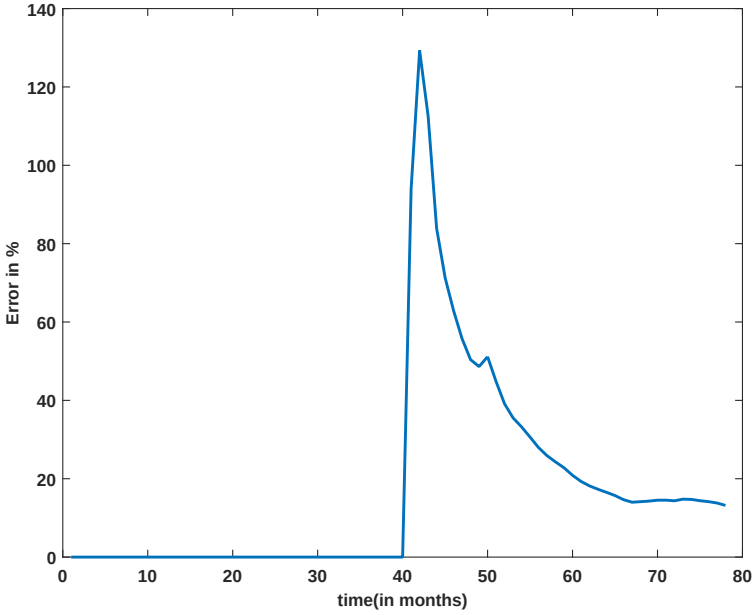

Figure C.18. Monthly cumulative oil flow rate error observed at Well #27

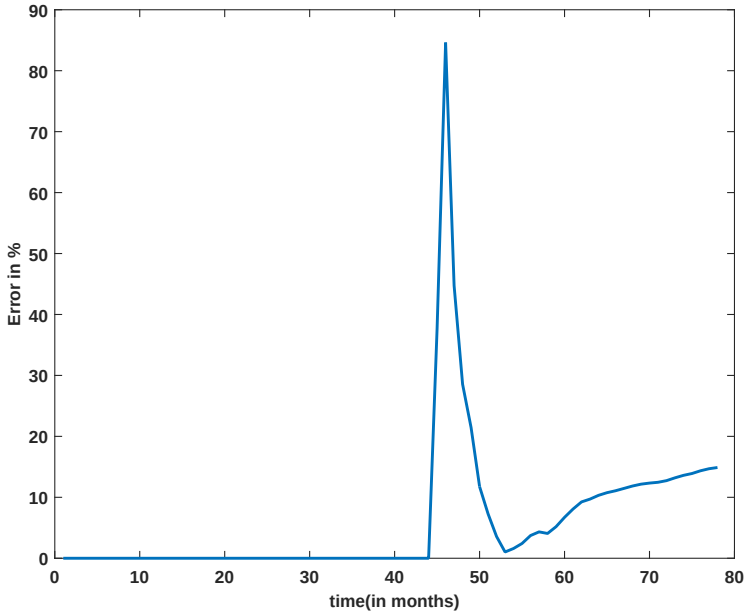

Figure C.19. Monthly cumulative gas flow rate error observed at Well #17

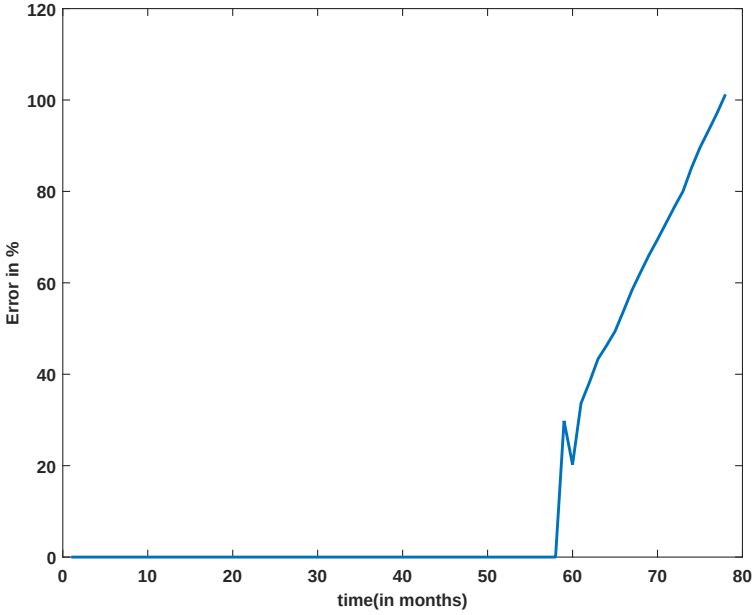

Figure C.20. Monthly cumulative gas flow rate error observed at Well #21

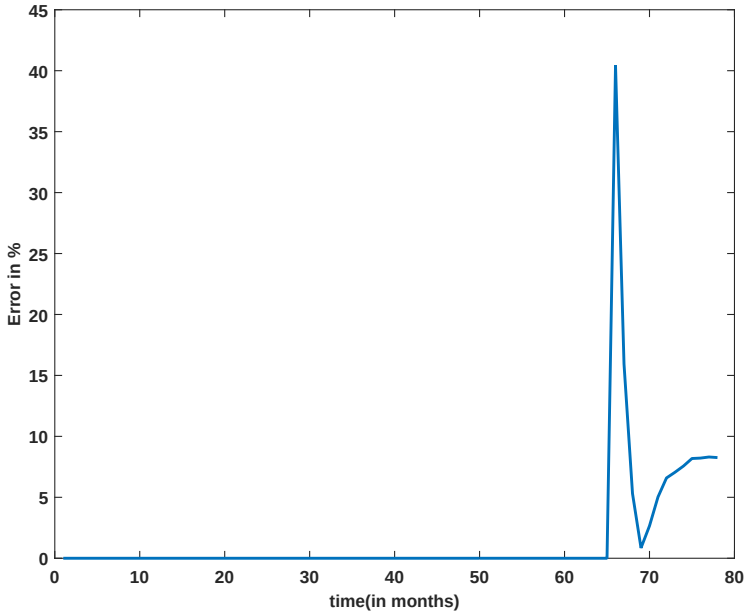

Figure C.21. Monthly cumulative gas flow rate error observed at Well #27

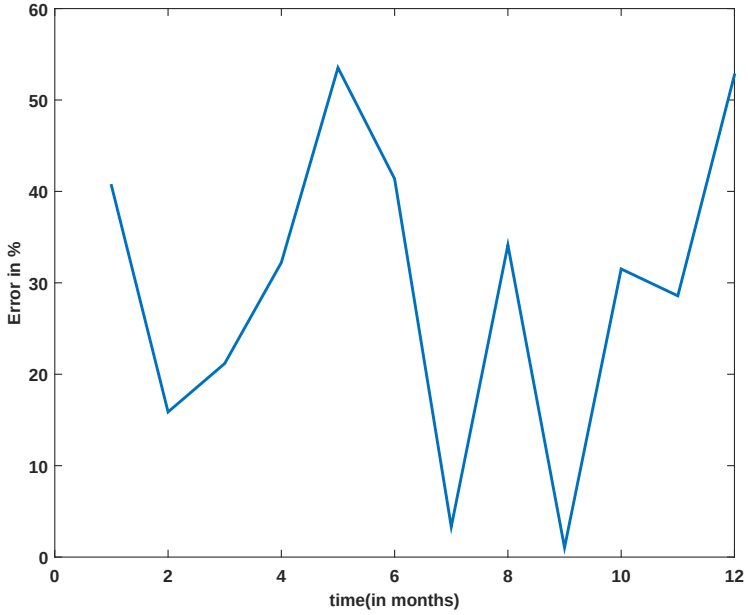

Figure C.22. Monthly cumulative water flow rate error observed at Well #30

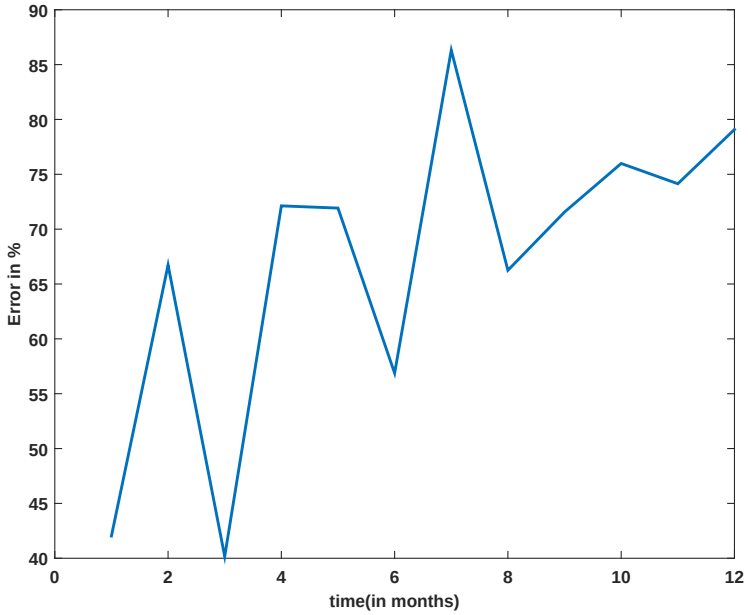

Figure C.23. Monthly cumulative water flow rate error observed at Well #31

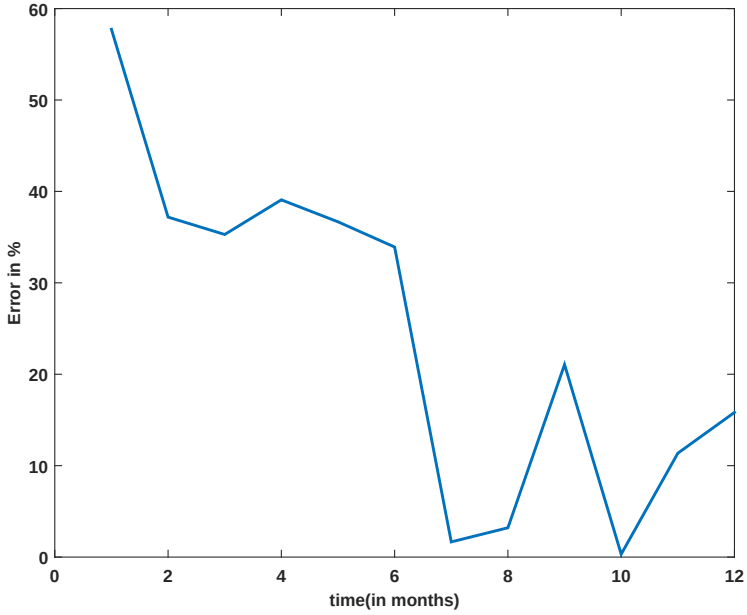

Figure C.24. Monthly cumulative water flow rate error observed at Well #21

Appendix D

Additional results from production performance networks

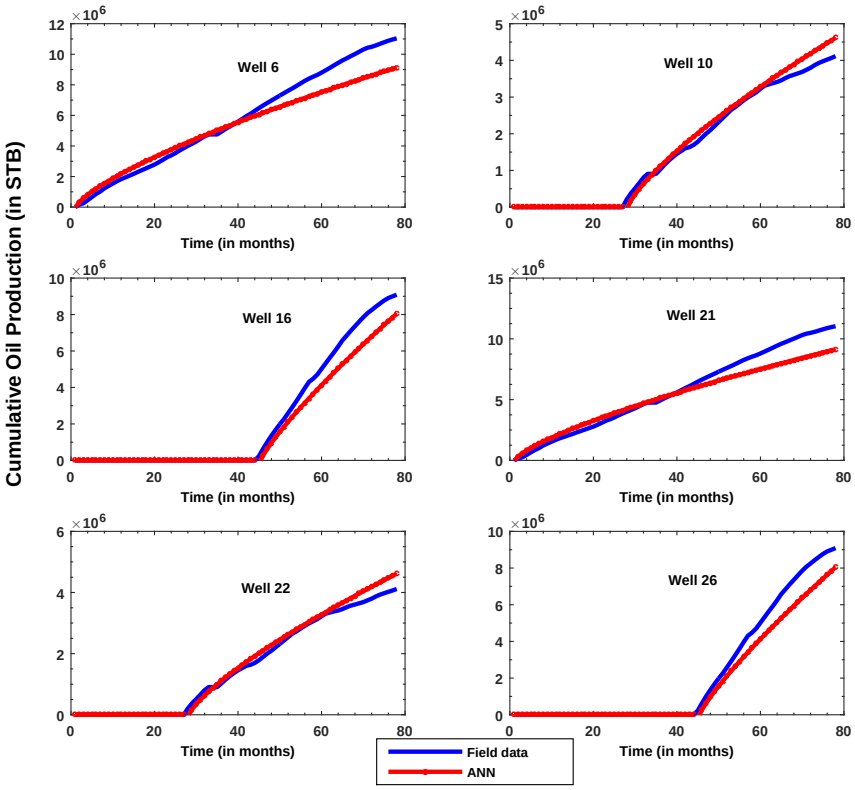

Figure D.1. Blind testing results of cumulative oil production networks

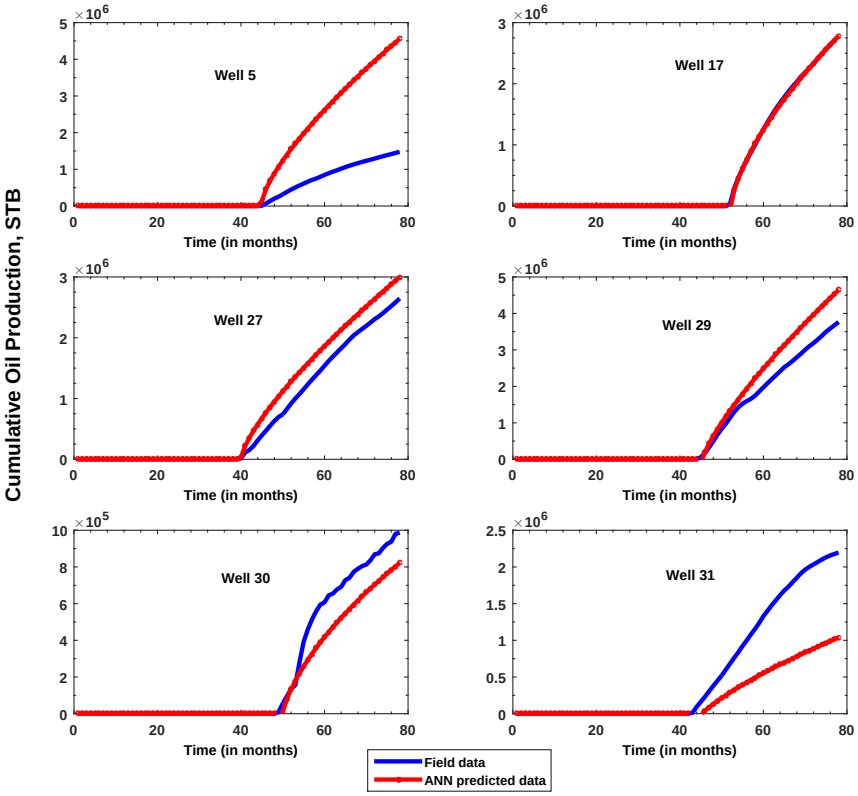

Figure D.2. Blind testing results of cumulative oil production networks

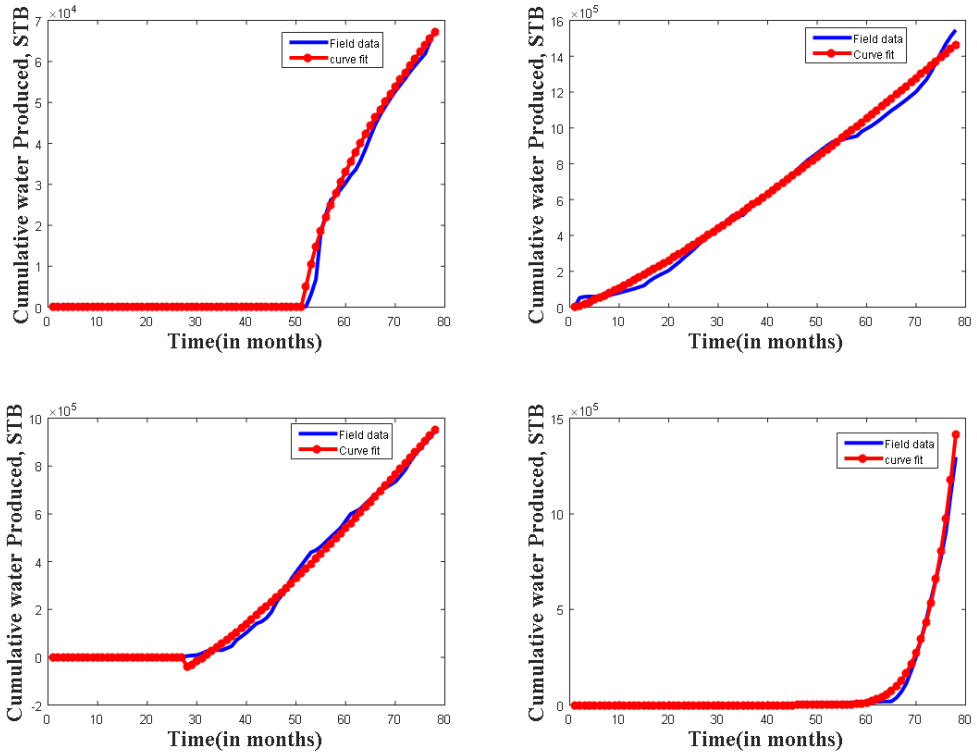

Figure D.3. Cumulative water curve fit -1

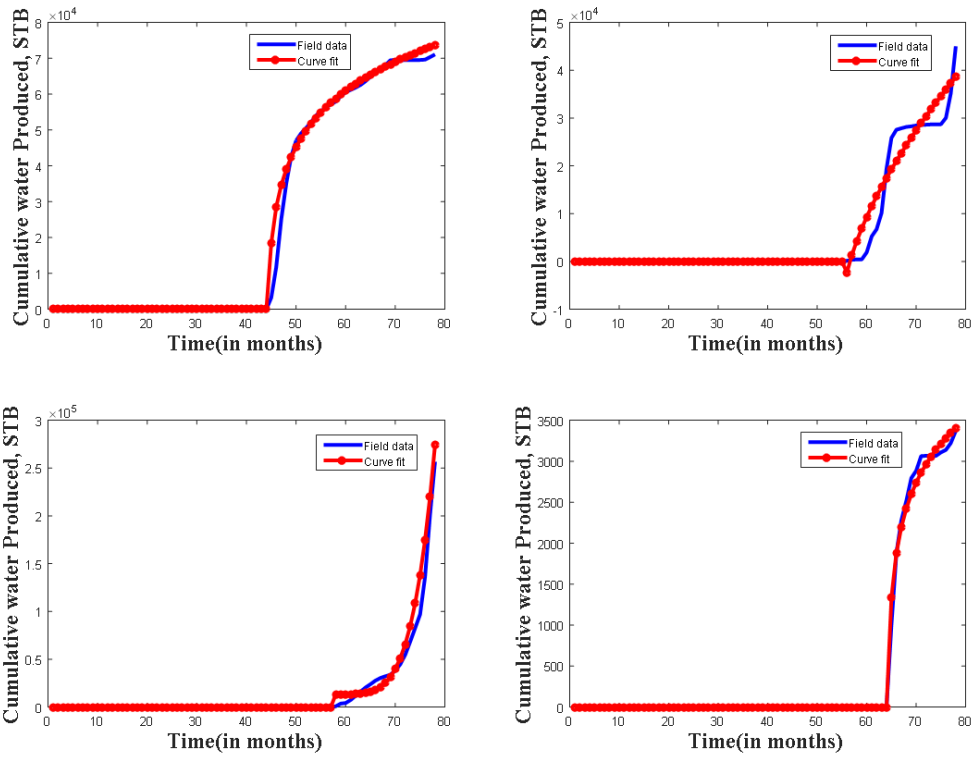

Figure D.4. Cumulative water curve fit -2

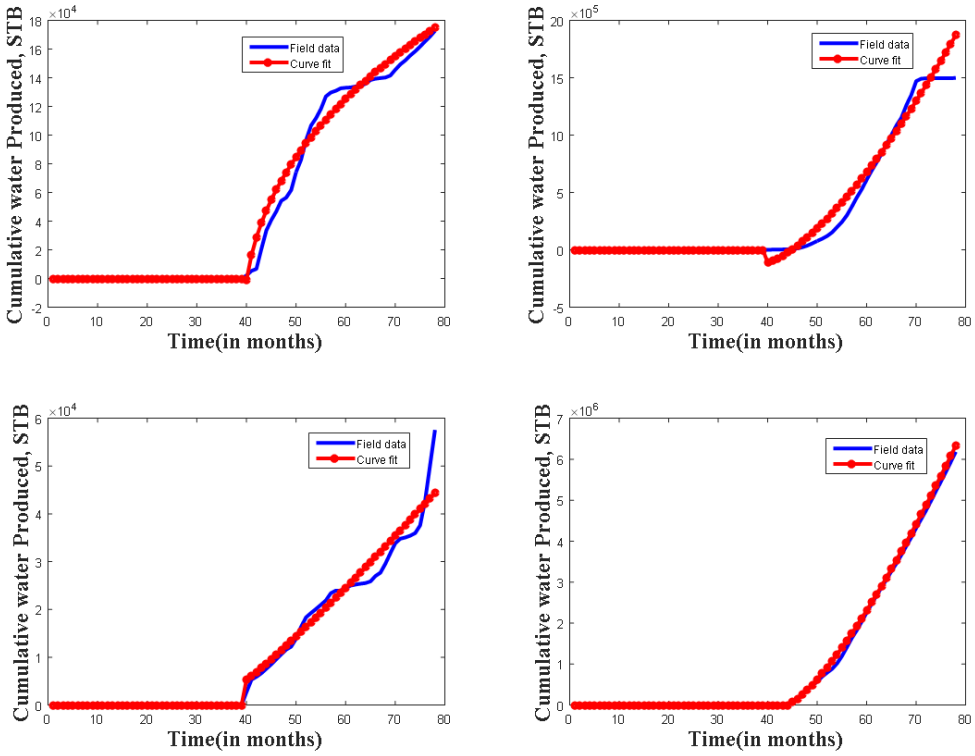

Figure D.5. Cumulative water curve fit -3

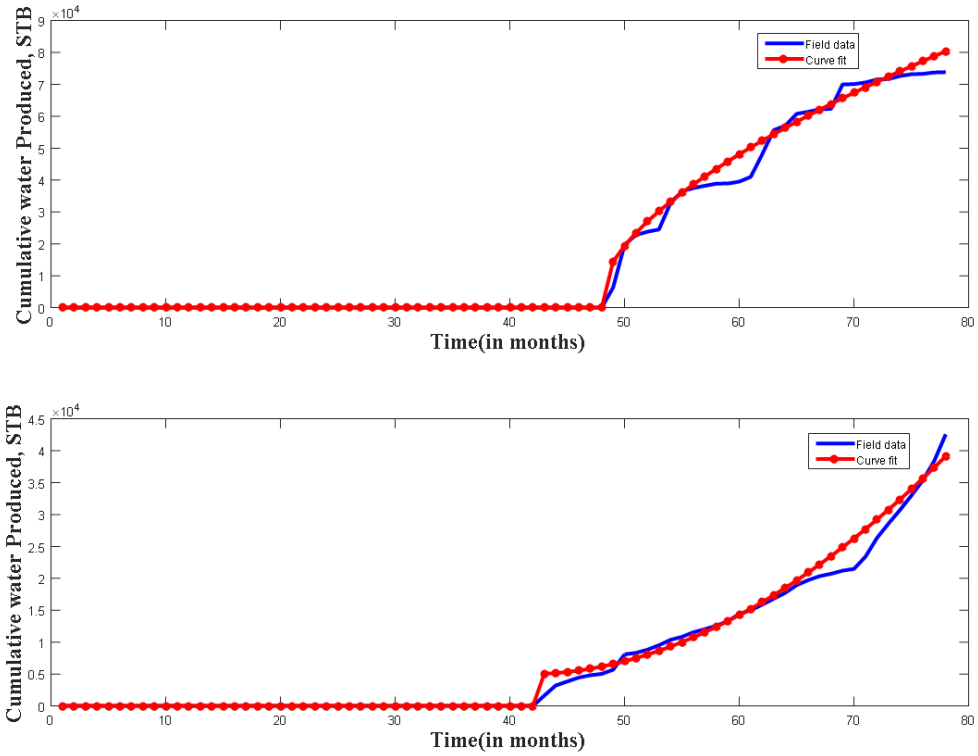

Figure D.6. Cumulative water curve fit -4

Vita

Sarath Pavan Ketineni

Sarath Ketineni is born and brought up in Andhra Pradesh, India and hails from a Telugu background. He obtained his bachelors of Technology in chemical engineering from Indian Institute of Technology (2008). After working for two years (2008-10) as a deputy manager in Essar Oil Limited, he moved to Penn State to pursue his graduate education.

He got his Masters of Science in Petroleum and Natural Gas Engineering at Pennsylvania State University in May 2012 and is pursuing his Doctorate in Petroleum and Natural Gas Engineering at Penn State working with Dr. Turgay Ertekin. He has accepted an offer to work with Chevron ETC as a Reservoir Simulation consultant starting September 2015.